sid.inpe.br/mtc-m21d/2022/03.23.20.13-TDI

# REMOTE SENSING QUANTIFICATION OF CARBON LOSSES IN FRAGMENTED TROPICAL FORESTS AT MULTIPLE GEOGRAPHICAL SCALES

Celso Henrique Leite Silva Junior

Doctorate Thesis of the Graduate Course in Remote Sensing, guided by Drs. Luiz Eduardo Oliveira e Cruz de Aragão, and Liana Oighenstein Anderson, approved in March 31, 2022.

URL of the original document:
<http://urlib.net/8JMKD3MGP3W34T/46J6KGH>

INPE
São José dos Campos
2022

**PUBLISHED BY:**

Instituto Nacional de Pesquisas Espaciais - INPE
Coordenação de Ensino, Pesquisa e Extensão (COEPE)
Divisão de Biblioteca (DIBIB)
CEP 12.227-010
São José dos Campos - SP - Brasil
Tel.:(012) 3208-6923/7348
E-mail: pubtc@inpe.br

sid.inpe.br/mtc-m21d/2022/03.23.20.13-TDI

# REMOTE SENSING QUANTIFICATION OF CARBON LOSSES IN FRAGMENTED TROPICAL FORESTS AT MULTIPLE GEOGRAPHICAL SCALES

Celso Henrique Leite Silva Junior

Doctorate Thesis of the Graduate Course in Remote Sensing, guided by Drs. Luiz Eduardo Oliveira e Cruz de Aragão, and Liana Oighenstein Anderson, approved in March 31, 2022.

URL of the original document:
<http://urlib.net/8JMKD3MGP3W34T/46J6KGH>

INPE
São José dos Campos
2022

Cataloging in Publication Data

Silva Junior, Celso Henrique Leite.

Si38r Remote sensing quantification of carbon losses in fragmented tropical forests at multiple geographical scales / Celso Henrique Leite Silva Junior. – São José dos Campos : INPE, 2022.

xxvii + 150 p. ; (sid.inpe.br/mtc-m21d/2022/03.23.20.13-TDI)

Thesis (Doctorate in Remote Sensing) – Instituto Nacional de Pesquisas Espaciais, São José dos Campos, 2022.

Guiding : Drs. Luiz Eduardo Oliveira e Cruz de Aragão, and Liana Oighenstein Anderson.

1. Landsat. 2. LiDAR. 3. GEDI. 4. Deforestation. 5. Forest degradation. I.Title.

CDU 528.8:504.122

MINISTÉRIO DA CIÊNCIA, TECNOLOGIA E INOVAÇÕES

**INSTITUTO NACIONAL DE PESQUISAS ESPACIAIS**
Serviço de Pós-Graduação - SEPGR

**DEFESA FINAL DE TESE DE CELSO HENRIQUE LEITE SILVA JUNIOR**
**BANCA Nº 075/2022, REG 135208/2018**

No dia 31 de março de 2022, as 09h, por teleconferência, o(a) aluno(a) mencionado(a) acima defendeu seu trabalho final (apresentação oral seguida de arguição) perante uma Banca Examinadora, cujos membros estão listados abaixo. O(A) aluno(a) foi APROVADO(A) pela Banca Examinadora, por unanimidade, em cumprimento ao requisito exigido para obtenção do Título de Doutor em Sensoriamento Remoto. O trabalho precisa da incorporação das correções sugeridas pela Banca Examinadora e revisão final pelo(s) orientador(es).

**Título: "Remote sensing quantification of carbon losses in fragmented tropical forests at multiple geographical scales"**

**Membros da banca:**

Dr. Yosio Edemir Shimabukuro – Presidente e Membro Interno – INPE
Dr. Luiz Eduardo Oliveira e Cruz de Aragão – Orientador – INPE
Dra. Liana Oighenstein Anderson – Orientadora – CEMADEN
Dra. Sonaira Souza da Silva – Membro Externo – UFAC
Dra. Ane Auxiliadora Costa Alencar – Membro Externo – IPAM
Dr. Jos Barlow – Membro Externo – Lancaster University – LU

Declaração de aprovação do Dr. Jos Barlow anexa ao processo.

Documento assinado eletronicamente por **Yosio Edemir Shimabukuro**, **Pesquisador**, em 05/04/2022, às 16:12 (horário oficial de Brasília), com fundamento no § 3º do art. 4º do Decreto nº 10.543, de 13 de novembro de 2020.

Documento assinado eletronicamente por **Liana Oighenstein Anderson**, **Pesquisador**, em 05/04/2022, às 18:00 (horário oficial de Brasília), com fundamento no § 3º do art. 4º do Decreto nº 10.543, de 13 de novembro de 2020.

Documento assinado eletronicamente por **Luiz Eduardo Oliveira E Cruz de Aragão**, **Chefe da Divisão de Observação da Terra e Geoinformática**, em 06/04/2022, às 09:32 (horário oficial de Brasília), com fundamento no § 3º do art. 4º do Decreto nº 10.543, de 13 de novembro de 2020.

Documento assinado eletronicamente por **Sonaira Souza da silva (E)**, **Usuário Externo**, em 13/04/2022, às 13:08 (horário oficial de Brasília), com fundamento no § 3º do art. 4º do Decreto nº 10.543, de 13 de novembro de 2020.

Documento assinado eletronicamente por **Ane Auxiliadora Costa Alencar (E)**, **Usuário Externo**, em 19/04/2022, às 21:37 (horário oficial de Brasília), com fundamento no § 3º do art. 4º do Decreto nº 10.543, de 13 de novembro de 2020.

A autenticidade deste documento pode ser conferida no site http://sei.mctic.gov.br/verifica.html, informando o código verificador **9585850** e o código CRC **46077A33**.

**Referência:** Processo nº 01340.002034/2022-64 SEI nº 9585850

*“Although the fig tree shall not blossom, neither shall fruit be in the vines; The labour of the olive shall fail, and the fields shall yield no meat; The flock shall be cut off from the fold, and there shall be no herd in the stalls: Yet I will rejoice in the LORD, I will joy in the God of my salvation”.*

*Habakkuk 3: 17-18 KJV*

*To my parents Celso and Lucia, and my sister Sandy.*

## ACKNOWLEDGEMENTS

To God, for the Gift of Life and Grace. Nothing would have been possible without Him, especially having hope amid a pandemic and the anxiety crises imposed by depression. Mental health in post-graduation programs is a serious problem and must be treated with care.

To my parents, Celso, and Lucia, for their love, sacrifice, encouragement, and unconditional support throughout my life. To Talita for her love, patience, and support at all times.

To my advisors, Dr Luiz Aragão and Dr Liana Anderson, for friendship, teachings, opportunities, and patience. Besides inspired me to do Science to transform society.

To all the members of TREES Lab who directly or indirectly helped and encouraged me throughout my PhD. Especially to Nathalia, Ana, João, Mikhaela, and Igor.

Finally, to the Brazilian people through the National Institute for Space Research - INPE and the Coordination for the Improvement of Higher Education Personnel - CAPES for the financial support. Scientists from different institutions in Brazil and worldwide who made the datasets used in the Thesis freely available.

## ABSTRACT

The tropical forests biomass is a crucial carbon reservoir. However, large-scale deforestation leads to a critical increase in tropical forest fragmentation and compromises essential ecosystem services. Due to the lack of a comprehensive assessment of the edge effects impacts on fragmented tropical forests, the main objective of this thesis was to establish a remote sensing-based method to assess the synergy between deforestation, forest fragmentation, and their negative impacts on the remaining tropical forests. We found that forest fires incidence and intensity vary with levels of habitat loss and forest fragmentation in the Central Brazilian Amazon. About 95% of active fires and the most intense ones occurred in the first kilometre from the forest edges. In Amazonia, we found that carbon losses associated with the edge effect (947 Tg C) corresponded to about one-third of losses from deforestation (2,592 Tg C). Despite a notable reduction of carbon losses from deforestation (7 Tg C $year^{-1}$), the losses from the edge effect remained unchanged, with an average of 63±8 Tg C $year^{-1}$. Thus, carbon losses edge effect is an additional unquantified flux that can counteract carbon emissions avoided by reducing deforestation. Furthermore, we found that selective logging and fire degradation can increase carbon losses at forest edges for the tropical scale. Over time, carbon losses at forest edges vary along different environmental gradients, with degradation being the most important for losses in America and Africa and maximum temperature in Asia. Between 1990 and 2020, carbon losses resulted in $CO_2$ emission of 18 thousand teragrams, or the equivalent of 19% of emissions from deforestation (93 thousand teragrams) in the same period. The uptake of $CO_2$ from the atmosphere by secondary tropical forests was not sufficient to offset these emissions. We concluded that we were able to make a comprehensive analysis of fragmented tropical forests and assess their impacts at different scales through remote sensing. Furthermore, we argue that collateral $CO_2$ emissions from the edge effect should be quantified and reported with emissions from deforestation for an inventory of greenhouse gases more consistent with the reality of the carbon cycle in tropical forests.



Keywords: Landsat. LiDAR. GEDI. Deforestation. Forest degradation.

# QUANTIFICAÇÃO DAS PERDAS DE CARBONO EM FLORESTAS TROPICAIS FRAGMENTADAS POR SENSORIAMENTO REMOTO EM MÚLTIPLAS ESCALAS GEOGRÁFICAS

## RESUMO

A biomassa das florestas tropicais é um crucial reservatório de carbono. No entanto, o desmatamento em larga escala tem levado a um aumento crítico da fragmentação das florestas tropicais e compromete os serviços ecossistêmicos essenciais. Devido à falta de uma avaliação abrangente dos impactos do efeito de borda em florestas tropicais fragmentadas, o objetivo geral desta tese foi estabelecer um método baseado em sensoriamento remoto para avaliar a sinergia entre desmatamento, fragmentação e seus impactos negativos sobre os remanescentes de florestas tropicais. Descobrimos que a incidência e a intensidade dos incêndios florestais variam com os níveis de perda de habitat e fragmentação florestal na Amazônia Central Brasileira. Cerca de 95% dos incêndios ativos e os mais intensos ocorreram no primeiro quilômetro das bordas da floresta. Na Amazônia, descobrimos que as perdas de carbono associadas ao efeito de borda (947 Tg C) corresponderam a cerca de um terço das perdas por desmatamento (2.592 Tg C). Apesar de uma notável redução das perdas de carbono por desmatamento (7 Tg C $ano^{-1}$), as perdas por efeito de borda permaneceram inalteradas, com média de 63±8 Tg C $ano^{-1}$. Assim, as perdas de carbono por efeito de borda são um fluxo adicional não quantificado que pode neutralizar as emissões de carbono evitadas pela redução do desmatamento. Além disso, descobrimos que a degradação florestal por extração seletiva de madeira e fogo podem aumentar as perdas de carbono nas bordas da floresta na escala tropical. As perdas de carbono nas bordas florestais à medida que envelhecem, variaram ao longo de diferentes gradientes ambientais, sendo a degradação a mais importante para perdas na América e África e temperatura máxima na Ásia. Entre 1990 e 2020, as perdas de carbono resultaram na emissão de 18 mil teragramas de $CO_2$ para a atmosfera ou o equivalente a 19% das emissões por desmatamento (93 mil teragramas) para o mesmo período. A absorção de $CO_2$ da atmosfera pelas florestas secundárias tropicais não foi suficiente para compensar essas emissões. Concluímos que fomos capazes de realizar uma análise abrangente das florestas tropicais fragmentadas e avaliar seus impactos em diferentes escalas por meio do sensoriamento remoto. Além disso, defendemos que as emissões de $CO_2$ decorrentes do efeito borda devem ser quantificadas e relatadas juntas as emissões por desmatamento para um inventário de gases de efeito estufa mais condizente com a realidade do ciclo do carbono das florestas tropicais.

Palavras-chave: Landsat. LiDAR. GEDI. Desmatamento. Degradação florestal.

## LIST OF FIGURES

**Page**

## LIST OF TABLES

**Page**.

## LIST OF ABBREVIATIONS

| | |
|---|---|
| AGB | *Above Ground Biomass* |
| AGC | *Above Ground Carbon* |
| ANOVA | Analysis of Variance |
| BIC | *Bayesian Information Criterion* |
| C | Carbon |
| ETM+ | *Enhanced Thematic Mapper Plus* |
| FIRMS | *Fire Information for Resource Management System* |
| GDAL | *Geospatial Data Abstraction Library* |
| GEDI | *Global Ecosystem Dynamics Investigation LIDAR* |
| GFC | *Global Forest Change* |
| GLAS | *Geoscience Laser Altimeter System* |
| GPS | *Global Positioning System* |
| GSW | *Global Surface Water* |
| ICESat | *NASA Ice, Cloud, and Land Elevation Satellite* |
| INPE | National Institute for Space Research |
| KW | *Kruskal-Wallis* |
| LiDAR | Light Detection And Ranging |
| DTM | Digital Terrain Model |
| MMA | Ministry of the Environment |
| MODIS | *Moderate Resolution Imaging Spectroradiometer* |
| CSM | Canopy Surface Model |
| NASA | *National Aeronautics and Space Administration* |
| OLI | *Operational Land Imager* |
| PDBFF | Biological Dynamics of Forest Fragments Project |
| PPCDAm | Action Plan for the Prevention and Control of Deforestation in Legal Amazon |
| PRODES | Monitoring of Deforestation in the Brazilian Legal Amazon by Satellite |
| RAISG | Amazon Network of Georeferenced Socio-Environmental Information |
| REDD | *Reducing Emissions from Deforestation and Forest Degradation* |
| SAR | *Synthetic Aperture Radar* |

| | |
|---|---|
| TM | *Thematic Mapper* |
| W | *Wilcoxon* |

## SUMMARY

**Page**

# 1 INTRODUCTION

The tropical forests store 193-229 Pg of carbon in their biomass (SAATCHI et al., 2011; BACCINI et al., 2012). However, this region is affected on a large scale by deforestation that converts forests into anthropic environments (KISSINGER; HEROLD; SY, 2012; MALHI et al., 2014; CARTER et al., 2018). Between 1990 and 2015, this region loss 10% of its forest cover (KEENAN et al., 2015). This forest area reduction compromises essential ecosystem services (FOLEY, 2005; BACCINI et al., 2017). In addition, rampant deforestation leads to a critical increase in tropical forest fragmentation (FISCHER et al., 2021).

The Paris Climate Agreement (UNFCCC - FRAMEWORK CONVENTION ON CLIMATE CHANGE, 2015a), which deals with measures to reduce greenhouse gas emissions by the signatory countries, reinforces the need to strengthen the global response to the threat of climate change. However, forest fragmentation led to edge effects, which adversely affects forest functioning, reducing carbon stocks (LAURANCE et al., 1997, 2018; SILVA JUNIOR et al., 2020a), lading to dioxide carbon ($CO_2$) emission into atmosphere. Thus, tropical forest edges, are an important source of $CO_2$ (NUMATA et al., 2011; PÜTZ et al., 2014; BRINCK et al., 2017; SILVA JUNIOR et al., 2020a), but yet explicitly measured and included in policies to reduce greenhouse gas emissions (SILVA JUNIOR et al., 2021a).

In the past, the decade-scale of tropical edge effect contribution to $CO_2$ emissions was limited by the lack of multi-temporal maps of forest cover with appropriate spatial resolution. On the other hand, recent advances in remote sensing datasets, especially with the widespread use of optical and non-optical multitemporal data, can fill these gaps. Here, we used a vast, remote sensing dataset to enable an unprecedented analysis of fragmented tropical forests. We start by analysing the relationship between forest fragmentation and fires in the Brazilian Central Amazon, going through the first Amazonian estimate of the loss of carbon stocks due to the edge effect, and finally at the first comprehensive assessment of the impact of the edge effects on carbon stocks of tropical forests.

## 1.1 Motivation and objectives

Due to the lack of a comprehensive assessment of the edge effects impacts on fragmented tropical forests, the main objective of the thesis was to establish a remote sensing-based method to assess the synergy between deforestation, forest fragmentation, and their negative impacts on the remaining tropical forests. Thus, the Thesis has three specific objectives:

1. To understand the relationship between the configuration of fragmented forest landscapes in the Brazilian Central Amazon and the occurrence and intensity of forest fires;
2. Quantify the extent and carbon stocks lost at forest edges of Amazonia;
3. Quantify the extent and carbon emissions and environmental factors associated with carbon loss at the edges of tropical forests over the past three decades.

## 1.2 Thesis outline

This document was drawn in a paper-format, which include two papers already published and one in the process of being finalized to submission. In the following sections it will be described: Chapter 2 is a literature review on tropical forest fragmentation; Chapter 3 presents a case study about the relationship between forest fragmentation and fires in the Central Brazilian Amazon; Chapter 4 introduces an LiDAR (Light Detection And Ranging) approach to quantify carbon stocks due to edge effects in Amazonia; Finally, Chapter 5 presents the first comprehensive 30-year analysis of fragmented tropical forests, including estimates of edge-effect carbon emissions and analysis of the role of the environmental gradient for the loss of carbon stocks at tropical forest edges.

# 2 LITERATURE REVIEW

## 2.1 Deforestation and forest fragmentation in the tropical region

The tropical region is located between the tropics of Capricorn (latitude 23.5° South) and Cancer (23.5° North), covering America, Africa, and Asia. Forests in this region play a crucial role, providing important ecosystem services. However, deforestation in this region continually converts forests into agricultural, livestock and urban areas (MALHI et al., 2014). The loss of forest cover caused an increase in the number of fragments and a reduction in the area of forest remnants in the region (TAUBERT et al., 2018).

### 2.1.1 Deforestation in the tropical region

In the tropical region, mappings with standardized methodologies and aimed at detecting changes in forest cover are rare. However, Hansen et al. (2013) examined Landsat data at a spatial resolution of 30 m and performed the first global mapping of forest gains and losses between 2000 and 2012. Although it contains uncertainties (HANSEN et al., 2014; TROPEK et al., 2014), these data are useful for a rapid and uniform assessment of forest cover loss in the tropical region. Figure 1 shows the annual forest cover losses from 2001 to 2018 detected by Hansen et al. (2013) and filtered for tropical forest areas (threshold of 80% tree cover applied) (SILVA JUNIOR, 2018; GASPARINI et al., 2019a).

Figure 2.1 - Annual Forest cover losses from 2001 to 2018 (left). Contribution of the American, African, and Asian continents to forest cover losses between 2001 and 2018 (right).

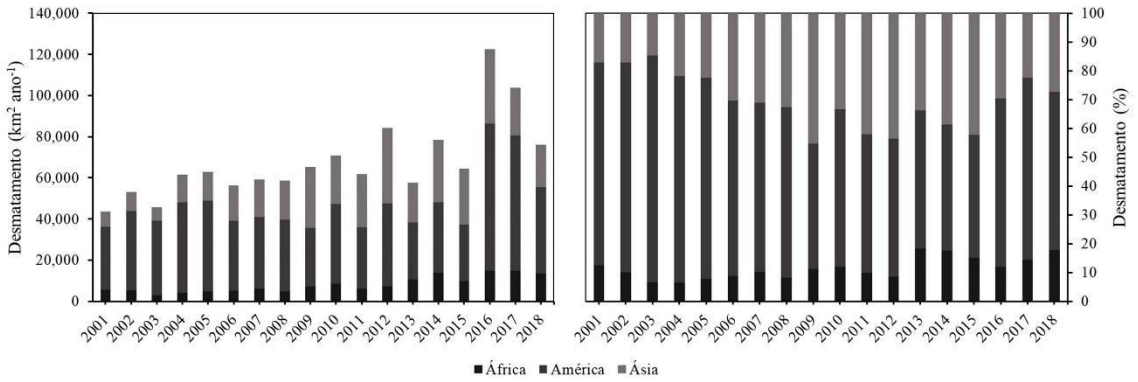


Source: Hansen et al. (2013).

In 2000, forest cover in the tropical region totalled 14,447,920 km$^2$, with 43% in Asia, 42% in America and 16% in Africa. Between 2001 and 2018, the region lost about 1,226,201 km$^2$ (approximately 8.49% compared to 2000) of its forest cover. This loss occurred at an average of 68,122±19,069 km$^2$ year$^{-1}$, with a significant increase trend ($p<0.05$; $R^2 = 0.55$) of 2,718 km$^2$ year$^{-1}$ (Figure 2.1; left) A peak of 122,498 km$^2$ was observed in 2018, while the smallest annual area of lost forest was observed in 2001 (43,660 km$^2$). America was responsible on average for 58±11% year$^{-1}$ of forest cover losses, while Asia and Africa accounted for 30±9% year$^{-1}$ and 12±4% year$^{-1}$, respectively (Figure 2.1; right).

America alone, between 2001 and 2018, 702,954 km$^2$ (approximately 11.72% of forest cover in 2000) of forest cover were lost, at an average of 39,053±11,677 km$^2$ year$^{-1}$, with no trend identified for the period ($p>0.05$; $R^2 = 0.12$) (Figure 2.2a). A peak of 71,626 km$^2$ was observed in 2016, while the smallest annual area of lost forest was observed in 2015 (27,541 km$^2$). In Africa, between 2001 and 2018, 144,904 km$^2$ (approximately 6.28% of forest cover in 2000) of forest cover were lost, at an average of 8050±3794 km$^2$ year$^{-1}$, with a significant increase trend ($p<0.05$; $R^2 = 0.78$) of 647 km$^2$ year$^{-1}$ (Figure 2.2b). A peak of 14,884 km$^2$ was observed in 2017, while the smallest annual area of lost forest was observed in 2003 (3058 km$^2$). However, in Asia between 2001 and 2018, 378,343 km$^2$ (approximately 6.16% of forest cover in 2000) of forest cover were lost, at an average of 21,019±8737 km$^2$ year$^{-1}$, with a significant increase trend ($p<0.05$; $R^2$

= 0.58) of 1,278 km$^2$ year$^{-1}$ (Figure 2.2c). A peak of 36,757 km$^2$ was observed in 2012, while the smallest annual area of lost forest was observed in 2003 (6,711 km$^2$).

Figure 2.2– (a) Annual loss of forest cover in tropical America. (b) Annual loss of forest cover in tropical Africa. (c) Annual loss of forest cover in tropical Asia. (d) Spatial distribution of forest cover losses between 2001 and 2018 grouped in pixels with 0.25-degree spatial resolution.

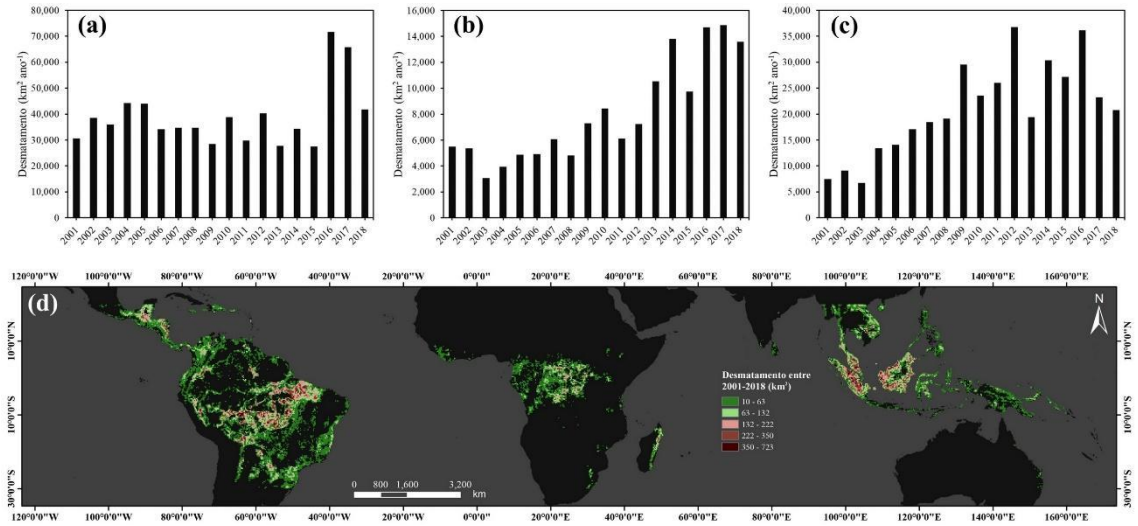


Spatially (Figure 2.2d), the largest losses (between 222 and 723 km$^2$ pixel$^{-1}$) of forest cover between 2001 and 2018 were mainly distributed in southern Mexico, Honduras, Nicaragua and in the south and east of the Amazon Basin in the American continent. On the other hand, on the African continent, the biggest losses were located mainly in the Congo Basin, while in Asia, they were located in Malaysia and Indonesia.

Although agricultural expansion has been identified as the main driver of deforestation in the tropics in the 20th century (GIBBS et al., 2010), other causes were observed from the beginning of the 21st century, varying regionally and temporally (BOUCHER et al., 2012; CURTIS et al., 2018) (Figure 2.3).

Figure 2.3 – Contribution of drivers of deforestation to deforestation in the tropical region. (a) Contribution of drivers of deforestation reported by 46 countries in the tropical region in the period 2000 to 2010 (FAO, 2010), where commercial agriculture includes the contribution of livestock. (b) Contribution of the drivers of deforestation reported for the tropical region from 2001 to 2015 (CURTIS et al., 2018). In the figures, commercial agriculture is understood to be large-scale, and subsistence to family agriculture, for example.

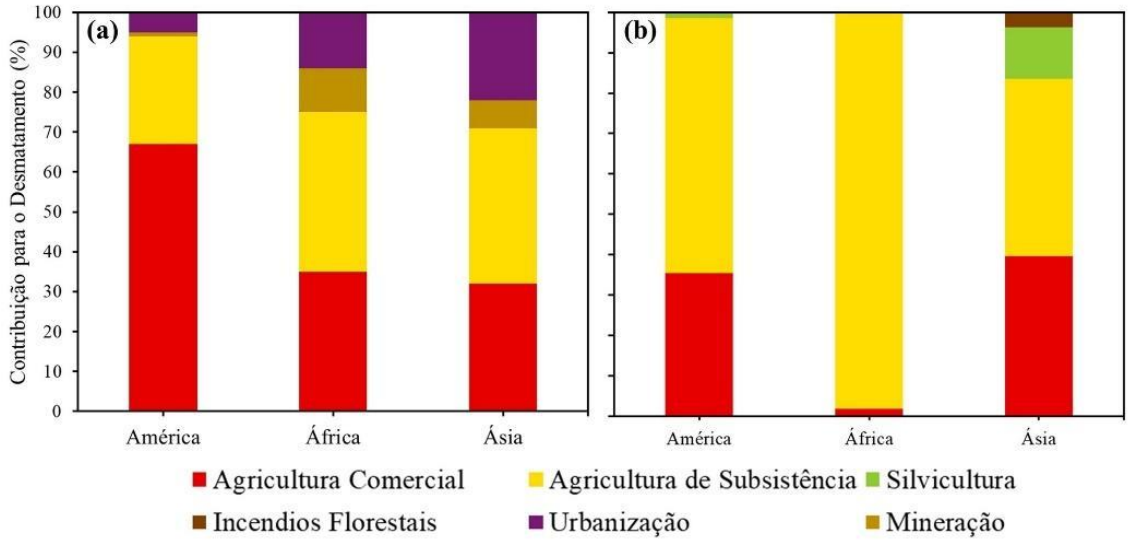


Source: Kissinger, Herold and Sy (2012) and Curtis et al. (2018).

According to data from the Food and Agriculture Organization of the United Nations - FAO (FAO, 2010) (Figure 2.3a), in America until 2010, approximately 67% of the deforested areas were destined to commercial agriculture, while the areas destined to mining and urban/infrastructure expansion together totalled a contribution of 6%. In contrast, Africa and Asia were similar with 40% and 39% of deforested areas, respectively, destined for subsistence agriculture. It is also important to highlight that of the three continents, Asia had 22% of the deforested areas destined for urban/infrastructure expansion, which reflects the large population growth in the region (DEFRIES et al., 2010).

In a global analysis based on remote sensing data (HANSEN et al., 2013), Curtis et al. (2018) classified those likely to be responsible for the loss of forest cover. According to this classification, focused here on the tropical region (Figure 2.3b), 63.14%, 98.11% and 43.91% of the deforested areas between 2001 and 2015 were destined for subsistence agriculture, in America, Africa and Asia, respectively. Commercial agriculture was more important in America (35.47%) and Africa (39.59%) than Asia (1.74%). On the other hand, forestry was more

important in Asia (12.86 %) than in America (1.08 %) and Africa (0.14 %), while urbanization was more important in Asia (0.11%) than in America (0%) and Africa (0.01%). Forest fires were responsible for 3.54% of the loss of forest cover in Asia, while America and Africa had zero values.

Although the two works mentioned above were carried out with different methods and have limitations and uncertainties, they converge in highlighting the importance of commercial agriculture as the main driver of deforestation in the tropics, mainly in America and Asia.

On the American continent, extensive areas of forest in the Brazilian portion of the Amazon Basin were converted into areas for soybean cultivation and cattle ranching (ALMEIDA et al., 2016), to meet external demands for food (NEPSTAD et al., 2014; GIBBS et al., 2015). In Ecuador and Colombia, on the other hand, forest areas have given way mainly to palm cultivation (KOH; WILCOVE, 2008; CASTIBLANCO; ETTER; AIDE, 2013; LÓPEZ ACEVEDO, 2018).

Still related to the forest areas that gave rise to palm cultivation, Nigeria and Ghana stand out in Africa, the third and fifth largest palm growers in 2013, respectively, according to FAO data (VIJAY et al., 2016b). On the other hand, in Asia, there is a consensus on the region's leadership in the significant replacement of forest areas for palm cultivation, to meet the growing international demand for vegetable oils and biofuels (FITZHERBERT et al., 2008; KOH; WILCOVE, 2008, 2009; WICKE et al., 2011; AFRIYANTI; KROEZE; SAAD, 2016; VIJAY et al., 2016a; AUSTIN et al., 2017).

Another emerging activity in the tropical region is mining in the Amazon region, especially gold, which has induced direct and collateral deforestation of forests in the region (ASNER; TUPAYACHI, 2016; WEISSE; NAUGHTON-TREVES, 2016; DEZÉCACHE et al., 2017; CABALLERO ESPEJO et al., 2018).

Identifying the causes and patterns of deforestation, as well as quantifying its extent in the tropics, is crucial to understanding fragmentation and its impacts in the region. The spatial and temporal patterns of deforestation are directly responsible for the spatial arrangements and geometries of forest fragments (LAURANCE; LAURANCE; DELAMONICA, 1998; SILVA JUNIOR et al., 2018).

In the Amazon region, for example, landscapes dominated by deforestation with a fishbone pattern, generally associated with subsistence agriculture and livestock, produce up to five times more forest edges than areas with a pattern of deforestation associated with commercial agricultural and livestock production (LAURANCE; LAURANCE; DELAMONICA, 1998).

### 2.1.2 Forest fragmentation in the tropical region

Deforestation in recent decades in the tropical region has resulted in significant fragmentation of forest remnants. Initial efforts made it possible to quantify fragmentation at different scales (spatial and temporal) using different methodologies. Work on a regional scale was limited mainly to the Amazon Basin and Atlantic Forest region. Below are the main findings regarding forest fragmentation in the tropical region.

In the Brazilian Amazon, Numata and Cochrane (2012) used forest maps (Monitoring the Brazilian Amazon Deforestation by Satellites - PRODES/INPE) resampled to 90-m spatial resolution, covering seven states of the Legal Brazilian Amazon in the period from 2001 to 2010 and estimated the quantity and size of forest fragments, in addition to the total extension of edges (1,000-m width). They found that the total number of fragments doubled in the analysed period, with 76,866 fragments in 2001 to 143,572 fragments in 2010 and forest edges increased from 467,237 $km^2$ in 2001 to 543,393 $km^2$ in 2010. For the year 2014, on the other hand, Vedovato et al. (2016) used a forest map (PRODES/INPE) resampled to 60-m spatial resolution to classify fragmentation across the Brazilian Legal Amazon and found that 101,440 $km^2$ (3.2%) of forest remnants corresponded to fragments (called islands), while 164,595 $km^2$ (5.2%) corresponded to edges (1,020-m width).

In the Amazonia-wide, Silva Junior et al. (2020a) used data from Hansen et al. (2013) to prepare forest maps (areas with tree cover equal to or greater than 80%) and estimate forest edge areas (120-m width) created between 2001 and 2015, having found that these areas increased from 16,212 $km^2$ in 2001 to 176,555 $km^2$ in 2015. Furthermore, Putz et al. (2014) used data from the Moderate-Resolution Imaging Spectroradiometer - MODIS sensor aboard the

Aqua and Terra satellites (250-m spatial resolution) in 2009 to estimate forest fragmentation in the Amazon Basin and found a total of 77,038 fragments with average area of 83.76 $km^2$ and 321,135 $km^2$ of total area of edges (1000-m width). For the Atlantic Forest, the same authors used Landsat data (spatial resolution resampled to 50 m) from 2005 and found a total of 245,173 fragments with an average area of 0.63 $km^2$ and 73,476 $km^2$ of total area of edges (1000-m width). These results show that in tropical America, fragmentation varied spatially and temporally with different magnitudes.

The authors cited above used different approaches to identify and quantify fragmentation. Among these approaches, there is the use of the Euclidean Distance technique (NUMATA; COCHRANE, 2012; SILVA JUNIOR, 2018), from the package *Patch Analyst*[1] (PÜTZ et al., 2014)and the MSPA - Morphological Segmentation of Binary Patterns[2] (VEDOVATO et al., 2016).

In the literature, two estimates of forest fragmentation at the tropical scale stand out (BRINCK et al., 2017; TAUBERT et al., 2018). Brinck et al. (2017) used a forest map for the year 2000, based on tree cover data from the Global Land Cover Facility - GLCF, while Taubert et al. (2018) used a map for the same year based on tree cover data prepared by Hansen et al. (2013). Both studies defined areas with tree cover equal to or greater than 30% and used an adapted version of the Hoshen-Copelman (HOSHEN; KOPELMAN, 1976) algorithm to quantify fragmentation. Table 1 summarizes the main results of the two works mentioned above.

[1] Rempel et al. (2019)

[2] Soille e Vogt (2009)

Table 2.1 - Synthesis of the main results obtained by Brinck et al. (2017) and Taubert et al. (2018). The results include quantification of the number of forest fragments, average area of forest fragments, area of forest edges and length of forest edges. *This value is not included in the reference, it was calculated here by the sum of the number of fragments from America, Africa, and Asia.

| Variable | Reference | America | Africa | Asia | Tropical region |
|---|---|---|---|---|---|
| Patches number | Brinck et al. (2017) | 23,491,573 | 22,894,239 | 7,593,226 | 53,979,038 |
| | Taubert et al. (2018) | 55,558,018 | 44,851,251 | 30,556,204 | 130,965,473* |
| Patches size ($km^2$) | Brinck et al. (2017) | 0.35 | 0.16 | 0,52 | 0.29 |
| | Taubert et al. (2018) | 0.17 | 0.13 | 0,13 | - |
| Forest edges area ($km^2$) | Brinck et al. (2017) | 1,310,000 | 940,000 | 700,000 | 2,950,000 |
| | Taubert et al. (2018) | - | - | - | - |
| Forest edges length (km) | Brinck et al. (2017) | - | - | - | - |
| | Taubert et al. (2018) | 22,000,000 | 18,000,000 | 10,000,000 | 50,000,000 |

Source: Brinck et al. (2017) and Taubert et al. (2018).

Although the magnitude of the estimates made by Taubert et al. (2018) are higher than the estimates by Brinck et al. (2017),the two works converge, showing an accentuated process of fragmentation in America in relation to Africa and Asia, at the beginning of the 21st century. Forest fragmentation in America is observed by the high number of fragments, these with a reduced average area, in addition to the extensive border areas. However, it is necessary to point out that in both works, the authors used a threshold of 30% to define forest areas. This threshold causes the overestimation of forest areas (GASPARINI et al., 2019a), thus including savannah formation areas in the analyses, causing a bias in the fragmentation estimates of the two works. Gasparini et al. (GASPARINI et al., 2019a), for example, suggest using a threshold between 80% and 85% to define forest areas more accurately in tree cover percentage data.

Although the initial efforts presented above have been undertaken, the multitemporal quantification of forest fragmentation for the tropical region is an unexplored gap in knowledge. Recent advances in the ability to process large volumes of geospatial data in the cloud (GORELICK et al., 2017) and the availability of forest cover datasets on a global scale with multitemporal

availability (HANSEN et al., 2013), mean an unprecedented opportunity to contribute to advancement in this field of knowledge.

### 2.1.3 Dynamics of fire in the tropical region

The tropical region has a natural forest fire regime characterized by a low frequency of fire (COCHRANE, 2003; BUSH et al., 2008; BOWMAN et al., 2011), while in savannah areas, this regime naturally has a high frequency (BOWMAN et al., 2009). However, in recent decades, this frequency has intensified in forest and non-forest areas, mainly due to human activities in the region (LEWIS; EDWARDS; GALBRAITH, 2015).

Figure 4 shows the temporal and spatial pattern of active fires across the tropical region between 2003 and 2018. During this period, the region had an impressive 11,744,186 active fires, an average of 734,012±66,725 active fires year$^{-1}$, with a maximum peak observed in 2007 (845,477 active fires) and a minimum in 2018 (624,289 active fires). However, the region had a significant downward trend ($p < 0.05$; $R^2 = 0.65$) of 11,634 active fires year$^{-1}$ between 2003 and 2018, corroborating the global reduction in burned areas observed between 2003 and 2015 (ANDELA et al., 2017).

Figure 2.4 – Spatio-temporal pattern of active fires throughout the tropical region. (a) Annual total of active fires in America between 2003 and 2018. (b) Annual total of active fires in Africa between 2003 and 2018. (c) Annual total of active fires in Asia between 2003 and 2018. (d) Spatial distribution of the annual average of active fires per pixel of 0.25 degrees between 2003 and 2018. (e) Spatial distribution of tree cover percentage in 2000 (HANSEN et al., 2013) resampled (averaged) in 0.25-degree spatial resolution pixels. (f-h) Monthly pattern of active fires in America, Africa, and Asia, respectively. In Figures 2.4f, 2.4g and 2.4h the black line represents the average and the shaded area the standard deviation.

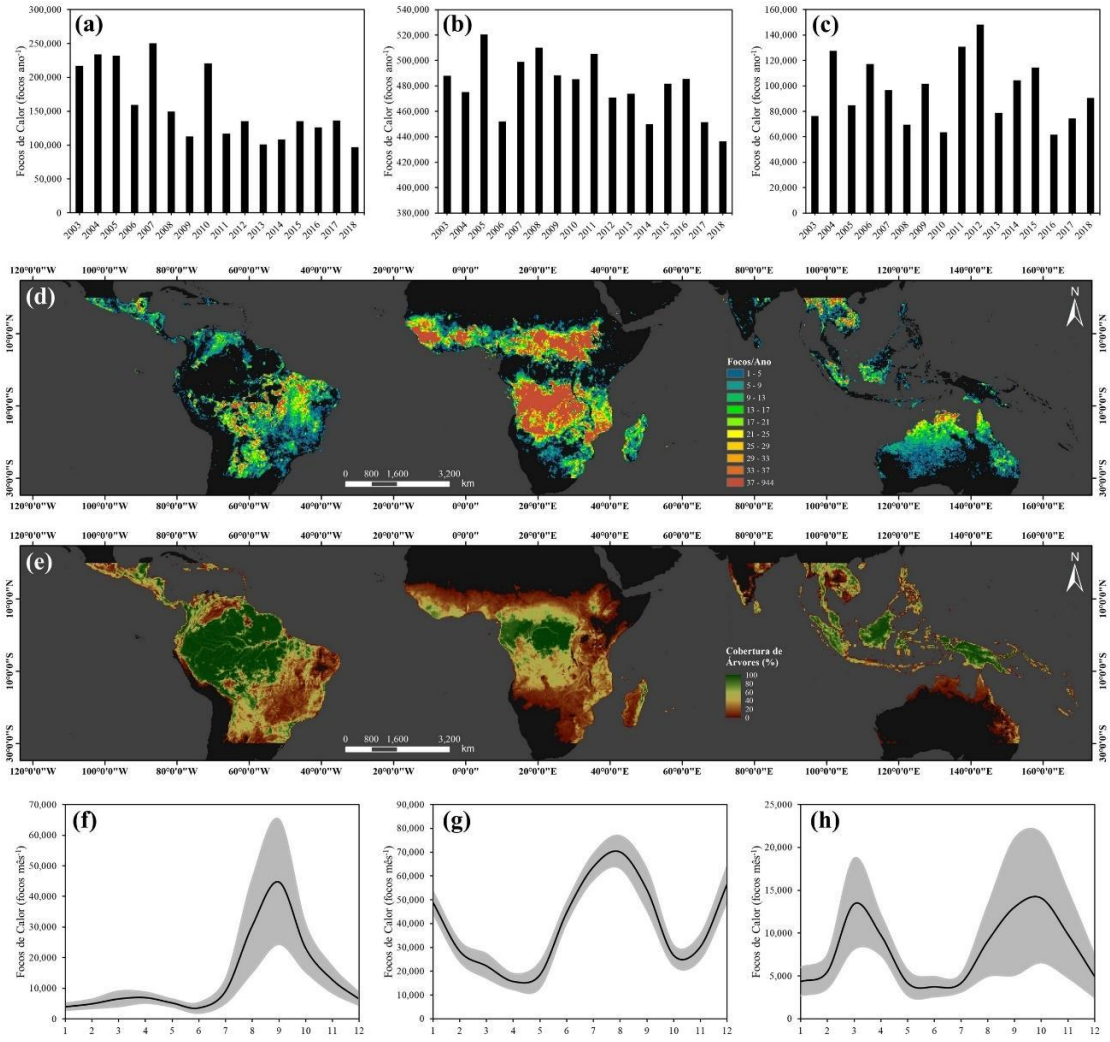


Source: Giglio et al. (2016) and NASA (2018).

On a regional scale (Figure 2.4a, 2.4b and 2.4c), Africa had 65% (7,673,004 active fires) of active fires detected in the tropical region between 2003 and 2018,

with an average of 479,563±22,720 active fires per year$^{-1}$, followed by America with 22% (2,530,484 active fires) and an average of 158,155±51,695 active fires year$^{-1}$ and Asia with 13% (1,540,698 active fires) and an average of 96,294±25,058 active fires year$^{-1}$. On the other hand, between 2003 and 2018, America and Africa had a significant downward trend ($p<0.05$) of 8,403 active fires year$^{-1}$ ($R^2=0.56$) and 2,575 active fires year$^{-1}$ ($R^2=0.27$), respectively, while Asia kept its rates constant over time ($p>0.05$; $R^2=0,01$).

Spatially (Figure 2.4d), active fires occurred especially in savannah areas and less frequently in forested areas. This fact is revealed by the overlap between cells with values between 37 and 944 active fires year$^{-1}$ and cells with tree cover between zero and 50 % (Figure 2.4e), which characterize savannah areas and the absence of active fires in central areas with tree cover greater than 70%. In addition, a high frequency of active fires was observed in the “Arc of Deforestation” region in the Amazon Basin and western Asia, regions heavily deforested between 2001 and 2018 (Figure 2.4d).

Monthly (Figure 2.4f, 2.4g and 2.4h), the occurrence of active fires differed strongly in terms of magnitude and variability in the three continents of the tropical region. In America (Figure 2.4f), the occurrence of active fires maintained an average below 10,000 active fires month$^{-1}$ between the months of January and June, increasing progressively from July onwards and reaching a peak of 44,753±20,389 active fires month$^{-1}$, then decreasing until December when it had an average of 12,797±4,299 active fires per month$^{-1}$. In Africa (Figure 2.4g), on the other hand, the monthly averages showed little variation, revealed by the low standard deviations, and two well-defined monthly peaks, one in December/January (48,759±4593 active fires month$^{-1}$ and 56,426±7448 active fires month$^{-1}$, respectively) and another in August (70.090±6815 active fires month$^{-1}$). Asia (Figure 4h) also presented two monthly peaks, one in March (70.090±6815 active fires month$^{-1}$) and another in October (70.090±6815 active fires month$^{1}$). In the American portion of the tropics, the fire regime is mainly governed by the Amazon Basin, which has its peaks of fire occurrence synchronized with the dry season in the region (rainfall below 100 mm$^{-1}$) (ARAGÃO et al., 2008; MARENGO et al., 2018). On the other hand, the African

and Asian portions, which have two monthly peaks, may be the result of the climate regimes of the northern and southern hemispheres simultaneously.

As pointed out in Figure 2.4d, in the tropical region the occurrence of fire is strongly linked to natural non-forest vegetation (e.g., savannahs), a result of natural occurrence or induced by human activities (ARCHIBALD; STAVER; LEVIN, 2012; DANIAU et al., 2013; ANDELA; VAN DER WERF, 2014; ARCHIBALD, 2016; MATAVELI et al., 2018). On the other hand, many studies carried out for the tropical region also relate fire to deforestation activities (slash and burn system), agriculture and livestock (JUÁREZ-OROZCO; SIEBE; FERNÁNDEZ Y FERNÁNDEZ, 2017).

However, forest fires in the tropical region emerge from fire escape from adjacent areas (CANO-CRESPO et al., 2015). This escape may originate from areas that were recently deforested and burned for cleaning, or from areas where agriculture and livestock are managed (ARAGÃO et al., 2008). Fire entry into the forest occurs through edges, which are a result of deforestation-induced fragmentation (ARMENTERAS; GONZÁLEZ; RETANA, 2013; SILVA JUNIOR et al., 2018).

In addition, the occurrence of El Niño causes a generalized reduction in rainfall and an increase in temperature throughout the tropical region (JIMÉNEZ-MUÑOZ et al., 2016; BURTON; RIFAI; MALHI, 2018; JIMENEZ et al., 2018). Thus, the fragmentation of forest remnants (NUMATA; COCHRANE, 2012; PÜTZ et al., 2014; VEDOVATO et al., 2016; BRINCK et al., 2017; SILVA JUNIOR, 2018; TAUBERT et al., 2018) associated with a drier and warmer environment, makes the vegetation more susceptible to the spread of fire (NEPSTAD et al., 2004, 2007; BRANDO et al., 2008; ARMENTERAS; GONZÁLEZ; RETANA, 2013; BRIENEN et al., 2015; SILVA JUNIOR et al., 2018). During the 2010 and 2015/2016 El Niño, for example, extensive areas of forest were consumed by fire in the Amazon portion of Brazil and Indonesia (ARAGÃO et al., 2018; LOHBERGER et al., 2018; SILVA JUNIOR et al., 2019a).

Thus, more comprehensive studies at the tropical scale are needed to improve the understanding of forest fires in the region and their relationship with El Niño years. Regional efforts should be concentrated in Africa and Asia, as Amazonia

is well studied. Furthermore, it is necessary to advance in the understanding of the relationship between fragmentation and forest fires in the tropical region, outside the Amazon Basin.

### 2.1.4 Edge effects impact on tropical forest carbon stocks

Forest fragmentation has a direct impact on forest biodiversity, which can reduce it between 13% and 75%, affecting important ecological functions (HADDAD et al., 2015). Forest remnants with a reduced area, for example, present a smaller variety of habitats than those with a larger area, causing a drastic loss of species of flora and fauna (LAURANCE; VASCONCELOS, 2009). In addition, the edge effect resulting from fragmentation reduces carbon stocks (due to tree mortality) and predisposes forest remnants to fire, the latter contributing to the intensification of the former (LAURANCE et al., 2018; SILVA JUNIOR et al., 2020a).

In the tropical region, the main findings regarding the effect of fragmentation on forest carbon stocks come from the Brazilian Amazon. These discoveries were made possible through long-term experiments carried out within the scope of the PDBFF - Biological Dynamics of Forest Fragments Project, based in the municipality of Manaus, state of Amazonas (LAURANCE et al., 2018).

Figure 2.5 shows the range in the forest of the main edge effects that include microclimate changes, tree mortality, forest fires and consequently the reduction of aboveground biomass.

Figure 2.5 – Reach of the main effects on board. The plus and minus signs represent the standard deviation of variables.

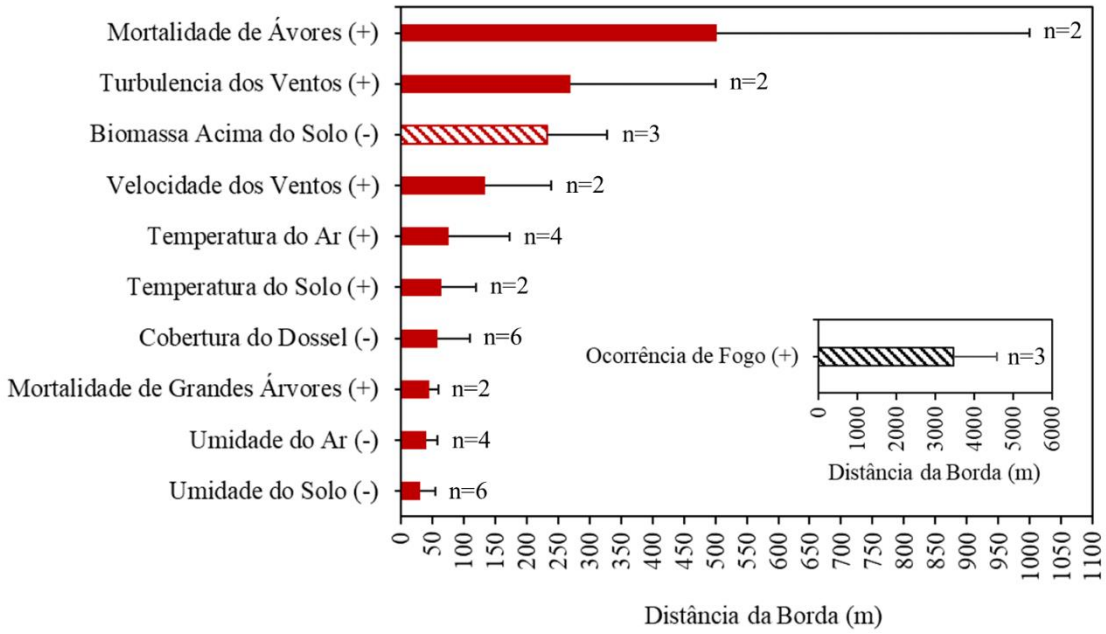


The figure was based on the compilation of results from the literature (BROADBENT et al., 2008; DE PAULA; COSTA; TABARELLI, 2011; ARMENTERAS; GONZÁLEZ; RETANA, 2013; SHAPIRO et al., 2016; LAURANCE et al., 2018; SILVA JUNIOR et al., 2018, 2020a).

After deforestation, edges (abrupt and artificial) are created between the remaining forest and the deforested areas, which cause physical and biotic changes in the forest (LAURANCE et al., 2018). The immediate effect observed is the increase in temperature and reduction in humidity due to differences in evapotranspiration between the forest and adjacent deforested areas (CAMARGO; KAPOS, 1995), reaching an average of 77±96-m for the increase in temperature and 40±19 m for moisture reduction (Figure 2.5). Furthermore, at the forest edges the wind becomes more turbulent (agitated) and with higher speed (FERREIRA; LAURANCE, 1997; LAURANCE et al., 1997), reaching an average of 270±230-m for the increase in turbulence and 135±105 m for speed increase (Figure 2.5). These microclimatic changes mentioned above, in turn, promote an increase in tree mortality rates, with an average range of 503±497 m

for trees in general and 45±15-m for large trees (Figure 2.5) (LAURANCE et al., 1997, 1998).

Tree mortality has a direct impact on the reduction of aboveground living biomass at forest edges. This reduction is significant at an average distance of 233±94-m (Figure 5). In Central Amazonia, a reduction in aboveground living biomass of around 11% is documented for up to 100-m in the first four years after fragmentation (LAURANCE; LAURANCE; DELAMONICA, 1998). However, Laurance, Laurance and Delamonica (1998) disregarding the occurrence of fire at forest edges in their field experiments, which can reach an average of 3,467±1,112 m (Figure 2.X) (COCHRANE; LAURANCE, 2002; ARMENTERAS; GONZÁLEZ; RETANA, 2013; SILVA JUNIOR et al., 2018), may increase the extent of aboveground biomass losses in the forest, due to increased tree mortality due to the direct impact of fire (SILVA et al., 2018b) or the wind-induced fall of live but fire-damaged trees (SILVÉRIO et al., 2019a). Silva Junior (2018), for example, found a loss of carbon stocks of 36.7% in the first five years after fragmentation, while De Paula et al. (2011) found 50% in forest edges with 100-m wide, although they did not relate this loss to the edge aging process.

On a large scale, some studies have quantified the loss of aboveground biomass and carbon stocks due to forest fragmentation for the tropical region (NUMATA et al., 2011; PÜTZ et al., 2014; BRINCK et al., 2017; SILVA JUNIOR, 2018).

On a regional scale, Numata et al. (2011) estimated a loss of between 126 and 221 Tg of carbon due to forest fragmentation for the Brazilian Amazon in the period from 2001 to 2013, Silva Junior (2020a) estimated 879 Tg of carbon lost in the Amazon Basin in the period from 2001 to 2015 and Pütz et al. (2014) estimated a loss of 599 Tg of carbon for the Amazon and 69 Tg for the Atlantic Forest for a period of 10 years.

On the tropical scale, Brinck et al. (2017) estimated a loss of 10.3 Gt of carbon (42% in America, 25% in Africa and 33% in Asia) due to fragmentation (loss of 50% of carbon in edges 100 m wide). This last work presents controversial results, the authors consider a loss of carbon stocks varying between 11 and 50% in forest edges with 100 m wide for the year 2000, however, it was not considered

that this loss occurs over time. As the forest edge ages, that is, it was assumed that all edges 100 m wide in the year 2000 lost up to 50% of their carbon stocks, although they are of different ages. This reinforces the need to improve the representativeness of the variability of tropical forests in these models, consequently improving the quantification of carbon stock losses due to fragmentation.

Although the impact of fragmentation on carbon stocks observed for the Amazon can be extrapolated to other tropical forests, investigations are still needed in representative regions of the tropics to improve the understanding of the impact of fragmentation on carbon stocks in this region. In addition, there are open scientific questions. The first concerns the extent to which carbon stocks are reduced at forest edges as a result of aging. The second is whether this range varies in different tropical regions. In addition, few of the works cited above have estimated the amount of lost carbon that goes into the atmosphere. The few that quantified it, only calculated the emission in the year in which the carbon stock was lost, disregarding the decomposition over time. Thus, efforts to fill these gaps are emerging.

## 2.2 The role of remote sensing in the quantification of forest fragmentation and its impacts on carbon stocks in the tropical region

Although field-scale studies have strongly contributed to the advancement of understanding of forest fragmentation and its impacts in recent decades, only sensing with its synoptic vision allows advances at the tropical scale. Below are the main remote sensing products at the tropical scale that can be used to quantify fragmentation, as well as methods developed to quantify carbon stocks using LiDAR (Light Detection And Ranging) data that can be used in forest fragmentation studies

### 2.2.1 Remote sensing products for quantification of forest fragmentation

The global mapping of forest cover is an important way to understand how forest changes affect the regional environmental and global climate balance, informing mitigation and adaptation strategies. Thus, in recent decades, efforts have been focused on the development of global sets of forest cover and change that are

reliable and consistent, as they are used, for example, as input in global circulation models, regional and global climate models, in dynamic modelling of the vegetation and its carbon stocks, among others (HIBBARD et al., 2010; HEROLD et al., 2011).

Forest cover data are the basis for forest fragmentation studies. Thus, a robust and consistent quantification of forest fragmentation and the modelling of its impact on forest carbon stocks largely depends on the chosen dataset. Technological advances in the computational field and the availability of Earth observation data in recent decades have allowed the development of various data sets on forest cover and dynamics, at different spatial and temporal scales. Table 2 summarizes some characteristics, advantages, and disadvantages of the main forest cover products available for the tropical region.

Table 2.2 - Main forest cover maps available for the tropical region. Spatial resolutions, temporal coverage, advantages, and disadvantages are presented.

| Dataset | Spatial Resolution (m) | Temporal Coverage | Advantages | Disadvantages |
|---|---|---|---|---|
| *GFC- Global Forest Change* (HANSEN et al., 2013) | 30 | 2000-2020 | High spatial resolution; Multitemporal; High temporal coverage. | May include forest fires; Includes planted forests; Includes secondary vegetation prior to 2000; Need to apply a tree cover percentage threshold. |
| *Roadless Project* (VANCUTSEM et al., 2021) | 30 | 1982-2020 | High temporal resolution; Multitemporal; Very high temporal coverage; Areas of forests already defined; Separates deforestation from degradation (selective logging and fire). | - |
| *ESA CCI Land Cover* (ESA - EUROPEAN SPACE AGENCY, 2017) | 300 | 1992-2015 | Multitemporal; Very high temporal coverage; Areas of forests already defined; Forest cover sorted by type. | Low spatial resolution; Includes secondary growth forest. |
| *MODIS Land Cover Type Product* (MCD12Q1) (FRIEDL; SULLA-MENASHE, 2019) | 500 | 2001-2021 | Multitemporal; High temporal resolution; Areas of forests already defined. | Low spatial resolution; Includes secondary growth forest. |
| *Landsat Tree Cover Continuous Fields* (SEXTON et al., 2013) | 30 | 2000 | High spatial resolution. | Fixed in time; Need for auxiliary data on forest cover loss; Includes secondary vegetation prior to 2000; Need to apply a tree cover percentage threshold; |
| *Primary Humid Tropical Forests* (TURUBANOVA et al., 2018) | 30 | 2001 | High spatial resolution; Areas of forests already defined. | Fixed in time; Need for auxiliary data on forest cover loss. |
| *Global PALSAR-2/PALSAR Forest/Non-Forest Map* (SHIMADA et al., 2014) | 25 | 2007-2017 | High spatial resolution; Areas of forests already defined. | Low temporal coverage; Includes secondary vegetation prior to 2007. |
| *Global TanDEM-X forest map* (MARTONE et al., 2018) | 50 | 2011-2017 (Temporal Mosaic) | High spatial resolution; Areas of forests already defined | Fixed in time; Need for auxiliary data on forest cover loss; Mapping based on multiple years (2011-2017); Includes secondary vegetation prior to 2011. |

Of the eight forest cover mappings in Table 2.2, two are based on RADAR data (SHIMADA et al., 2014; MARTONE et al., 2018) and six on optical data. The spatial resolution of the mappings ranged from 25 m to 500 m, with 50% with a resolution of 30 m (based on Landsat data). Two of the mappings have coarser spatial resolution (ESA - EUROPEAN SPACE AGENCY, 2017; FRIEDL; SULLA-MENASHE, 2019), the *ESA CCI Land Cover* with 300 m, based on MERIS data - *Medium Resolution Imaging Spectrometer* and the MODIS MCD12Q1 with 500 m, based on MODIS data - *Moderate-Resolution Imaging Spectroradiometer*. Only two mappings have very high temporal coverage (VANCUTSEM; FRÉDÉRIC, 2016; ESA - EUROPEAN SPACE AGENCY, 2017), although the *ESA CCI Land Cover* is limited by its coarse spatial resolution (300m). Three of the mappings are fixed in time (SEXTON et al., 2013; MARTONE et al., 2018; TURUBANOVA et al., 2018), and auxiliary forest cover loss data is needed to build multitemporal maps. Most of the mappings have the forest classes already defined, while two of the mappings (HANSEN et al., 2013; SEXTON et al., 2013) require the application of a threshold to define forest areas. In addition, the *ESA CCI Land Cover* mapping, for example, maps areas of secondary growth forest, which makes temporal studies with forest edges difficult, as these end up disappearing with the mapping of secondary growth areas.

The accuracy of these mappings varies according to the scale evaluated (global and regional). In addition, different methods were used to validate these products, which makes comparisons difficult. Validations aimed at the tropical region are still necessary, with a view to applications in forest fragmentation. On the other hand, the *GFC* mapping (HANSEN et al., 2013) and the Roadless Project (VANCUTSEM et al., 2021) certainly present the best characteristics for applications in forest fragmentation in the tropical region, considering their spatial resolution, temporal coverage and as there is still no consensus on a final forest cover and change product for the tropical region.

## 2.3 Use of LiDAR for estimating carbon stocks in tropical forests

### 2.3.1 LiDAR as a remote sensing system

Categorized as an active remote sensing technology, LiDAR (Light Detection And Ranging) includes land, air and orbital platforms. The system works by emitting laser beams towards the earth's surface, operating in the visible to infrared range of the electromagnetic spectrum. The emitted beam interacts with surface objects, where part of the radiation is reflected, returning, and being registered by the sensor.

From the strength of the return signal, it is possible to obtain information about the targets on the surface. However, the most useful information for forestry applications is the return time of each pulse, which allows the calculation of the distance between the surface targets and the sensor (LARGE; HERITAGE, 2009), and consequently the altitude, latitude, and longitude of each return. The distance between the target and the sensor is calculated by the relationship: $(c \times t)/2$, where $c$ is the speed of light and $t$ is the time between emission and registration of the laser pulse in the sensor.

From the registration of the direction of the laser beam, information from the differential GPS (Global Positioning System) and from the INS (Inertial Measurement Unit; records the rolling, pitching and yaw) on board the platform, allow obtaining three-dimensional coordinates (3-D) of every point on the Earth's surface (WEHR; LOHR, 1999; REUTEBUCH; ANDERSEN; MCGAUGHEY, 2005; LARGE; HERITAGE, 2009; HASSEBO, 2012; CHEN, 2014) (Figure 2.6).

Figure 2.6 – Principles and components of an Airborne LiDAR System. The double dashed arrows represent the communication between the GPS equipment (ground station and on board the plane) and the satellite constellation.

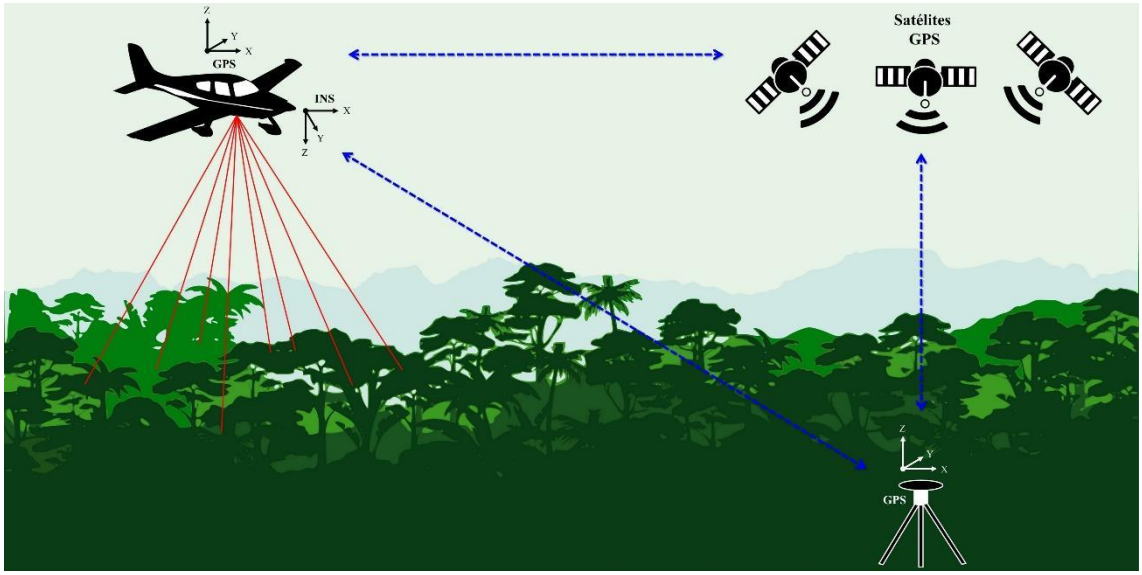


The recording of the return signal can occur in two ways: by discrete pulse or continuous wave (full waveform) (Figure 2.7). In discrete return (cloud of points, commonly used in forestry applications), each point contains information with 3-D coordinates (latitude, longitude, and altitude), the signal strength and the type of return (first, last or intermediate). On the other hand, in continuous feedback, the distribution of the entire feedback signal is recorded according to the time or distance of the feedback (GIONGO et al., 2010).

Figure 2.7 - Return signal recording in airborne LiDAR Systems.

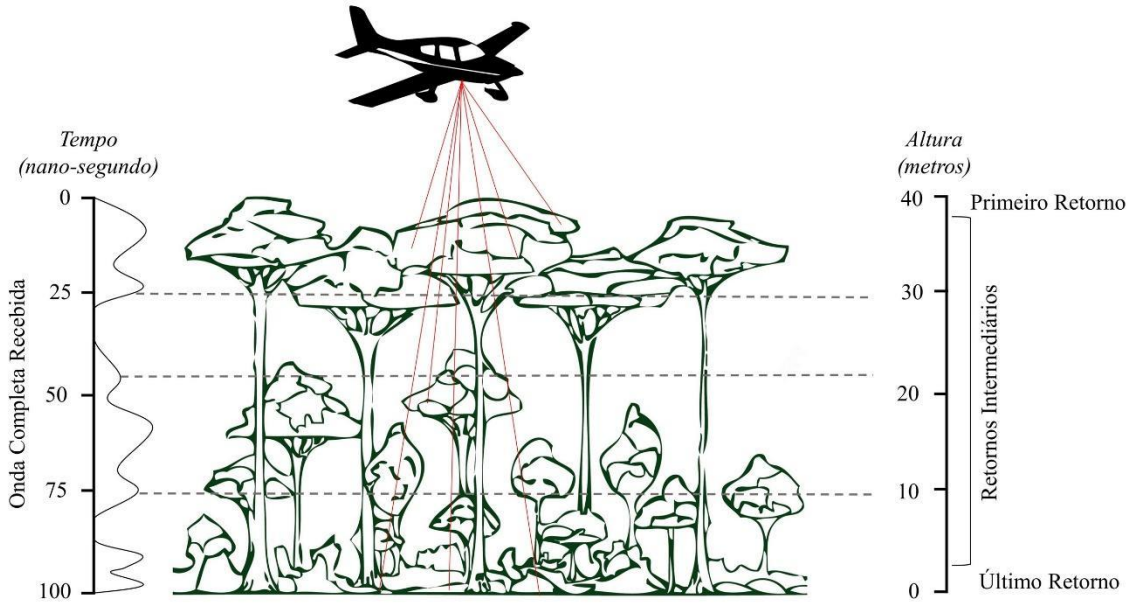


The first pulses that interact with the surface and return to the sensor (first returns) contain the signal that reaches the top of the forest canopy. The next set of pulses represents the return of leaves and branches from the vegetation. As the laser beam travels through the forest canopy, understory data is obtained. The last returns correspond to the terrain, the latter used to create the digital terrain models (GIONGO et al., 2010).

### 2.3.2 Estimation of forest carbon stocks using LiDAR

The estimation of forest carbon stocks plays an important role in studies of the carbon cycle in tropical forests, given the growing concern about the increase in anthropogenic carbon emissions into the atmosphere. Methodologies for estimating forest biomass are an important tool for mitigation mechanisms such as REDD - Reducing Emissions from Deforestation and Forest Degradation (SINHA et al., 2015).

Traditionally, there are two basic methods for estimating forest carbon, the direct and the indirect. The direct method is characterized by clearing the vegetation, weighing the entire mass, and later estimating forest carbon, while the indirect method uses allometric equations to estimate forest carbon.

Direct methods limit the collection of forest carbon in large areas, such as tropical forests, as it is an expensive and slow process. However, indirect measurements

of forest carbon using remote sensing data have become a viable option in large-scale applications (LE MAIRE et al., 2011). One result of these applications is the currently available forest carbon maps for the tropical region (Table 3).

Table 2.3 - Main forest carbon maps available for the tropical region and their respective characteristics.

| Map | Extension | Base year | Spatial resolution (m) | Reference |
|---|---|---|---|---|
| Saatchi Map | Pantropical | 2000 | 1,000 | (SAATCHI et al., 2011) |
| Baccini 500 Map | Pantropical | 2007-2008 | 500 | (SAATCHI et al., 2011) |
| Baccini 30 Map | Global | 2000 | 30 | (BACCINI et al., 2012; GFW - GLOBAL FOREST WATCH, 2019) |
| Avitabile Map | Pantropical | ~2000 | 1,000 | (AVITABILE et al., 2016) |
| Ruesch & Gibbs Map | Global | 2000 | 1,000 | (RUESCH; GIBBS, 2008) |
| Hu Map | Global | 2000-2004 | 1,000 | (HU et al., 2016) |
| ESA Biomass Climate Change Initiative | Global | 2010, 2017 and 2018 | 100 | (SANTORO; CARTUS, 2021) |

Although useful, these maps have uncertainties propagated from the acquisition of field data (used for calibration) to the method used to extrapolate forest carbon estimates. So, in general, each map comes with an uncertainty map so that users can assess inherent errors. It is important to highlight that the maps presented in Table 3 are centred on the year 2000, which makes it impossible to carry out studies with time series prior to that year, thus making efforts to build forest carbon maps centred on the 20th century.

Although the forest carbon maps mentioned above are useful for several studies, they are fixed in time and generalist, which limits applications that require multitemporal data and with a good ability to detect the local variability of forest carbon. An emerging alternative is the estimation of forest carbon using LiDAR - Light Detection And Ranging airborne data.

Estimates of carbon stocks via LiDAR can be performed by the area-based method or by the method based on individualization of trees (CHEN, 2014), with the use of the former being the most suitable for tropical forests. The use of the

method based on individualization of trees is still less accurate compared to the method based on area due to the complexity of tropical tree shapes and understory vegetation, which makes it difficult to separate a particular tree in the LiDAR point cloud (COOMES et al., 2017). However, these limitations can be addressed with advances in individualizing trees based on terrestrial LiDAR data (BURT; DISNEY; CALDERS, 2018; GONZALEZ DE TANAGO et al., 2018; PEREIRA et al., 2019).

Table 4 shows the main area-based methodologies developed to estimate carbon stocks from LiDAR data in the tropical region.

Table 2.4 - Methods for estimating carbon stocks from LiDAR data available for the tropical region.

| Reference | Type | Spatial resolution (m) | Equation |
|---|---|---|---|
| Asner et al. (2010) | Regional (Peru) | 30 | Equation: $AGC = 0.3531 * MCH^{1,9252}$. Where *AGC* is carbon above ground and *MCH* is the average height of the canopy profile. The equation has $R^2$ = 0.85 and RMSE not evaluated. |
| Mascaro et al. (2011) | Regional (Panama) | 60 | Equation: $ACD = 1.4110 * MCH^{1,4126}$. Where *ACD* is the above-ground carbon density and *MCH* is the average height of the canopy profile. The equation has $R^2$ = 0.85 and RMSE = 16.6 Mg C $ha^{-1}$. |
| Asner et al. (2012) | Universal | 60 | Equation: $ACD = 2.04 * MCH^{0,436} * BA^{0,946} * WD^{0,912}$. Where ACD is the aboveground carbon density, MCH is the average height of the canopy profile, BA is the regional basal area, and WD is the regional wood density. The equation has $R^2$ = 0.80 and RMSE = 27.6 Mg C $ha^{-1}$. |
| Asner e Mascaro (2014) | Universal | 100 | Equation: $ACD = 3.8358 * TCH^{0,2807} * BA^{0,9721} * \rho_{BA}^{1,3763}$. Where *ACD* is the density of carbon above ground, *THC* is the average height of the top of the canopy, BA is the regional basal area and $\rho_{BA}$ is the wood density weighted by the basal area. The equation has $R^2$ = 0.92 and RMSE = 17.1 Mg C $ha^{-1}$. |
| Longo et al. (2016) | Regional (Brazil; Amazon Biome) | 50 | Longo et al. (2016) developed two equations: (1) $ACD = 0.20 * \underline{h} * k_h^{0,66} * h_5^{0,11} * h_{10}^{-0,32} * h_{IQ}^{0,50} * h_{100}^{-0,82}$ (2) $ACD = 0.025 * TCH^{1,99}$. Where *ACD* is the aboveground carbon density, $\underline{h}$ is the average height of returns, $k_h$ is the kurtosis of the distribution of all heights of returns, $h_5$ and $h_{10}$ are the percentiles 5 and 10 from all heights of returns, $h_{IQ}$ is the interquartile range, $h_{100}$ is the maximum height and *TCH* is the average height of the top of the canopy. The first equation has $R^2$ = 0.70 and RMSE = 41.7 Mg C $ha^{-1}$, while the second has $R^2$ = 0.68 and RMSE = 43.3 Mg C $ha^{-1}$. |
| Xu et al. (2017) | Regional (Democratic Republic of Congo) | 100 | Xu et al. (2017) developed two equations: (1) $AGB = 1.88 * MCH^{1,55}$ and (2) $AGB = 10.43 * (MCH * WD)^{1,19}$. Where *AGB* is the above-ground biomass, *MCH* is the average canopy height and *WD* is the density of wood. The first equation has $R^2$ = 0.76 and RMSE = 60.33 Mg $ha^{-1}$ (30.17 Mg C $ha^{-1}$), while the second has $R^2$ = 0.82 and RMSE = 51.43 Mg $ha^{-1}$ (25.72 Mg C $ha^{-1}$). |
| Ferraz et al. (2018) | Regional (Indonesia) | 50 | Equation: $AGB = 0.03 * MCH^{2,65}$. Where *AGB* is the above-ground biomass, *MCH* is the average canopy height. The equation has $R^2$ = 0.81 and RMSE = 62.21 Mg $ha^{-1}$ (31.11 Mg C $ha^{-1}$). |
| Jucker et al. (2018) | Regional (Borneo) | 100 | Equation: $ACD = 0.567 * TCH^{0,554} * BA^{1,081} * WD^{0,186}$. Where *ACD* is the density of carbon above ground, *THC* is the average height of the top of the canopy, BA is the basal area and *WD* is the density of wood. The equation has RMSE = 19 Mg C $ha^{-1}$ and $R^2$ not evaluated. |
| Becknell et al. (2018) | Regional (Brazil; Atlantic Forest Biome) | 50 | Equation: $AGB = \frac{590,2}{1+e^{-0,202*(P95-23,24)}}$. Where *AGB* is the above-ground biomass and *P95* is the 95th percentile of canopy height. The equation has $R^2$ not evaluated and RMSE = 44.85 Mg $ha^{-1}$ (22.42 Mg C $ha^{-1}$). |

The use and development of methods for estimating forest carbon by LiDAR has grown in recent decades in the tropical region (Table 2.4). Asner et al. (2010), for example, developed an equation to estimate carbon stocks using LiDAR data for the Peruvian Amazon, supporting calculations of carbon emissions from deforestation and forest degradation. On the other hand, Becknell et al. (2018) developed an equation to estimate aboveground biomass via LiDAR, supporting the analysis of the distribution of this variable in secondary growth forests in the Brazilian Atlantic Forest.

Of the equations compiled in Table 2.4, two are universal, that is, they were calibrated using data from different continents, and eight are local, covering the American, African, and Asian continents. The pixel size in which the equation is applied varied between 30 m and 100 m, which is defined by the size of the field plots used to calibrate the models. In addition, there is a consensus in the literature that as the model pixel size increases, the uncertainties associated with carbon estimation progressively reduce (ASNER et al., 2010; ZOLKOS; GOETZ; DUBAYAH, 2013; MAUYA et al., 2015), that is, although a finer resolution is necessary for some applications, it is also necessary to consider the inherent uncertainties in the estimates.

Of the nine equations in Table 4, eight follow the power law, expressed as $y = a * x^b * ... z^c$, while only the equation developed by Becknell et al. (2018) follows a sigmoid-like function. In general, the equations used simple metrics based on canopy height. However, some equations (ASNER et al., 2012; ASNER; MASCARO, 2014; XU et al., 2017; JUCKER et al., 2018) used regional variables such as basal area and wood density to improve estimates. Although generated at low computational cost, LiDAR metrics based on canopy height tend to saturate in areas of high biomass, since in these regions, at a certain point of forest development, the accumulation of biomass is no longer accompanied by an increase in the canopy height of the vegetation. Equation 1, developed by Longo et al. (2016), for example, uses LiDAR metrics that consider different strata of the forest, which reduce problems with saturation in the estimates, although the metrics have a higher computational cost to generate. Thus, it is up to the user to consider, based on its application, the best equation to be used.

In general, the universal equations had an average $R^2$ of 0.86±0.06 (n=2), while the regional equations had an average $R^2$ of 0.78±0.06 (n=7). At the same time, the universal equations had a mean RMSE (Root Mean Square Error) of 22.35±5.25 Tg C $ha^{-1}$ (n=2) and the regional ones an average of 28.75±9.21 Tg C $ha^{-1}$ (n=8). The better explanatory power of biomass through LiDAR variables and the lower uncertainty associated with the universal equations can be explained by the larger sampling compared to the regional equations.

Finally, it is important to highlight the contribution of LiDAR instruments on board orbital platforms for forest carbon estimates. The first device of this kind, the *Geoscience Laser Altimeter System* (GLAS) on board the satellite *Ice, Cloud, and Land Elevation Satellite* (ICESat), was operational from 2003 to 2009 and carried out an unprecedented data collection. These data were combined with other satellite-derived data to produce continuous biomass maps (DUNCANSON; NIEMANN; WULDER, 2010; SAATCHI et al., 2011; MITCHARD et al., 2012). In 2018, the sensor LiDAR GEDI (*Global Ecosystem Dynamics Investigation*) was launched (STYSLEY et al., 2015) which is on board the International Space Station (ISS) (STAVROS et al., 2017). GEDI, among other products, will provide aboveground biomass data with spatial resolution ranging from 25 m to 1 km (SILVA et al., 2018a; HANCOCK et al., 2019).

# 3 DEFORESTATION-INDUCED FRAGMENTATION INCREASES FOREST FIRE OCCURRENCE IN CENTRAL BRAZILIAN AMAZONIA[3]

## 3.1 Introduction

Tropical forests are globally important reservoirs of carbon (C) and biodiversity (BONAN, 2008; BACCINI et al., 2012; SULLIVAN et al., 2017). Vegetation in this region stores between 350-600 Pg C (HOUGHTON; HALL; GOETZ, 2009; PAN et al., 2011; SAATCHI et al., 2011; BACCINI et al., 2012; CIAIS et al., 2013), while the atmosphere stores about 750 Pg C (GRACE, 2004). The loss of these C stocks due to deforestation and forest degradation is estimated to be approximately 1.1 Pg C $year^{-1}$ (MALHI, 2010; HOUGHTON et al., 2012; GRACE; MITCHARD; GLOOR, 2014). Amazonia, specifically, is home to more than half of the world's remaining rainforest areas (CAPOBIANCO, 2001). However, in the Brazilian Amazonia, intense land-use and land-cover changes and forest degradation threaten the forest structure, biodiversity, and ecological functions (COE et al., 2013).

The intense occupation of Brazilian Amazonia from the 70s (FEARNSIDE, 2005) aiming to expand agricultural and livestock activities and to increase the wood supply, besides a general lack of enforcement of environmental laws, caused the dramatic increase of deforestation rates, reaching a peak of 27,772 $km^2$ in 2004 (NEPSTAD et al., 2014; INSTITUTO NACIONAL DE PESQUISAS ESPACIAIS (INPE), 2017). After 2005, a steep decrease in deforestation rates was observed, which can be attributed to a combination of factors including governmental enforcement of environmental laws, restrictions on access to credit, expansion of protected areas, and civil society interventions in the soy and beef supply chains (NEPSTAD et al., 2014). Nonetheless, the deforestation rate increased markedly in 2015 and 2016 (INSTITUTO NACIONAL DE PESQUISAS ESPACIAIS (INPE),

[3] This chapter is an adapted version of the published paper: SILVA JUNIOR, C. H. L. et al. Deforestation-induced fragmentation increases forest fire occurrence in central Brazilian Amazonia. **Forests**, v. 9, n. 6, p. 305, 2018.

2017) (24% and 27% in relation to the previous year respectively), raising concerns that the recent weakening of environmental-protection policies could be already reversing the Brazilian progress in reducing the Amazonian Forest destruction.

Whether at a slower or faster pace, continued deforestation cumulatively causes forest habitat loss, altering habitat configuration such as the change in spatial arrangement of the remaining habitat through forest fragmentation. Metrics of habitat configuration, such as the number and mean size of forest patches and edge length covary with habitat amount. Understanding these relationships is important to correctly interpret the effects of habitat fragmentation on tropical forests (VILLARD; METZGER, 2014). Following Farhig (2003) (2003) the mean patch size of remaining forests is expected to decrease linearly with the reduction in habitat amount while both the number of patches and the total edge are expected to rise up to a certain threshold of habitat loss and then decrease with increasing deforestation.

Forest edges resulting from landscape fragmentation are highly fire-prone due to increased dryness, higher fuel load compared to forest interior and proximity to ignition sources from adjacent management areas (COCHRANE, 2001; LAURANCE; WILLIAMSON, 2001; COCHRANE; LAURANCE, 2002; ALENCAR; SOLÓRZANO; NEPSTAD, 2004; ARAGÃO; SHIMABUKURO, 2010; CANO-CRESPO et al., 2015). Fragmentation and its resulting edge effects may act synergistically with the ongoing large-scale changes in climate and fire regimes, threatening the Amazonian Forest ecological integrity (ARAGÃO et al., 2007; COE et al., 2013).

Much of the literature on the effects of habitat loss and changes in habitat configuration has focused on biodiversity maintenance and population persistence. Studies concerning the effect of habitat loss and configuration on forest fires incidence and intensity at the landscape scale are rare in the Brazilian Amazonia, especially in active deforestation frontiers, where the interactions between deforestation, forest fragmentation and fire are evident. In other regions of the Amazon Basin, some authors have demonstrated a positive response of

fire incidence and intensity to increased fragmentation and forest edges in the landscape (COCHRANE, 2001; COCHRANE; LAURANCE, 2002; ALENCAR; SOLÓRZANO; NEPSTAD, 2004; ARMENTERAS; GONZÁLEZ; RETANA, 2013; ARMENTERAS et al., 2017).

In Brazil, the Forest Code (Federal Law 12.727/2012) is the main national law regulating the conservation of forests within private properties (BRASIL, 2012). This law determines that, within the Amazon Biome, at least 80% of each rural property should not be deforested to ensure the sustainable use of natural resources, assisting in the conservation and rehabilitation of ecological processes, promoting the conservation of biodiversity, as well as the shelter and protection of wildlife and native flora. The question of whether such a high level of habitat maintenance is necessary to reduce fire incidence in the region, however, has not been directly addressed yet.

To fill this gap, we relate, for the first time, habitat configuration metrics with fire incidence and intensity in an active Brazilian Amazonia deforestation frontier, aiming to identify the relationships between forest fragmentation and fire on the landscape scale. To achieve this, we address the following question: What is the relationship between habitat loss and measures of habitat configuration, and their implications for fire incidence and intensity in a central Amazonian landscape?

### 3.2 Study area

Our study site was located in the northern region of Novo Progresso municipality, State of Pará, Central Brazilian Amazonia, with an area of 30,000 $km^2$ (3 x $10^6$ ha) (Figure 1), which corresponds approximately to the area of Belgium. This region is known as a frontier of deforestation because of high rates of deforestation in the last 10 years. The vegetation is predominantly composed of the Dense Ombrophilous Forest, with trees that can reach heights up to 50 meters (VIEIRA et al., 2004).

The initial occupation of this area was associated with governmental settlement projects and the construction of road infrastructure, mainly the construction of BR-163 highway (PINHEIRO et al., 2016). During the 70's and 80's, a

spontaneous colonization phenomenon occurred in the region, characterized by the occupation of land by small subsistence farmers and gold miners (PINHEIRO et al., 2016). There are three main deforestation patterns present in the study area (i) fishbone, associated with settlements, (ii) rectangular patches, related to large rural properties, and (iii) stem of the rose pattern associated with mining areas, mainly in BR-163 (ARIMA et al., 2015).

Figure 3.1 - Location map of the study area. On the main map, in green are the old-growth and secondary forest areas, in magenta the productive lands and in purple the burned areas. Composition of Landsat 8 images (OLI sensor) for the dry season of the year 2014 (Red-Shortwave Infrared 1; Green-Near Infrared; Blue-Red).

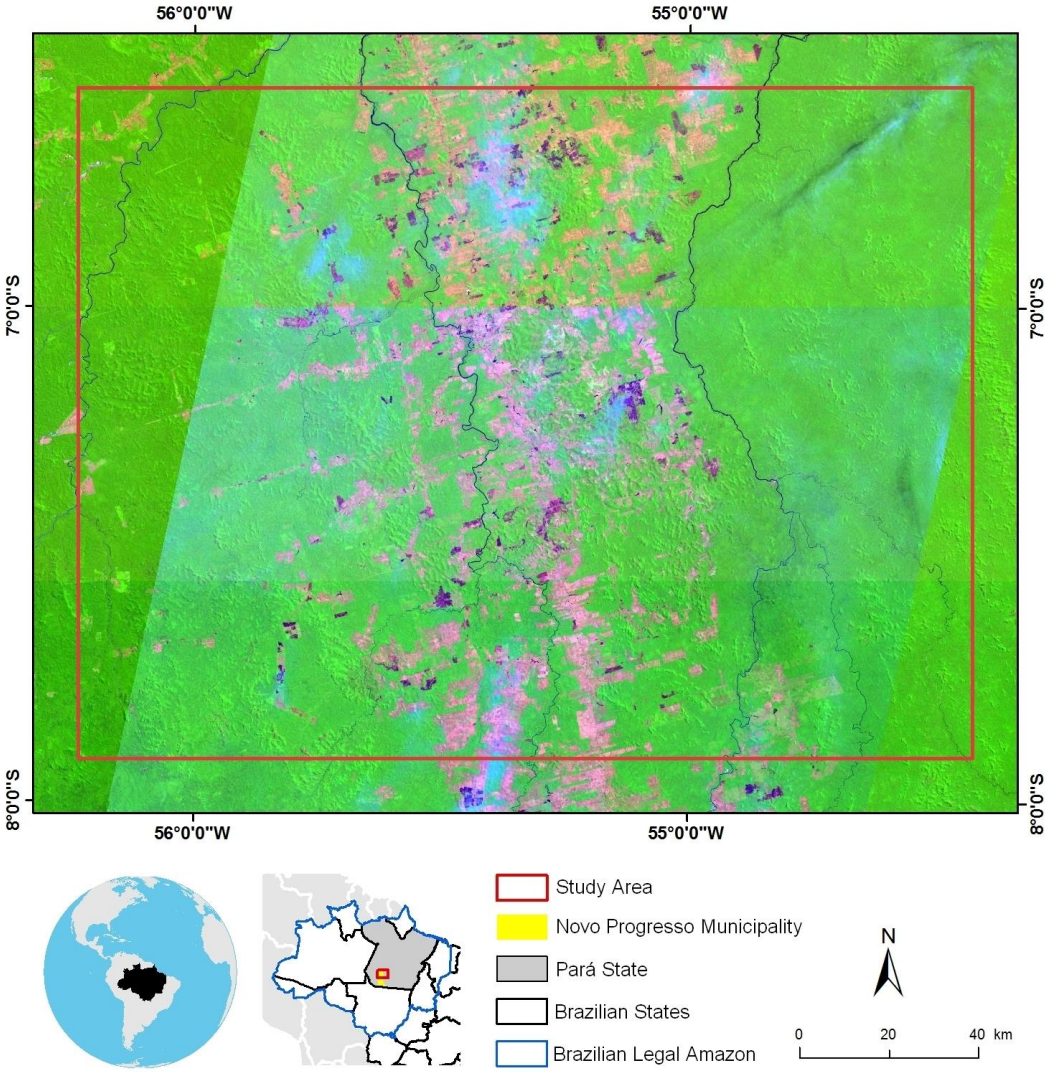

## 3.3 Datasets

### 3.3.1 Forest cover map

Land-use and land-cover data were obtained from the Amazonia Land-use Land-cover Monitoring Project (TerraClass Project/INPE) (ALMEIDA et al., 2016). We used data for the year 2014, which corresponds to the last year of available mapping.

The TerraClass Project data are the result of a combination of deforestation data from the Brazilian Amazonia Deforestation Monitoring Project (PRODES/INPE) (INSTITUTO NACIONAL DE PESQUISAS ESPACIAIS (INPE), 2017) and the land use classification based on orbital images from Landsat, Terra/Aqua and SPOT-5 satellites.

We regrouped the original classes of the TerraClass Project into two new classes: Forest Cover and Deforested Areas (Table 1). To eliminate natural edges in the analyses, we jointed the areas of Cerrado (Brazilian Savannas) and water bodies to the Forest Cover class.

Table 3.1 - Regroups of the original classes of the Amazonia Land-use Land-cover Monitoring Project (TerraClass Project) to obtain the forest cover map.

| Original classes | New classes |
|---|---|
| Forest, Secondary Forest, Cerrado (Brazilian Savanna) and Hydrography | Forest Cover |
| Annual Crops, Urban area, Deforestation in 2014, Mining, Mosaic of Uses, Others, Pasture with exposed soil, Herbaceous Pastures, Shrubby Pasture and Regeneration with Pasture | Deforested Areas |

### 3.3.2 Active fire data

Active fire data were obtained for the period between January and December 2014 from the Fire Information for Resource Management System (FIRMS). These data are derived from the MODIS Active Fire Product (MCD14ML, Collection 6) (GIGLIO; SCHROEDER; JUSTICE, 2016), adjusted to 1 km of

spatial resolution. To generate the product, a contextual algorithm compares the daily data of the medium and thermal infrared bands with reference data (without thermal anomalies). Subsequently, false detections are rejected by examining the brightness temperature of neighbouring pixels (GIGLIO et al., 2003).

Fire Radiative Power (FRP) values are considered an indicator of fire intensity (given in Megawatts or MW) and are commonly related to the amount of biomass consumed during the fire, where the higher the FRP value, the greater is the amount of biomass consumed (WOOSTER et al., 2005).

During 2014 the number of detected active fires (N = 35,873) in Pará State was near the average from 1999 to 2017 (n=32,602) (INSTITUTO NACIONAL DE PESQUISAS ESPACIAIS (INPE), 2018) and the year presented a normal climatology (Figure A1) (ARAGÃO et al., 2018).

Figure 3.2 – (a) Seasonal rainfall pattern (the vertical black lines are the standard deviations). (b) Normalized rainfall anomalies (1998-2014) calculated based on the methodology proposed by Aragão et al. (2007). Data extracted from product 3B43-v7 of the Tropical Rainfall Measuring Mission Satellite (TRMM).

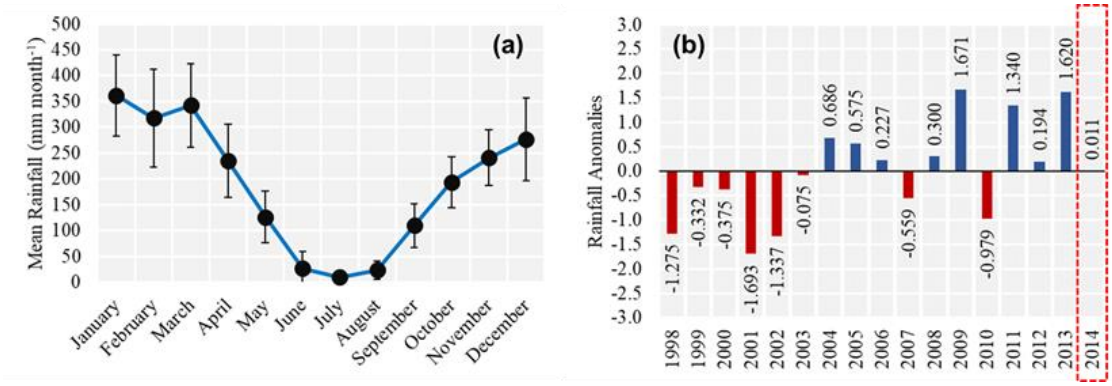


## 3.4 Methods

### 3.4.1 Landscape, fire incidence and fire intensity metrics

Firstly, we use the forest cover map to calculate landscape metrics using the LecoS plug-in (Landscape Ecology Statistics; version 2.0.7) (JUNG, 2016) implemented in the QGIS software (version 2.18 LTR) (QGIS DEVELOPMENT TEAM, 2017). These metrics and its modifications are commonly used in the literature for analysis related to forest fires (HAYES; ROBESON, 2011;

ARMENTERAS; GONZÁLEZ; RETANA, 2013) and are based on the Fragstats software (MCGARIGAL, 2015).

For our analysis, we used 300 grid cells of 10 km by 10 km. This spatial resolution captures satisfactorily the different patterns of fragmentation in our study area. According to Saito et al. (SAITO et al., 2011) the size of the cells does not statistically affect the results of the landscape metrics, and the user then chooses the size of the cells based on the phenomenon and scale analysed. The following metrics were adopted (Table 2): (1) Habitat Loss (percentage of deforestation), (2) Edges Proportion, (3) Number of Forest Patches, and (4) Mean Forest Patch Area.

Then, for each cell, two metrics were calculated for the active fire data. The first metric was the Fire Density (FD; as a proxy of fire incidence), which corresponds to the cumulative number of active fires in 2014 that occurred within forest areas in each cell divided by the total forest in that cell. The second metric was the FRP Mean (as a proxy of fire intensity), which was calculated by averaging the FRP values of active fires falling within the forest areas in each cell.

Table 3.2 – Landscape metrics used and their respective descriptions.

| Landscape metric | Abbreviation | Equation | Description |
|---|---|---|---|
| Habitat Loss | HL | $\frac{\sum_{j=1}^{n} a_{ij}}{A}(100)$ | The sum of all deforested areas within a cell, divided by total cell area, and multiplied by 100 (to convert to a percentage). The final unit is given in percentage (%). Where $a_{ij}$ is the area (km$^2$) of patch *ij*, and *A* is total cell area (km$^2$). |
| Edges Proportion | EP | $\frac{\sum_{k=1}^{n} e_{ik}}{\sum_{j=1}^{n} a_{ij}}$ | The sum of the lengths of all forest edge segments within a cell, divided by total area of all forest patches. The final unit is given in kilometres of edge per square kilometres of forest (km km$^{-2}$). Where $e_{ik}$ is the total length (km) of edge in patch *i*, and $a_{ij}$ is the area (km$^2$) of patch *ij*. |
| Number of Forest Patches | NFP | $n_i$ | The number of forest patches within a cell ($n_i$). |
| Mean Forest Patch Area | MFPA | $\frac{\sum_{j=1}^{n} a_{ij}}{n_i}$ | The mean area of all forest patches in each cell. The final unit is given in square kilometres (km$^2$). Where $a_{ij}$ is the area (km$^2$) of patch *ij*, and $n_i$ is the total of patches within a cell. |

### 3.4.2 Statistical analysis

To evaluate the relationship among the variables (Fire Density, FRP Mean, and landscape metrics), we fitted curves using LOESS Regression (Locally Weighted Scatterplot Smoothing – LOESS), which is a form of local regression model (CLEVELAND; GROSSE; SHYU, 1992; CLEVELAND; LOADER, 1996). This method is a non-parametric strategy for fitting a smooth curve to data, where noisy data values, sparse data points or weak interrelationships interfere with your ability to see a line of best fit (TATE et al., 2005). We used the span 0.75 (default setting) in LOESS Regression analyses.

In order to verify the existence of significant differences in the incidence and intensity of fire as a function of the landscape metrics, we used the Kruskal-Wallis non-parametric test. This test is equivalent to Analysis of Variance (ANOVA), which compares three or more groups to test the hypothesis that they have the

same distribution (HETTMANSPERGER; MCKEAN, 2010; GIBBONS; CHAKRABORTI, 2011; BONNINI et al., 2014). To identify how the analysed variables, differ, a paired posthoc test was performed. To perform the posthoc test, we use the Fisher's least significant difference criterion with Bonferroni adjustment methods correction (CONOVER, 1999a). For all tests, the significance level of 95% (p-value < 0.05) was adopted.

We use the R software (version 3.4.4) for all analysis (R CORE TEAM, 2018). For LOESS Regression, we use the "loess" native function (RIPLEY, 2018). In the Kruskal-Wallis test, we use the "agricolae" package (MENDIBURU, 2017).

We also separated and quantified active fires and the respective FRP values at three edge distances (1, 2 and greater than 2-km), both within forest areas (hereafter referred as edge of forest cover) and out of forest areas (hereafter referred as edge of deforested areas). Additionally, we calculated the percentage of active fires per FRP intervals, as suggested by Armenteras et al. (2013): $\leq$50 MW, 50 to $\leq$ 500 MW, 500 to $\leq$ 1000 MW and > 1000 MW.

## 3.5 Results

### 3.5.1 Relationship between habitat loss and measures of habitat configuration

Our results showed that the analysed landscape metrics exhibited different relationships with habitat loss (HL; Figure 2). The number of forest patches (NFP), as well as its variance, increases with HL until it reaches 70%, the maximum level of deforestation within a grid cell found in the study area (Figure 2a). The mean forest patch area (MFPA) decreases sharply between 0 and 10% of HL and continues to decrease smoothly from about 10% to 70% of HL, with a lower variance in the larger HL values (Figure 2b). Similarly, to NFP, EP and its variance increase with HL, mostly from 20% of HL onwards (Figure 2c).

Figure 3.3– Landscape metrics as a function of Habitat Loss (HL): (a) relationship between Habitat Loss and Number of Forest Patches (NFP); (b) relationship between Habitat Loss and Mean of Forest Patches Areas (MFPA); (c) relationship between Habitat Loss and Edges Proportion (EP). Shaded areas represent 95% confidence intervals.

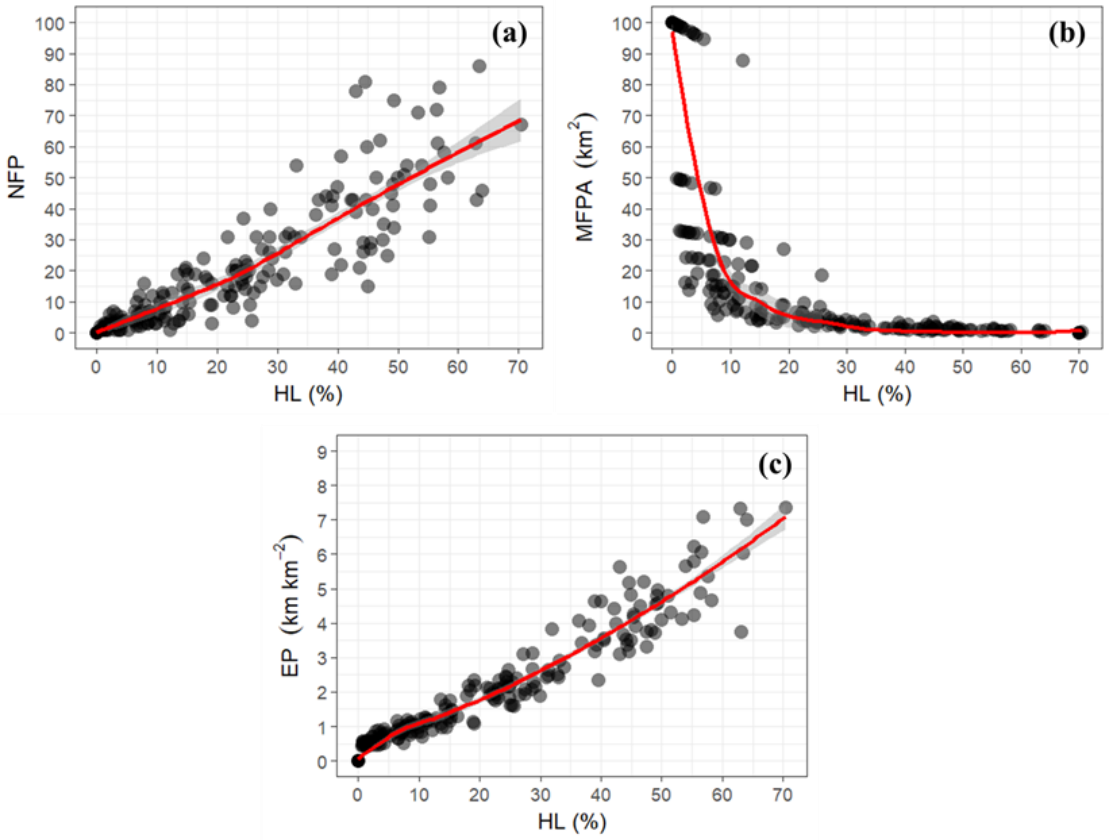


The Kruskal-Wallis test showed that the NFP (KW = 196.04; p-value < 0.05; Figure S2a) and the EP (KW = 205.07; p-value < 0.05; FigureS2c) were significantly lower only in the interval between 0-20% of HL, while the MFPA (KW = 201.38; p-value < 0.05; FigureS2b) was significantly higher in the same interval.

Figure 3.4 – Boxplot of the habitat loss (HL) intervals for the number of forest patches (a; NFP), mean of forest patches areas (b; MFPA) and edges proportion (c; EP). The letters represent the groups resulting from the Kruskal-Wallis post-hoc test. For all analyses, a significance level of 95% (p-value < 0.05) was adopted.

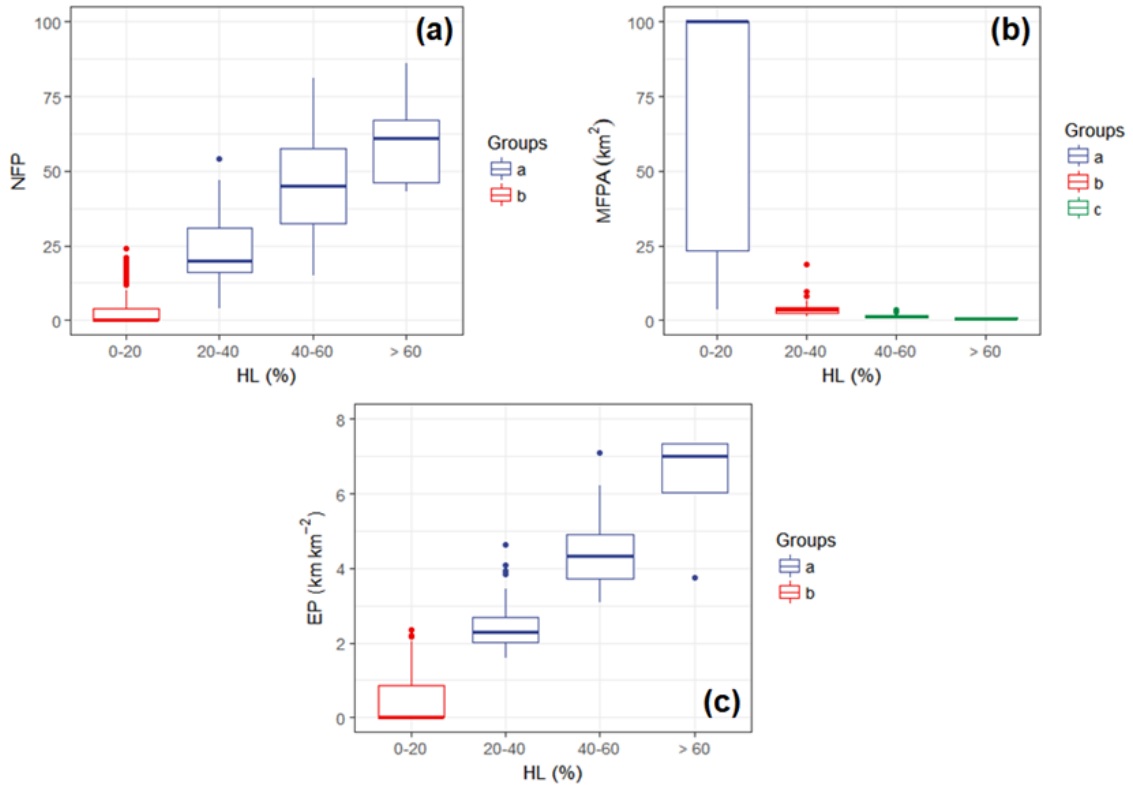


### 3.5.2 Relationship between habitat configuration and fire incidence and intensity

Fire density (FD) increased with HL, with greater variability in the higher levels of deforestation (Figure 3a). Furthermore, the FD increased until NFP reaches ~35 per grid cell, and then stabilized (Figure 3b). The FD decreased sharply up to 25 $km^2$ of MFPA, tending to zero after that. On the other hand, the FD increased up to 5 km $km^{-2}$ of EP, after which it plateaus.

Figure 3.5 – Fire Density (FD) as a function of (a) Habitat Loss (HL); (b) Number of Forest Patches (NFP); (c) Mean Forest Patches areas (MFPA) and (d) Edges Proportion (EP). Shaded areas represent 95% confidence intervals. The missing confidence intervals in some regions of the graphs are the result of the dispersion in the data at the upper end of the distribution.

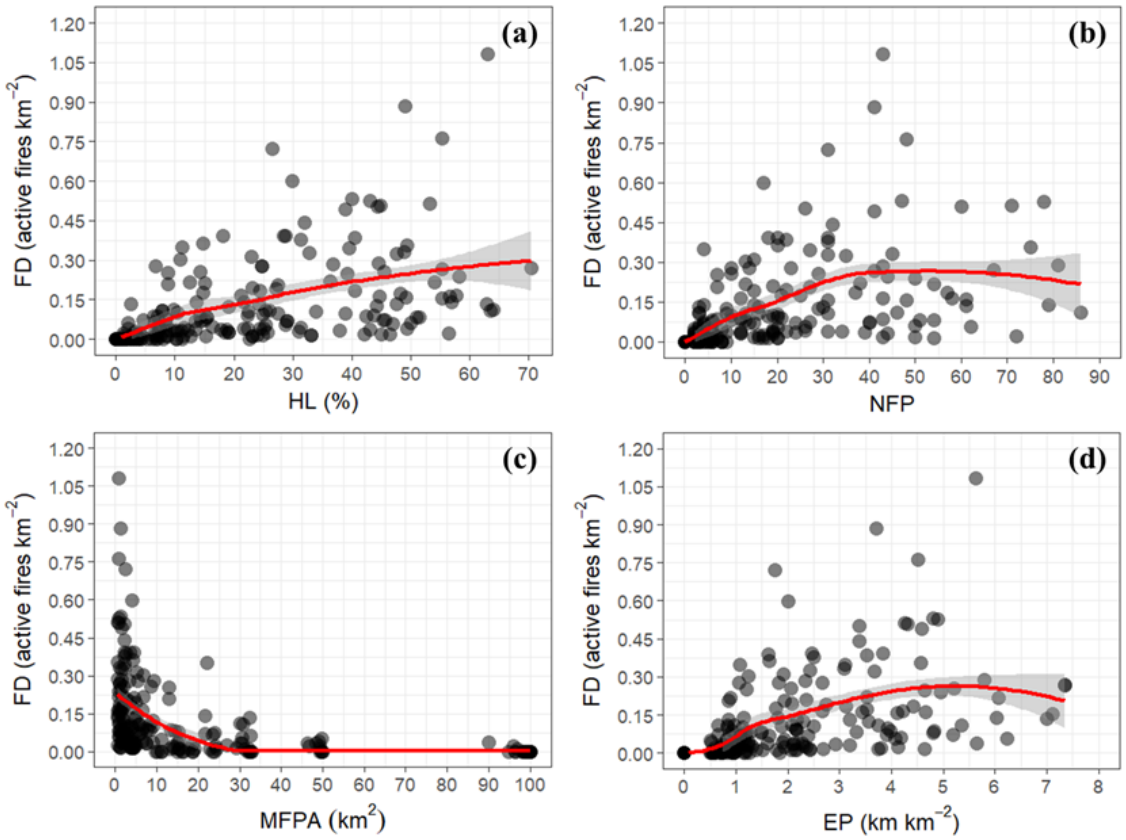


The Kruskal-Wallis test showed that FD was significantly lower only in the interval between 0-10% of the HL (KW = 191.76; p-value < 0.05; Figure S3a), between 0-10 NFP (KW = 180.68; p-value < 0.05; FigureS3b), between 90-100 km$^2$ of MFPA (KW = 224.86; p-value < 0.05; FigureS3c) and finally between 0-1 km km$^{-2}$ of EP (KW = 166.82; p-value < 0.05; FigureS3d).

Figure 3.6 – Boxplot of the fire density for the habitat loss intervals (a; HL), number of forest patches (b; NFP), mean of forest patches areas (c; MFPA) and edges proportion (d; EP). The letters represent the groups resulting from the Kruskal-Wallis post-hoc test. For all analyses, a significance level of 95% ($p<0.05$) was adopted

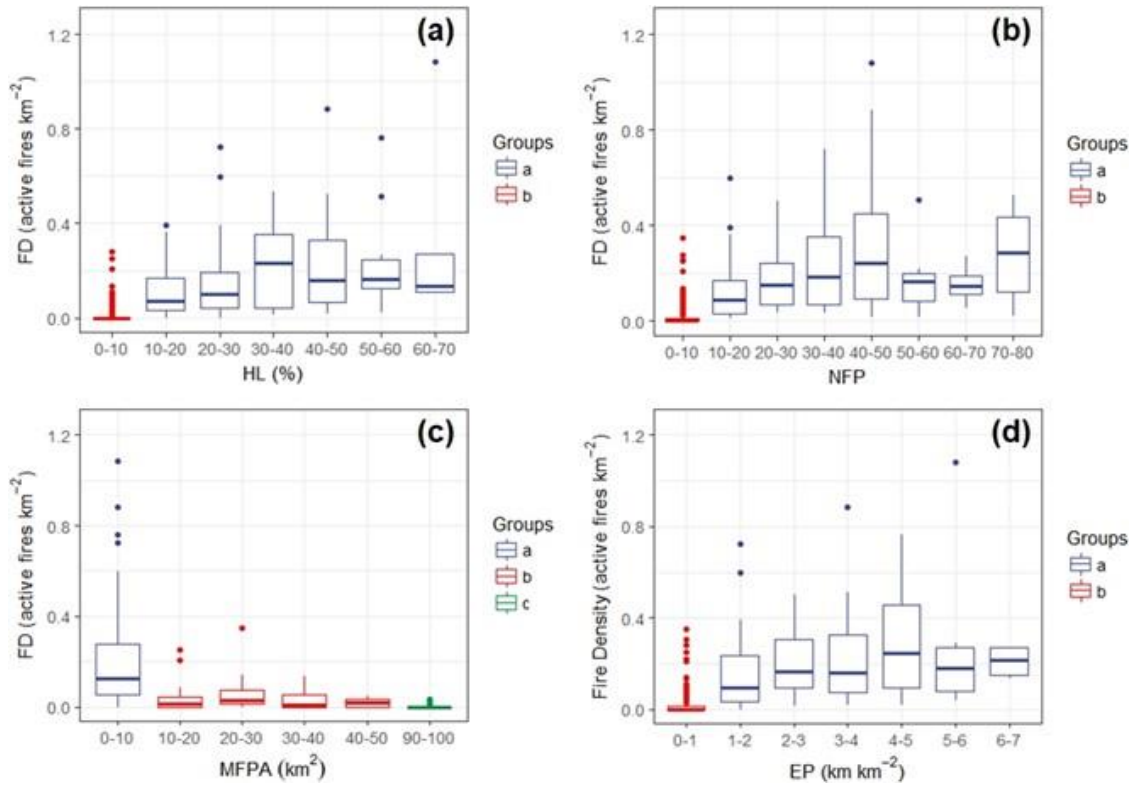


The fragmentation effect on the fire intensity, as measured by the Mean FRP, is presented in Figure 4. The Mean FRP increased until ~35% of HL and then decreased until the higher registered levels of HL (Figure 4a). The Mean FRP increased with the increase in the NFP up to 25 but decreased smoothly from about 25 to 80 forest patches (Figure 4b). A tendency of decrease in the Mean FRP was registered as the MFPA increases up to 50 km$^2$. On the other hand, the Mean FRP increased with the increase of the EP up to 3 km km$^{-2}$, with a subsequent decrease up to 7.5 km km$^{-2}$.

Figure 3.7 – Mean FRP as a function of (a) Habitat Loss; (b) Number of Forest Patches (NFP); (c) Mean of Forest Patches Areas (MFPA) and (d) Edges Proportion (EP). Shaded areas represent 95% confidence intervals. The missing confidence intervals in some regions of the graphs are the result of the dispersion in the data at the upper end of the distribution.

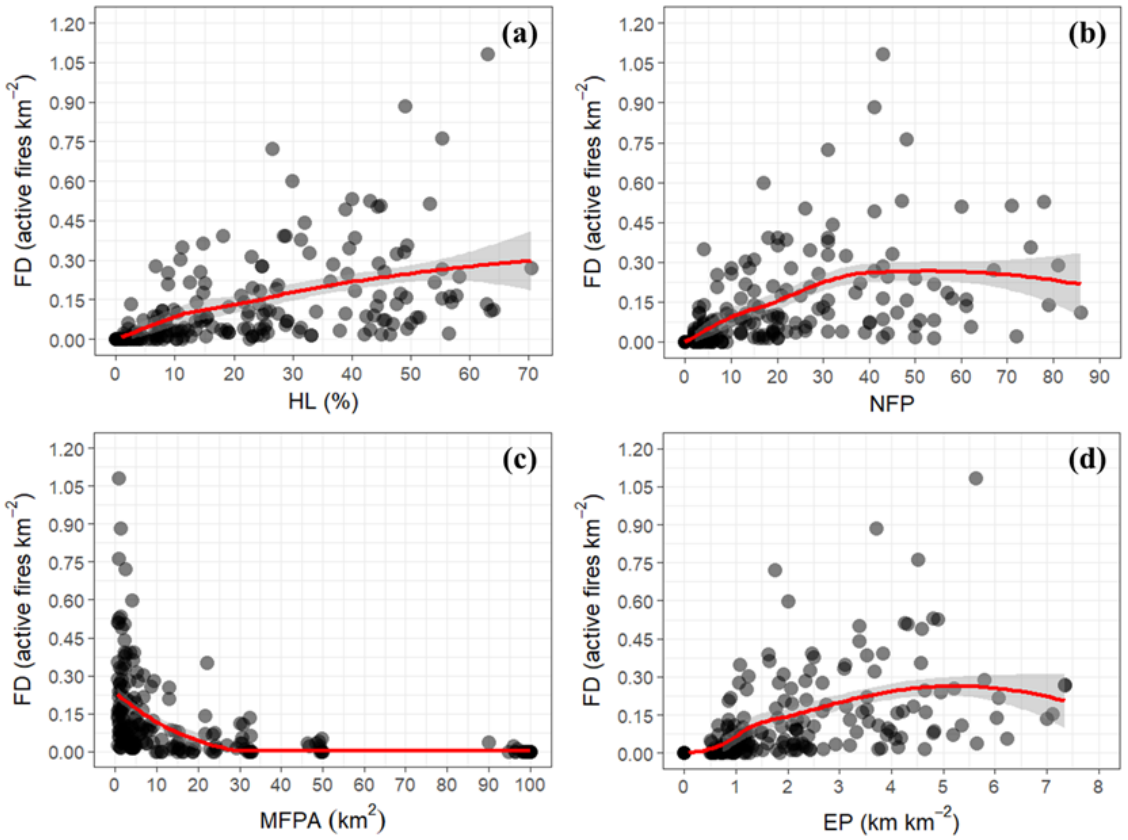


The Kruskal-Wallis test indicated that forest fire intensity (measured as mean FRP) was significantly lower at the lowest levels of fragmentation: 0-10% of HL (KW = 162.90; p-value < 0.05; FigureS4a), between 0-10 NFP (KW = 145.49; p-value < 0.05; FigureS4b), between 90-100 km$^2$ of MFPA (KW = 204.28; p-value < 0.05; FigureS4c) and between 0-1 km km$^{-2}$ of EP (KW = 121.89; p-value < 0.05; FigureS4d).

Figure 3.8 – Boxplot of the Fire Radiative Power (FRP) for the habitat loss intervals (a), number of forest patches (b; NFP), mean of forest patches areas (c; MFPA) and edges proportion (d; EP). The letters represent the groups resulting from the Kruskal-Wallis post-hoc test. For all analyses, a significance level of 95% (p-value < 0.05) was adopted.

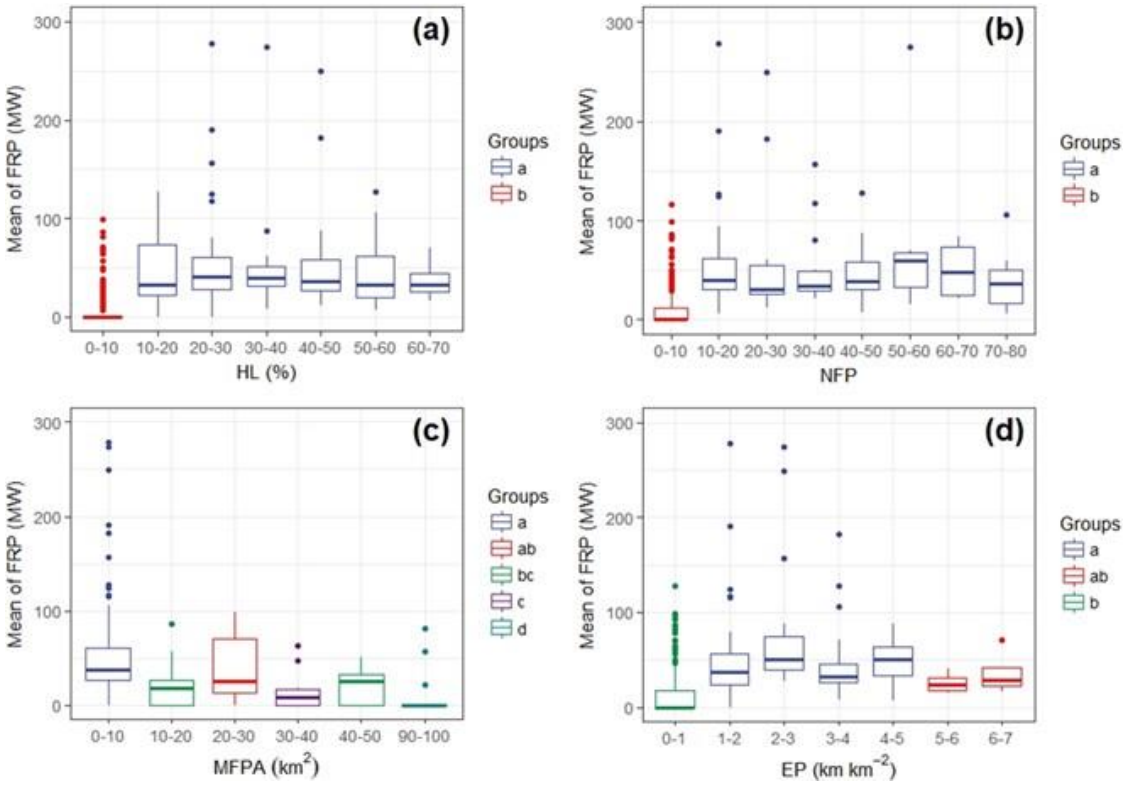


Most of the active fires detected were located within 1 km from the forest edges (Table 3), corresponding to 95% and 98% of fires occurring in forest and deforested areas, respectively.

Table 3.3 – Total of active fires per edge distance. (*) No active fires were observed.

| Class | Edge distance (km) | Number of active fires | % |
|---|---|---|---|
| Forest Cover | > 3 | 10 | 0.62 |
| | 2 | 66 | 4.07 |
| | 1 | 1,546 | 95.31 |
| Deforested Areas | 1 | 2,477 | 98.92 |
| | 2 | 27 | 1.08 |
| | > 3 (*) | 0 | 0 |

Most active fires were classified as low intensity (FRP less than 50 MW), representing between 70 and 90% of the total of active fires analysed for each edge distance (Table4). Between 10 and 28% of the total active fires were in the 50-500 MW intensity category. The few observed higher intensities of active fires (FRP greater than 500 MW) were located in the first kilometre from the forest edges only. Corroborating the previous evidence, the Kruskal-Wallis test showed a significant difference between the FRP values for 45evelorent edge distances in the forest areas (KW = 6.95; p-value < 0.05; FigureS5a), where the highest FRP values were observed only in the first kilometre from the forest edges. For the deforested areas, no significant difference was observed (KW = 2.99; p-value > 0.05; FigureS5b).

Figure 3.9 – Boxplot of Fire Radiative Power (FRP) for different distances from the edges in forest areas (a) and in deforested areas (b). The letters represent the groups resulting from the Kruskal-Wallis post-hoc test (p-value = 0.03 for Figure S5a and p-value = 0.22 for Figure S5b). (*) No active fires were observed. The log transformations were performed only to improve visualization of the data in the figure (the Kruskal-Wallis and post-hoc tests were performed using the original data). For all analyses, a significance level of 95% (p-value < 0.05) was adopted.

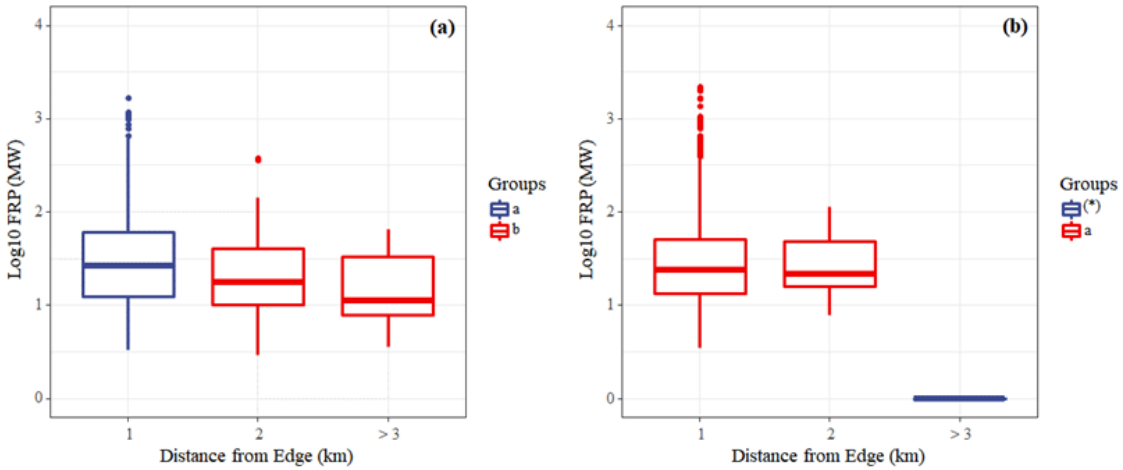

Table 3.4 – Percentage of Fire Radiative Power (FRP) per edges distance interval and fire intensity class. (*) no active fires were observed.

| Class | Edge distance (km) | Class of FRP (%) | | | |
|---|---|---|---|---|---|
| | | < 50MW | 50-500 MW | 500-1000 MW | > 1000 MW |
| Forest Cover | > 3 | 90.00 | 10.00 | 0 | 0 |
| | 2 | 75.76 | 24.24 | 0 | 0 |
| | 1 | 70.63 | 28.01 | 0.97 | 0.39 |
| Deforested Areas | 1 | 74.44 | 24.34 | 0.93 | 0.28 |
| | 2 | 74.07 | 25.93 | 0 | 0 |
| | > 3 (*) | 0 | 0 | 0 | 0 |

## 3.6 Discussion

### 3.6.1 Relationship between habitat loss and measures of habitat configuration

Due to the complexity of anthropic actions in the Amazon region, deforestation occurs in different patterns, resulting in different spatial configurations of patches and forest edges (FAHRIG, 2003; ARIMA et al., 2015; VEDOVATO et al., 2016). Here, we show that in Central Amazonia, the NFP increases as deforestation progresses to levels up to 70% of HL. The increasing number of forest patches and its variability with increasing habitat loss is similar to the one found by Oliveira Filho and Metzger (OLIVEIRA FILHO; METZGER, 2006) for the “fishbone” fragmentation pattern. This relationship was also found by Villard and Metzger (VILLARD; METZGER, 2014) in simulated landscapes. Although the maximum HL observed in our study area was 70%, the NFP should necessarily decrease at some point as deforestation approaches the 100% level. According to literature review carried out by Fahrig (FAHRIG, 2003), the number of forest patches is expected to increase up to a certain degree of deforestation (~80% of habitat loss) and decrease in the lower levels of habitat amount.

The non-linear relationship between the MFPA and HL found in our study area differed from the one previously presented by Fahrig (FAHRIG, 2003) in a global study (meta-analysis) for real landscapes but is similar to that documented by Oliveira Filho and Metzger (OLIVEIRA FILHO; METZGER, 2006) in real and

simulated landscapes in the Brazilian Amazonia. According to Oliveira Filho and Metzger (OLIVEIRA FILHO; METZGER, 2006), this response pattern is usually associated with the “fishbone” fragmentation pattern and small settlements, as they produce small patches close to each other, similar to our study area.

The theoretical model proposed by Fahrig (FAHRIG, 2003) describes a significant increase in the total edges up to 50% of habitat removal level, tending progressively to zero after this threshold. However, in our study area, there was no reduction in EP up to at least 70% of HL, indicating a greater inflection point than that observed by Fahrig (FAHRIG, 2003). The same pattern was observed by Numata et al. (NUMATA et al., 2010) when analysing the forest fragmentation in old deforestation frontiers in the state of Rondônia (Brazilian Amazonia) with different patterns and levels of deforestation, and by Laurance et al (LAURANCE; LAURANCE; DELAMONICA, 1998) when simulating the deforestation scenario for the same state. This pattern occurs over time as the habitat loss progresses to intermediate levels, increasing the number of forest patches and consequently the density of forest edges. On the other hand, when forest removal approaches 100%, the number of forest patches and total area are reduced dramatically, resulting in a lower edge density in the landscape (FAHRIG, 2003; LIU; HE; WU, 2016).

### 3.6.2 Relationship between habitat configuration and fire incidence and intensity

Our results suggest that the landscape structure partly explains the variation of fire incidence and intensity in forest areas, similar to the results found by Armenteras et al. [25] in the Colombian Amazon. More fragmented landscapes, with smaller patches and a greater proportion of edges, tend to be more vulnerable to fire than landscapes with continuous and intact forests. The effect of fragmentation on the incidence and intensity of fire observed here is likely a result of changes in the original structural configuration of the forest, which changes mass and energy balance. Fragmented forests tend to be drier than a continuous forest cover, due to the lower humidity retention, higher temperature, and greater exposure to dry air masses and winds (COCHRANE; LAURANCE,

2008). This dry condition causes a higher tree mortality (generally large trees) (LAURANCE et al., 2017), resulting in a large amount of fuel load available (dead biomass), which increases the susceptibility of forest to fire (BERENGUER et al., 2014).

Although fragmentation makes forests more susceptible to fire, the occurrence of fire is conditioned to the presence of ignition sources. In Amazonia, these sources are mostly associated with the escape of fire from newly deforested areas (Figure A1b) or from the management of agricultural and pasture areas (Figure A1c) (ARAGÃO et al., 2008; CANO-CRESPO et al., 2015; ROSAN; ANDERSON; VEDOVATO, 2017). This explains the observed variation in fire occurrence and intensity at different levels of landscape fragmentation in our results. This issue becomes even clearer when we observe that over than 95% of the active fires occurred in the first kilometre from the edge, in both forested and deforested areas, indicating the escape of fires into forests. We verified that fire penetrates forest areas up to a distance of 3 km, which corroborates other studies carried out in the Amazon region (COCHRANE, 2001; COCHRANE; LAURANCE, 2002; BRIANT; GOND; LAURANCE, 2010; ARMENTERAS; GONZÁLEZ; RETANA, 2013; ARMENTERAS et al., 2017). All active fires of higher intensity (FRP above 500 MW) occurred in the first kilometre in the forest areas, with a significant difference when compared to the other edge distances. This can be explained by the greater amount of fuel available, due to the high rate of trees mortality closer to the forest edges (LAURANCE et al., 2017).

The great variability in the incidence and intensity of fire observed at different levels of fragmentation in our results are likely related to the combined existence of ignition sources and fuel availability in the landscape. Conversely, it is important to note that our results are based on a year considered normal from the point of view of the amount of rainfall (Figure S1). Thus, the effects of fragmentation on fire incidence and intensity can be more significant during drought years (ARAGÃO et al., 2007, 2018), increasing carbon emissions into the atmosphere (ANDERSON et al., 2015; ARAGÃO et al., 2018). This scenario is worrying since the occurrence of extreme droughts events have become

increasingly frequent in Amazonia, and fire occurrence is predicted to increase in the region due to climate and land use change synergies (MALHI et al., 2008; MARENGO; ESPINOZA, 2016; LE PAGE et al., 2017).

### 3.6.3 Implications of the effect of fragmentation on fire occurrence in Amazonia for the Brazilian forest code

Land use regulation is a critical component of forest governance and conservation strategies (STICKLER et al., 2013). In Brazil, the Brazilian Forest Code (BFC) is the main law for regulating land use with the objective of conserving native vegetation. Two instruments of this legislation are highlighted, the first is the Legal Reserve (LR), which requires the maintenance of at least 80% of intact forest areas on private properties in the Amazon biome; and the other is the Permanent Preservation Area (PPA), that includes both Riparian Preservation Areas (RPA) that protect riverside forest buffers, and Hilltop Preservation Areas in high elevations and steep slopes (SOARES-FILHO et al., 2014).

Our results showed that forest removal values limited by 20% guarantee a smaller number of patches (0-20 patches per 100 $km^{-2}$) with larger average areas (90-100 $km^2$) and a lower proportion of forest edges (0-2 km $km^{-2}$) in relation to higher levels of habitat loss. This HL threshold coincides with values where the incidence and intensity of fire are significantly smaller when compared to the other levels of HL. The susceptibility of the landscape to forest fires clearly increases with greater HL. Therefore, maintaining native vegetation in at least 80% of the rural properties area, as prescribed in the LR definition for the Amazon biome, allow for low levels of fire incidence, even if ignition sources are present. Regions with a lower proportion of forest cover are clearly more susceptible to forest degradation due to fire, unless appropriate prevention and management techniques are applied.

In 2012 the BFC was reviewed and based on our results we argue that some of the current BFC rules for LR and PPA areas can contribute to increasing fire incidence and intensity in the Amazon region, since they substituted some

instruments established in the previous version of the law. The most worrying from a conservation point of view is that “small” properties (from 40 ha to 440 ha depending on the region) were exempted from recovering areas of LR deforested illegally before 2008. Furthermore, the vegetation of PPA within a property is now considered part of the LR, while before the law’s modification the PPA and the LR areas were computed separately, as they serve to different conservation purposes. Additionally, the requirements for restoration of PPA and maintenance of LR were reduced. The LR requirement for 80% intact forest was reduced to 50% when (1) the proportion of conservation areas and indigenous territories within Amazonian municipalities is equal to or higher than 50% or (2) conservation areas and indigenous territories represent 65% of the state territory. These legal modifications together reduced the country’s “forest debt” by 58% (SOARES-FILHO et al., 2014), which may allow the maintenance of the fragmentation of Amazonian landscapes, keeping them susceptible to the occurrence of fire, as we demonstrated in our results.

Another legal modification allowed the rural owner who has forest liabilities to compensate for it in other properties located anywhere in the same biome. Given the vast extent of Brazilian biomes, this implies that an owner may compensate for an illegally deforested area by restoring another over 3,000 km away. Such restoration effort, if undertaken in a region where forest cover is already well preserved, would not recover the landscape structure and local environmental services where it is needed most. Thus, the displacement of restoration efforts from highly fragmented to more preserved areas would make the former regions more susceptible to the incidence of fire.

According to the BFC, economic exploitation is allowed in the LR areas, including the collection of non-timber forest products (fruits, vines, leaves and seeds), and the commercial and non-commercial selective extraction of wood. The sustainable economic exploitation of the forest is important for the rural owner as a source of income, avoiding the deforestation of the LR areas. However, good forest management practices should be applied. Selective logging can increase the forest susceptibility to fire (HOLDSWORTH; UHL, 1997) due the canopy

damage (UHL; VIEIRA, 1989; VERISSIMO et al., 1992; PEREIRA et al., 2002; ASNER et al., 2006) that allows the penetration of solar radiation, raising the temperature and decreasing the humidity within the forest. These microclimate changes associated with the greater amount of dead biomass caused mainly by the logging operations (UHL et al., 1997), resulting in more severe fires (SIEGERT et al., 2001; GERWING, 2002).

This whole context is worrisome since the main sources of fire ignition in the Amazonia are related to the management of adjacent agricultural and livestock areas. The flexibilization of the Forest Code in comparison to its predecessor allowed the maintenance of extensive fragmented areas, mainly in the region of the deforestation arc, where there are intense anthropic activities (VEDOVATO et al., 2016), and therefore abundant ignition sources.

## 3.7 Conclusions

We conclude that the susceptibility of the landscape to forest fires increases at the beginning of the deforestation process. In general, our results reinforce the need to guarantee low levels of fragmentation in the Brazilian Amazonia in order to avoid the degradation of its forests by fire and the related carbon emissions (ANDERSON et al., 2015; ARAGÃO et al., 2018). Future work could examine whether the relations found here are kept or modified during extreme drought events.

The reduction of forest liabilities resulting from the last modification of the forest code increases the probability of occurrence of forest degradation by fire since it allows the existence of areas with less than 80% of forest cover, contributing to the maintenance of high levels of fragmentation.

We anticipate that forest degradation by fire will continue to increase in the region especially in light of the mentioned environmental law relaxation and its synergistic effects with climate change. All of this can affect efforts to Reduce Emissions from Deforestation and Forest Degradation (REDD). Therefore, actions to prevent and manage forest fires are necessary, mostly for the properties where forest liabilities exist and are compensated in other regions.

## 3.8 Graphical Abstract

Figure 3.10 – Graphic summary of the main results found in this chapter. (a) Intact forest, with controlled microclimate, less penetration of solar radiation and action of the winds. (b) Deforested forest, resulting in a changed microclimate (higher temperature and lower humidity due to greater penetrability of solar radiation and wind action) and higher mortality rate of trees near the edges, resulting in a greater amount of available fuel material. (c) Fragmented forest, more susceptible to the occurrence of fire (more intense near the forest edge) due to the edge effect and fire escape from the agriculture and livestock management areas.

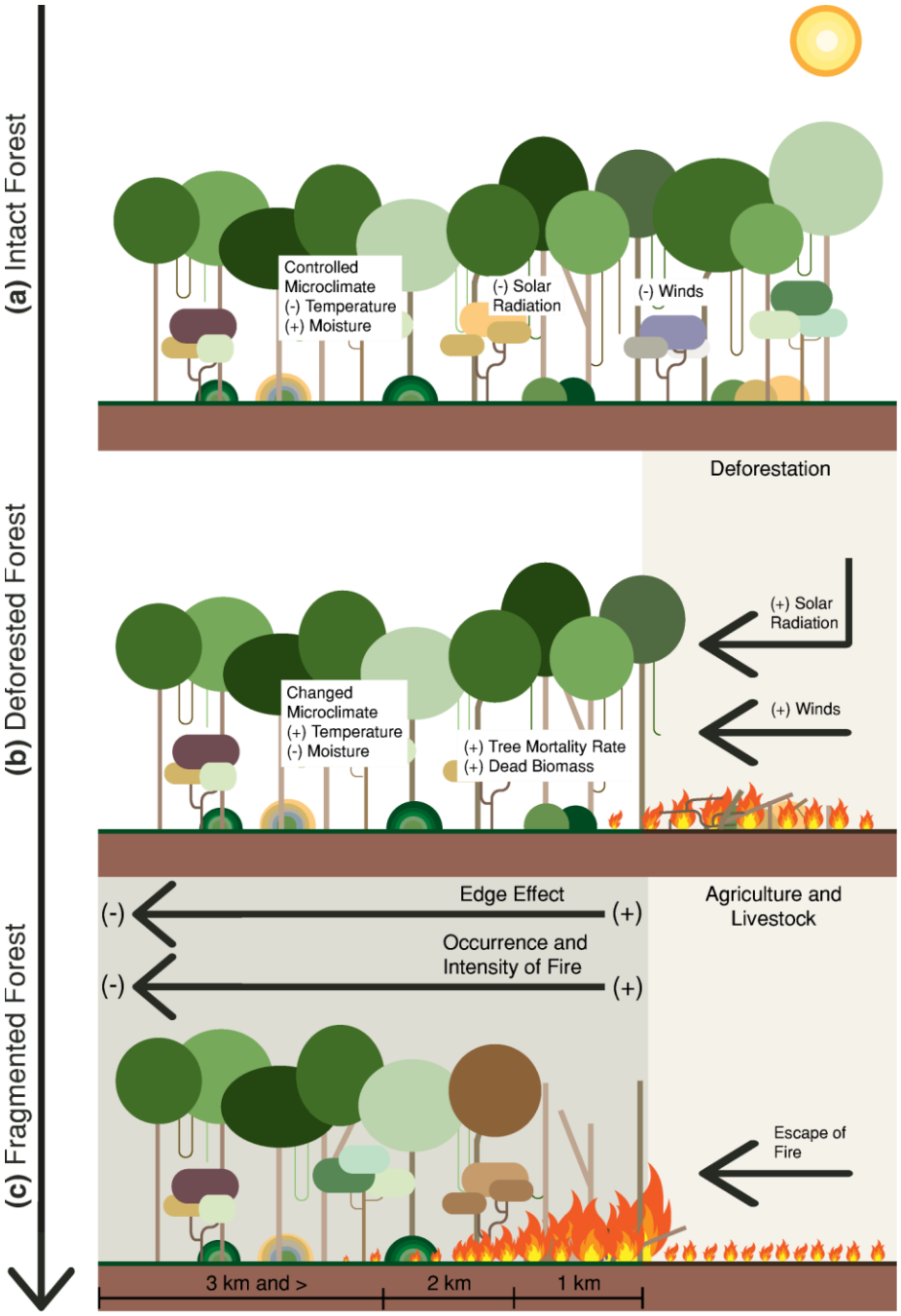

# 4 PERSISTENT COLLAPSE OF BIOMASS IN AMAZONIAN FOREST EDGES FOLLOWING DEFORESTATION LEADS TO UNACCOUNTED CARBON LOSSES[4]

## 4.1 Introduction

Tropical forests play a crucial role in the global carbon cycle, with carbon stocks varying between 193-229 Pg (SAATCHI et al., 2011; BACCINI et al., 2012), representing about 54% of the global above-ground carbon (AGC) stock (LIU et al., 2015). The area of these forests, however, declined by 10%, from 19.65 million square kilometres ($km^2$) in 1990 to 17.70 million $km^2$ in 2015, because of land use and land cover changes (KEENAN et al., 2015). The magnitude of these forest changes affects essential ecosystem services, including carbon storage, biodiversity, climate regulation, nutrient cycling, and water supply (FOLEY, 2005; BACCINI et al., 2017).

In the Amazon, the world's largest continuous tropical forest, deforestation has continuously converted old-growth forests into agricultural and livestock areas, fragmenting the landscape extensively. Forest fragmentation is associated with the increased number of forest patches and augmentation of the extent of forest edges perimeter and area (VEDOVATO et al., 2016; SILVA JUNIOR et al., 2018). These changes in forest cover configuration cause direct carbon losses from edge effect and agricultural fire incursion into adjacent stand forests (FERREIRA; LAURANCE, 1997; LAURANCE et al., 1997; NASCIMENTO; LAURANCE, 2004; BROADBENT et al., 2008; ARMENTERAS; GONZÁLEZ; RETANA, 2013; CHAPLIN-KRAMER et al., 2015; ARMENTERAS et al., 2017; SILVA JUNIOR et al., 2018). The exposure of the Earth's forests to edge effect is widespread (RIITTERS et al., 2000; TAUBERT et al., 2018; HANSEN et al., 2020). Globally, about 70% of forests were within one-kilometre of forest edges in 2000 (HADDAD

[4] This chapter is an adapted version of the published paper: SILVA JUNIOR, C. H. L. et al. Persistent collapse of biomass in Amazonian forest edges following deforestation leads to unaccounted carbon losses. **Science advances**, v. 6, n. 40, p. eaaz8360, 2020. It is representing advances and improvements that made able the implementation of Silva Junior (2018) method in the Google Earth Engine - GEE platform (GORELICK et al., 2017), having supported the next Thesis' chapter.

et al., 2015). However, only 5.2% of the forests in the Brazilian Amazon were in this same edge zone in 2014 (VEDOVATO et al., 2016).

Pioneering investigations from the BDFFP (Biological Dynamics of Forest Fragments Project), in the Brazilian Central Amazonia, found significant carbon losses at forest edges (depth of 100-m) induced by microclimatic changes within the canopy, leading to increased tree mortality rates (FERREIRA; LAURANCE, 1997; LAURANCE et al., 1997; NASCIMENTO; LAURANCE, 2004). However, the magnitude of carbon losses at these forest edges is still poorly quantified at large-scales due to the scarcity of quantitative datasets for tropical forests. Efforts to accurately incorporate this source to regional and global carbon budgets are urgently needed for improving the estimations of the contribution of land use and cover changes to the atmospheric carbon burden. This quantification is critical for the effectiveness of sustainable 54eveloppment policies and must be explicitly included either in national greenhouse gas inventories of tropical countries and in REDD+ (Reducing Emissions from Deforestation and Degradation) reports (UNFCCC – UNITED NATIONS FRAMEWORK CONVENTION ON CLIMATE CHANGE, 2019). Initial attempts were already made to quantify the carbon losses caused by edge effect in Amazonia (NUMATA et al., 2010, 2011; PÜTZ et al., 2014; HISSA et al., 2016; BRINCK et al., 2017; ALMEIDA et al., 2019; MAXWELL et al., 2019); nonetheless, these studies were constrained by the availability of synoptic data, the accuracy of models, the spatial resolution of the remote sensing data used or the study area extent.

Representing the environmental variability of edge effect and associated carbon stocks across the Amazon is a challenge, due to its large area. In this context, remote sensing technologies play an essential role in quantifying both the extent of fragmentation-induced forest edges and the negative impact of edge effect on forest carbon stocks. The recent availability of 30-m spatial resolution forest change data sets (HANSEN et al., 2013) based on optical images from the Landsat series of Earth Observation satellites, provides a unique opportunity to quantify forest edge extent and age in detail at pan-Amazon scale. This information integrated with airborne LiDAR (Light Detection And Ranging)

technology collected over Amazonian forests offers a powerful combination for estimating forest carbon stocks in these areas, based on accurate models of forest structure (LEFSKY et al., 2002; LONGO et al., 2016) (Figure 4.1).

Figure 4.1 – LiDAR point cloud profile. Point cloud data collected in 2014 in the northeast of the Pará state, Brazil with 420 meters o-f length. The points represent the vegetation height, which was normalised by the terrain altimetry. (a) Structure of a non-degraded old-growth forest, where the trees height reaches up to 40m. (b) Forest edge (width of 120m), where the height of the vegetation reaches up to 25m. (c) Deforested area with vegetation regrowth (height up to 5m).

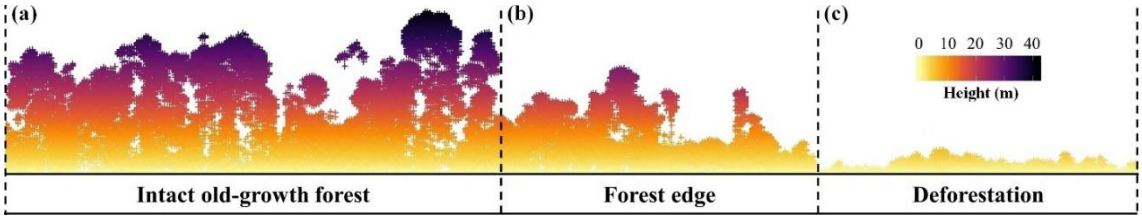


Therefore, in this study we aim to provide a unique spatially and temporally explicit quantification of carbon losses from forest edges and estimate the additional contribution to gross deforestation-induced carbon losses. Specifically, we: (i) analysed 16 years (2000-2015) of readily available 30m spatial resolution Landsat-based forest-cover and change datasets (HANSEN et al., 2013) to quantify the dynamics and age distribution of forest edges in Amazonia; (ii) processed an airborne LiDAR dataset collected across several locations in the studied area to build an empirical carbon loss model as a function of forest edge age; and finally (iii) modelled the edge-induced carbon loss across the entire Amazonia by applying the LiDAR-based carbon loss model across all pixels of the forest edge age maps. our model is grounded on the observation (ORDWAY; ASNER, 2020) and concept (MELITO; METZGER; DE OLIVEIRA, 2018) that tropical forest edges formed by deforestation continuously reduce their carbon stocks with age. Thus, we hypothesize that direct carbon losses by deforestation are followed by incremental indirect carbon losses induced by the aging of forest edges in Amazonia.

## 4.2 Results

### 4.2.1 Forest edge dynamics and age distribution

The dynamics of forest edges creation and erosion (defined here as the complete removal of canopy cover of the forest edge) is explained directly by the pattern and pace of deforestation. In Figure 2, we present our findings regarding Amazonian Forest edges dynamics (Figure 2a and 2b) and their age distribution (Figure 2c and 2d). We estimate that 5% of the standing forest cover in 2000 was deforested between 2001 and 2015, or a gross forest loss of 273,195 $km^2$, at an average of 18,213±4,303 $km^2$ $year^{-1}$ (Figure 2a). We observed a deforestation peak of 26,376 $km^2$ in 2004 and a minimum value in 2013 (12,578 $km^2$). However, the Mann-Kendall test (*MK*) showed that annual deforestation overall decreased significantly at a rate of 683 $km^2$ $year^{-1}$ (*MK*=-0.49 and $p<0.05$) along the 15-year period.

During the interval studied, Brazil was the country with the highest deforestation rate (14,835±4706 $km^2$ $year^{-1}$), contributing with an average of 62±10% $year^{-1}$ of overall deforestation in Amazonia (Figure S1). Brazil is also the leader in relative contribution rate (percentage of annual deforestation in relation to the Amazonia area of each country), with an average of 0.355±0.109% $year^{-1}$ (Table S1). In contrast, French Guiana had the lowest deforestation rate (33±18 $km^2$ $year^{-1}$), contributing with an average of 0.20±0.10% $year^{-1}$ of overall Amazonian deforestation, with a relative contribution rate average of 0.040±0.021% $year^{-1}$ (Table S1). However, across all Amazonian countries, only Brazil had a significant negative temporal trend in deforestation, at a rate of 773 $km^2$ $year^{-1}$ (*MK*=-0.55 and $p<0.05$), while Peru had the highest significant temporal trend of increase, at a rate of 68 $km^2$ $year^{-1}$ (*MK*=0.67 and $p<0.05$). Details about annual deforestation rates and temporal trends for all countries in the Amazonia can be found in Figure 4.3.

Figure 4.2 – Forest edges creation, erosion, and age composition in Amazonia. (a) Temporal forest edges variation in Amazonia, where the black bars are the annual forest edges increment rate, and the blue line is the total gross forest area increment from 2001. (b) Boxplots of forest edges erosion rates (as a negative percentage) for the Amazonia, where the bold horizontal lines are the medians, the blue dots are the averages, the shaded area is the frequency distribution function, and *n* is the number of observations. (c) Spatial distribution of forest edges age in 2015 in Amazonia; ages were aggregated by the average in a 10-km by 10-km grid-cell to improve visualization. (d) Dot plots of forest edge age (each dot corresponds to a single grid-cell in Figure2c) in Amazonian countries in 2015, where the vertical bars are the standard deviations, the black dots are the averages, the grey dots are the data observations, and *n* is the number of observations. The letters in bold represent the groups defined by the posthoc test.

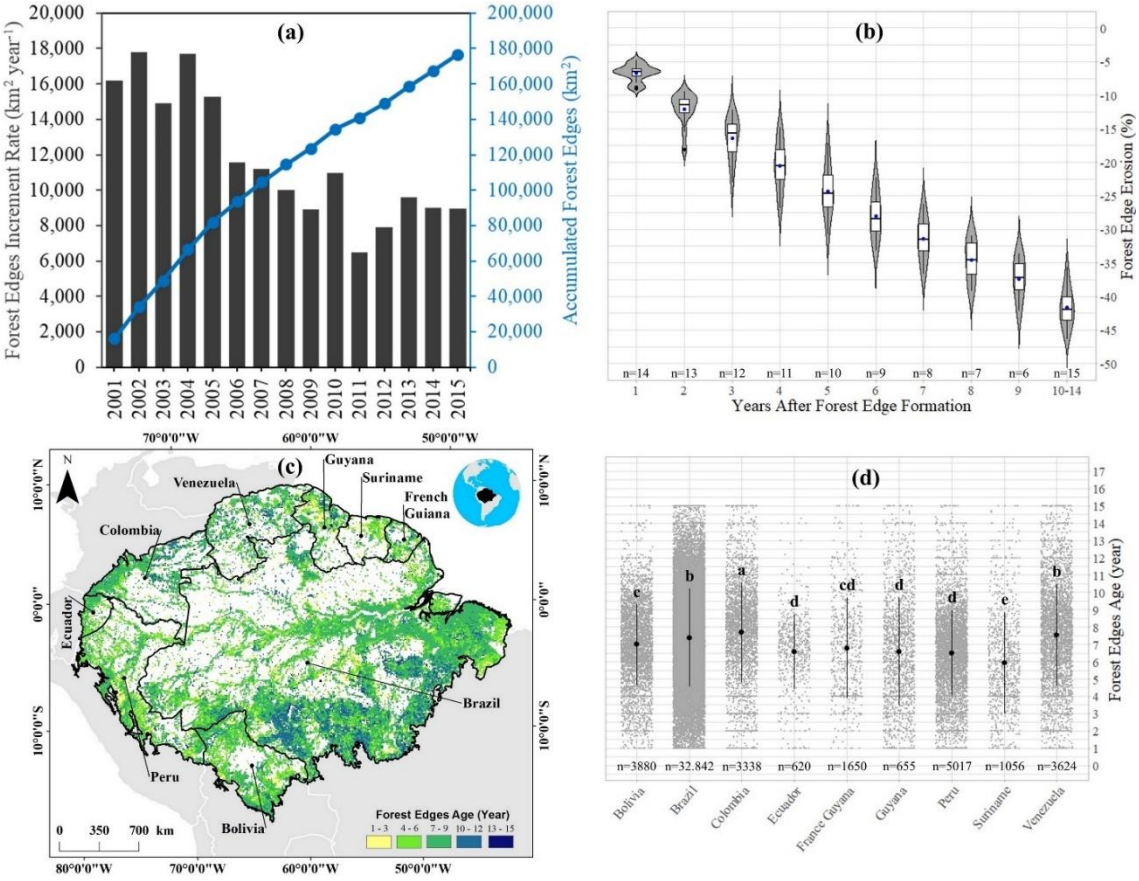

Figure 4.3 – Annual deforestation rates in Amazonian countries, and their respective contributions (as percentage) to the total Amazonia deforestation. Deforestation in the 2016-2019 period was measured from version 1.7 of the Global Forest Change dataset (GFC; https://earthenginepartners.appspot.com/science-2013-global-forest/download_v1.7.html). The Brazilian Amazon official deforestation rates were obtained from PRODES program (The Brazilian Amazon Deforestation Monitoring Program; http://terrabrasilis.dpi.inpe.br/en/home-page). After 2015, the difference between magnitudes of forest cover losses of GFC and PRODES data was due to the increase in drought-induced forest fires in the late 2015 and early 2016 (ARAGÃO et al., 2018; SILVA JUNIOR et al., 2019b) that were detected by the GFC and not detected by PRODES (responsible for mapping the clear-cut deforestation in the Brazilian Amazon).

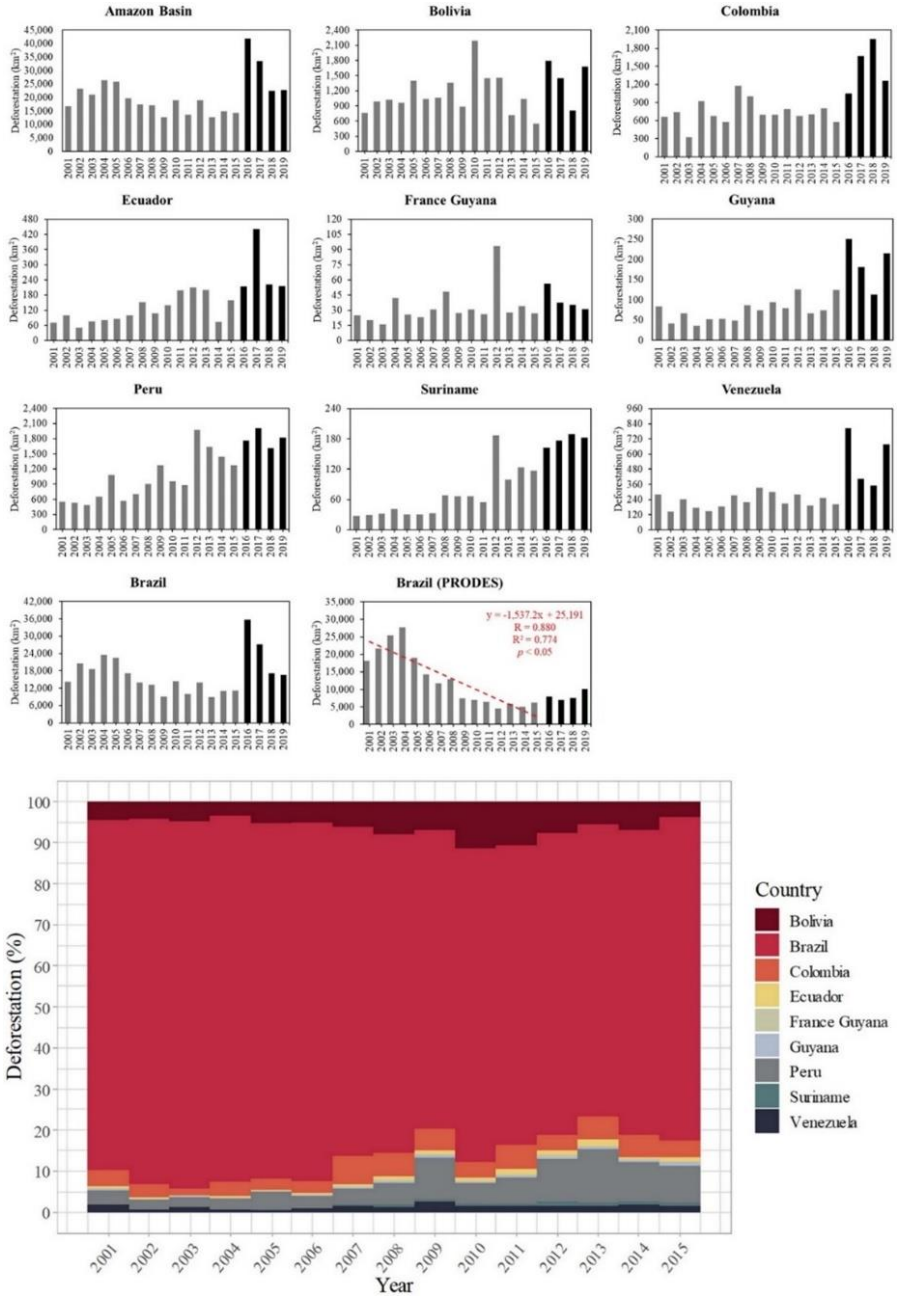

Table 4.1 – Temporal trends of deforestation rates for each Amazonian country. Where S is the Man-Kendall statistics and SD the standard deviation. The S statistic with an asterisk (*) means a significant temporal trend at 95% of significance level ($p < 0.05$).

| Country | S | Sen's Slope (km$^2$ year$^{-1}$) | Average±SD (km$^2$ year$^{-1}$) |
|---|---|---|---|
| Bolivia | 0.13 | 8.66 | 1,126±400 |
| Brazil | -0.55* | -773 | 14,835±4,706 |
| Colombia | 0.09 | 2.13 | 734±198 |
| Ecuador | 0.59* | 9.12 | 120±52 |
| France Guiana | 0.37 | 0.67 | 33±18 |
| Guyana | 0.45* | 3.71 | 73±27 |
| Peru | 0.67* | 67.97 | 994±450 |
| Suriname | 0.75* | 6.71 | 67±46 |
| Venezuela | 0.15 | 2.42 | 229±57 |

In 2015, we estimated that forests edges, considering a depth of 120-m (LAURANCE et al., 1997; NUMATA et al., 2017), covered an area of 176,555 km$^2$ across the whole Amazonia (Figure 2a). This represents about 65% of the total deforested area between 2001 and 2015 or 3% of the total forest area in 2015 over the region. On average 11,770±3,546 km$^2$ year$^{-1}$ of new forest edges were created in Amazonia, with a maximum area of 17,815 km$^2$ in 2012 and a minimum of 6,481 km$^2$ in 2011 (Figure 2a). Brazil and Peru had the highest annual edge creation average, contributing with 7,600±3,427 km$^2$ year$^{-1}$ and 1,510±300 km$^2$ year$^{-1}$, respectively. In addition, we quantified that on average 7±1%, 24±4% and 42±3% of the forest edges were eroded by forest clearing process after one, five and 10 to 14 years of their creation, respectively (Figure 2b).

Similar to the patterns found for deforestation rates in the Amazonia, the creation of forest edges decreased significantly at a rate of 707 km$^2$ year$^{-1}$ ($MK$=0.74 and $p$<0.05) between 2001 and 2015 (Figure 2a). Across all Amazonian countries (Table S1), Brazil and Colombia had a significant decreased trend in edge formation ($p$<0.05), with rates of 683 km$^2$ year$^{-1}$ and 49 km$^2$ year$^{-1}$, respectively. Conversely, Guyana and Suriname had a significant increased trend ($p$<0.05), with rates of 5 km$^2$ year$^{-1}$ and 11 km$^2$ year$^{-1}$, respectively. Details about temporal trends of forest edge dynamics for the Amazonian countries are shown in Figure S2 and Table S3.

Figure 4.4 – Annual rates of forest edges increment in Amazonian countries, and their respective contributions (as percentage) to the total Amazonia Forest edge area.

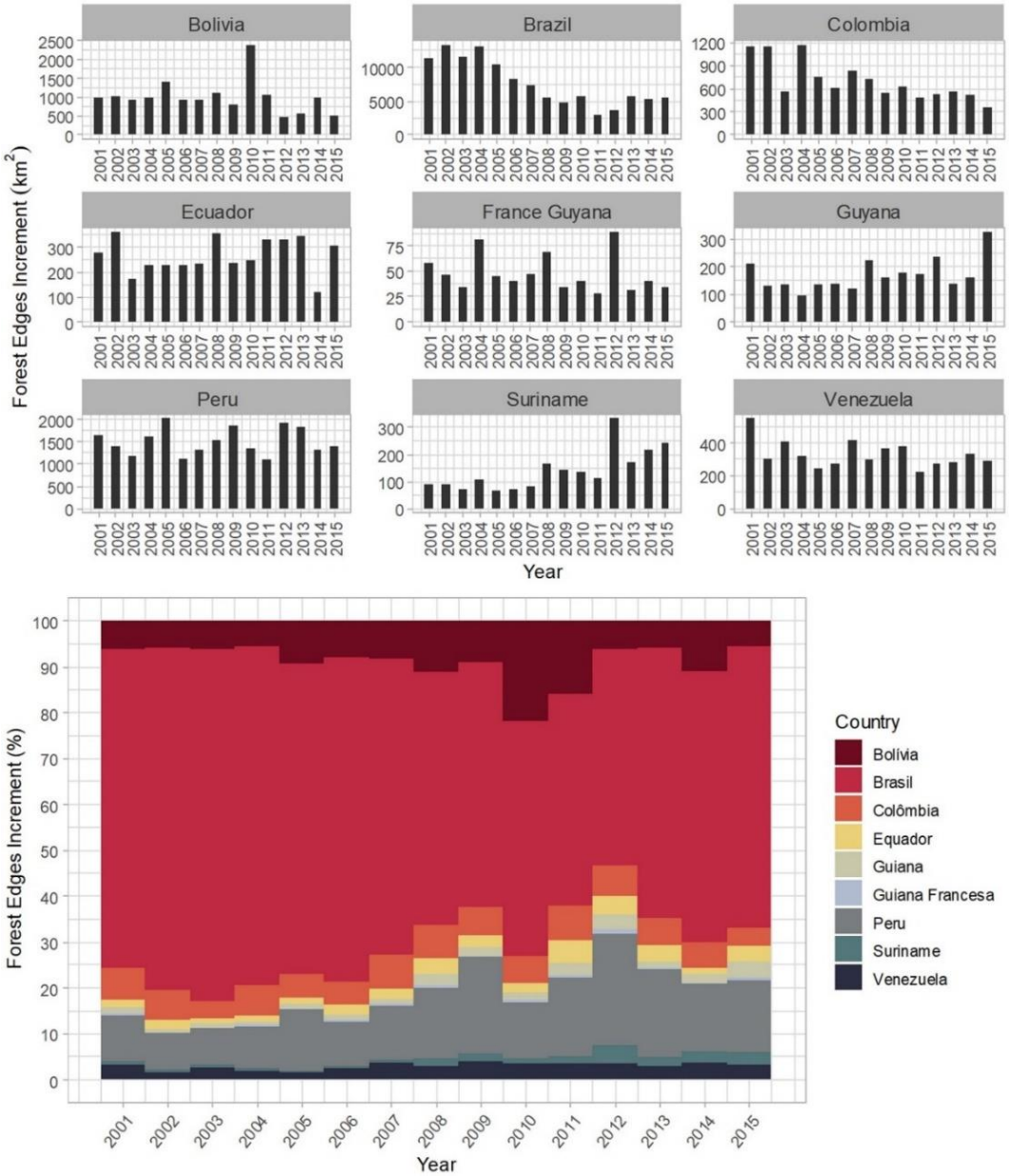

Table 4.2 – Temporal trends of forest edge increments for each Amazonian country. Where S is the Man-Kendall statistics and SD the standard deviation. The S statistic with an asterisk (*) means a significant temporal trend at 95% of significance level ($p < 0.05$).

| Country | S | Sen Slope ($km^2$ $year^{-1}$) | Average±SD ($km^2$ $year^{-1}$) |
|---|---|---|---|
| Bolivia | -0.27 | -23 | 1000±455 |
| Brazil | -0.67* | -683 | 7600±3427 |
| Colombia | -0.65* | -49 | 705±261 |
| Ecuador | 0.17 | 4 | 266±72 |
| France Guiana | -0.29 | -1 | 171±59 |
| Guyana | 0.41* | 5 | 48±18 |
| Peru | -0.01 | -3 | 1510±300 |
| Suriname | 0.63* | 11 | 139±76 |
| Venezuela | -0.25 | -6 | 330±83 |

In 2015, we observed that the oldest edges (between 10 and 15 years old) were distributed mainly over the Brazilian Arc of Deforestation (VELASCO GOMEZ et al., 2015), an old Amazonian deforestation frontier located in the southeast flank of Amazonia (Figure 2c). We also observed old forest edges in the southern portion of Bolivia and in the north of Amazonia, including three countries: Colombia, Venezuela, and Guyana. On the other hand, the youngest forest edges (between 1 to 3 years old) dominated not only the new active deforestation frontiers in southern Bolivia, western Peru, and northern Colombia, but also areas in the central Brazilian Amazon.

On average, forest edges in Amazonia were 7±3 years old in 2015. The edge age distribution was close to uniform: 23% of the forest edges ages were between 1 and 3 years, 21% between 4 and 6 years, 19% between 7 and 9 years, 20% between 10 and 12 years and 16% between 13 and 15 years. Considering all the Amazonian countries, the age of forest edges spanned from an average of 6±3 years in Suriname to 8±3 years in Colombia (Figure 2d and Table 1). The Kruskal-Wallis test (*KW*) showed a significant difference (*KW*=1,179 and $p<0.05$) in the age of forest edges among the Amazonian countries (Figure 2d). For instance, we found that forest edge age was significantly ($p<0.05$) lower in Suriname (group e) and higher in Colombia (group a). However, the age of forest edges in the pair Brazil and Venezuela (group b), and in the group Ecuador, Guyana, and Peru (group d) were statistically indistinguishable from each other. Finally, the age of

forest edges in French Guiana (cd group) was not distinguishable from countries belonging to groups c and d simultaneously.

Table 4.3 – Average and median of the forest edges ages for the Amazonian countries. SD is the standard derivation.

| Country | Forest edges ages (years) | |
|---|---|---|
| | Average±SD | Median |
| Bolivia | 7.00±2.35 | 7.01 |
| Brazil | 7.38±2.84 | 7.54 |
| Colombia | 7.67±2.88 | 7.96 |
| Ecuador | 6.58±2.17 | 6.84 |
| France Guyana | 6.57±3.11 | 6.41 |
| Guyana | 6.78±2.91 | 6.57 |
| Peru | 6.48±2.50 | 6.56 |
| Suriname | 5.94±2.93 | 5.49 |
| Venezuela | 7.53±2.94 | 7.59 |

### 4.2.2 Spatial-temporal variation in above-ground carbon losses

By combining the age information from the mapped forest edges with the airborne LiDAR data we stablished a relationship depicting the loss of above-ground forest carbon as a function of the age of forest edges (see Materials and Methods) to investigate the spatial and temporal changes of carbon stocks associated to edge effect across Amazonia. As shown in Fig 3a and 3b, between 2001 and 2015, carbon losses related to edge effect ranged from 0.001 up to 0.252 Tg C per grid-cell (100 $km^2$), while losses from deforestation ranged from 0.001 up to 0.799 Tg C per grid-cell. More than 60% of the grid-cells had values of carbon loss varying between 0.001 and 0.022 Tg C, both for edge effect and deforestation (Figure 3c and 3d). Spatially, absolute carbon loss values associated to edge effect and deforestation presented similar patterns across Amazonia (Fig 3a and 3b), with substantial accumulated losses over the Brazilian Arc of Deforestation (VELASCO GOMEZ et al., 2015) and the southwest Amazonian flank. The lower accumulated losses were spatially distributed over the central and the northern part of the Amazon Forest.

Figure 4.5 – Spatial variability of carbon losses in Amazonia. Spatial variability of carbon losses between 2001 and 2015 from (a) edge effect and (b) deforestation. Histograms of frequency distribution of carbon losses related to (c) the edge effect presented in Figure3a and (d) the deforestation presented in Figure3b. I Percent contribution of edge effect and deforestation to the total carbon loss of each pixel in Amazonia. Carbon losses were aggregated by the sum in a 10-km by 10-km grid-cell to improve visualization in Figure 3a and Figure 3b.

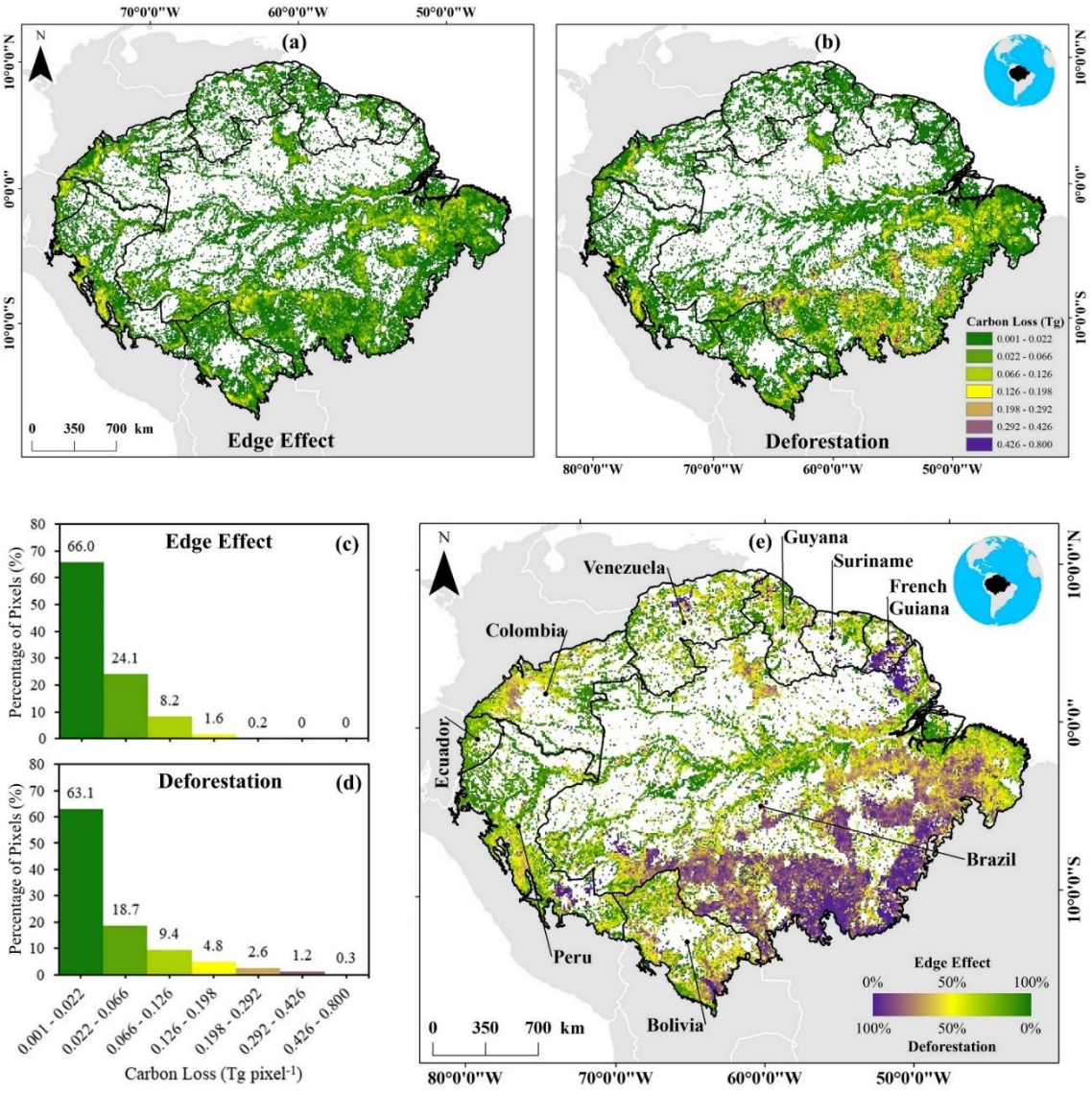


Figure 3e shows the relative contribution of edge effect and deforestation for the total carbon loss between 2001 and 2015 as a percentage of each grid-cell. Remarkably, we found that relative contribution of edge effect and deforestation for the carbon loss of grid-cells were heterogeneous across Amazonia during the

studied period. While carbon losses from edge effect dominated mainly the central Amazonia region, carbon loss associated to deforestation were more evident along the Brazilian Arc of Deforestation (VELASCO GOMEZ et al., 2015), and areas in Peru, Bolivia, and southern French Guiana.

Between 2001 and 2015, we estimated a total gross carbon loss from edge effect of 947 Tg C (0.95 Pg C), with an average of 63±8 Tg C $year^{-1}$ between 2001 and 2015 in Amazonia. We did not identify any temporal trend in the time-series (*Sen's Slope*=-0.22 Tg C $year^{-1}$, *MK*=-0.01 and *p*>0.05). We observed a carbon loss peak of 78 Tg C in 2005, while we recorded a minimum loss of 41 Tg C related to edge effect in 2001 (Figure 4a). In contrast, the total gross carbon loss from deforestation was 2,592 Tg C (2.59 Pg C), with an average of 173±46 Tg C $year^{-1}$, and a significant negative temporal trend of 6.90 Tg C $year^{-1}$ (*MK*=-0.51 and p<0.05) between 2001 and 2015. Unlike the observed pattern of carbon loss from forest edges, the peak of deforestation-related carbon loss occurred in 2004 (261 Tg C) and the minimum was recorded in 2013 (114 Tg C) (Figure 4b). Across all Amazonian countries, Brazil had the most substantial contribution for the Amazonia-wide carbon loss from both forest edges and deforestation, representing an average of 67±6% $year^{-1}$and 79±7% $year^{-1}$, respectively (Figure 4a and Figure 4b). At the same time, Suriname's forest edges and deforestation had the lowest contribution, with an average of 1.03±0.57% $year^{-1}$ and 0.48±0.35% $year^{-1}$ respectively (Figure 4a and Figure 4b).

Figure 4.6 – Temporal variability of carbon losses in Amazonia. (a) Temporal carbon loss variability by fragmentation. (b) Temporal carbon loss variability by deforestation. The bottom panels show the contribution as a percentage of each country to the annual carbon loss by edge effect (c) and deforestation (d).

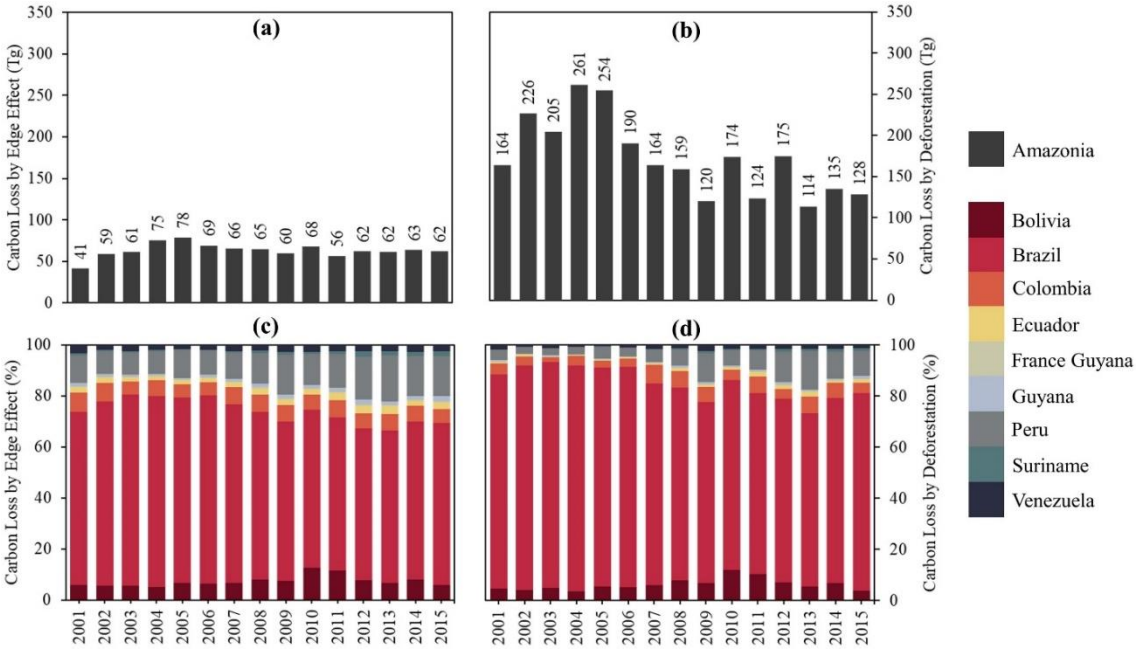


Overall, our findings show that the deforestation process leads to a collateral carbon loss of 37% related to the dynamics of forest edges in the Amazonia. Most strikingly, unlike the carbon loss from deforestation, which declined significantly during the analysed period, the additional carbon loss associated to the edge effect remained unchanged over time. It is interesting to note that the difference between carbon losses from deforestation and edge effect decreases over time. In 2001 deforestation promoted a loss of 122 Tg C greater than that observed for the edges, however, in 2015 this difference decreased to 66 Tg C (Figure S3a). During the studied period, hence, the carbon loss from forest edges that contributed to 25% of the loss from deforestation in 2001 increased to 48% in 2015 (Figure S3b). It is also important to note that in 2013 carbon loss induced by edge effect was more than half (54%) of the direct deforestation loss (Figure S3b).

Figure 4.7 – Comparison between the annual carbon losses from fragmentation and deforestation. (a) Annual difference between carbon losses from deforestation and from fragmentation. (b) Annual proportion of carbon losses from edge effect in relation to carbon losses from deforestation (losses from edge effect divided by losses from deforestation). Where “Def” is Deforestation an “EE” is Edge Effect.

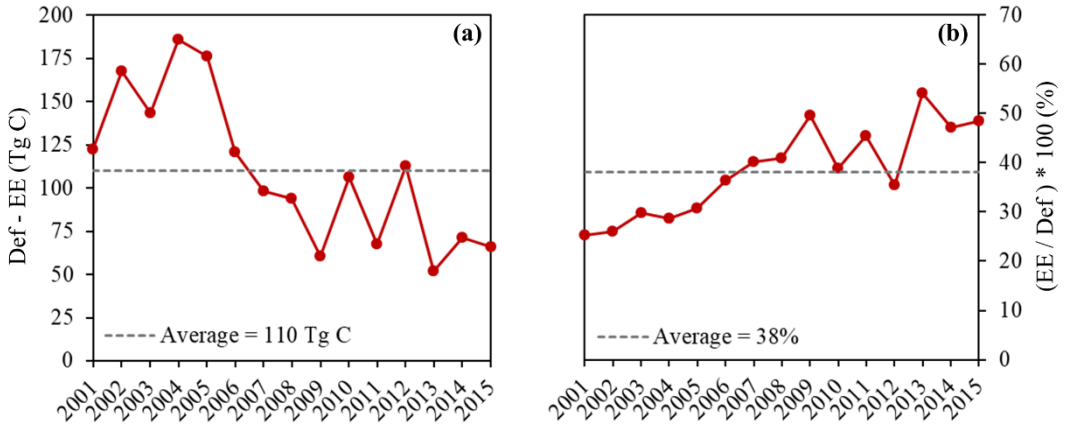


The analysis of temporal trend and average of carbon losses associated to edge effect and deforestation across all Amazonian countries (Table 2), showed that Ecuador, Guyana, Peru, and Suriname had a significant ($p$<0.05) positive trend in carbon losses both by edge effect and deforestation, varying between 0.01 and 0.41 Tg C year$^{-1}$ for edge effect, and between 0.01 and 0.65 Tg C year$^{-1}$ for deforestation. Only Brazil had a significant ($p$<0.05) negative temporal trend of deforestation-associated carbon loss, although loss from edges remained unchanged ($p$>0.05) over time. In contrast, Venezuela had a significant ($p$<0.05) positive trend in carbon loss from deforestation, but losses from edge effect remained unchanged ($p$>0.05) over time.

Table 4.4 – Temporal trend and average carbon losses induced by edge effect and deforestation for all Amazonian countries. Where S is the Man-Kendell statistics and SD the standard derivation. The S statistic with an asterisk (*) means a significant temporal trend at 95% of significance level ($p<0.05$).

| Country | Edge Effect | | | Deforestation | | |
|---|---|---|---|---|---|---|
| | S | Sen's Slope (Tg C year$^{-1}$) | Average±SD (Tg C year$^{-1}$) | S | Sen's Slope (Tg C year$^{-1}$) | Average±SD (Tg C year$^{-1}$) |
| Bolivia | 0.37 | 0.14 | 5±1.41 | -0.03 | -0.02 | 10±3.60 |
| Brazil | -0.31 | -0.58 | 42±7.67 | -0.61* | -8.41 | 139±47.68 |
| Colombia | -0.11 | -0.03 | 4±0.47 | -0.15 | -0.02 | 8±1.97 |
| Ecuador | 0.71* | 0.06 | 1±0.34 | 0.51* | 0.08 | 1±0.53 |
| France Guiana | 0.35 | 0.01 | 0±0.06 | 0.15 | 0.01 | 0±0.20 |
| Guyana | 0.71* | 0.04 | 1±0.23 | 0.41* | 0.04 | 1±0.28 |
| Peru | 0.73* | 0.41 | 8±1.97 | 0.63* | 0.65 | 11±4.25 |
| Suriname | 0.83* | 0.07 | 1±0.36 | 0.75* | 0.07 | 1±0.49 |
| Venezuela | 0.45* | 0.02 | 1±0.17 | 0.09 | 0.01 | 2±0.52 |

## 4.3 Discussion

### 4.3.1 Trends in deforestation across Amazonian countries

From our approach, we observed a significant decline in forest clearing processes between 2001 and 2015 in Amazonia. This decline followed the reduction in the deforestation rates observed in Brazil. The reduction of deforestation rates observed here for the Brazilian portion of Amazonia corroborates the progressive decline reported by the official deforestation system operating in Brazil (Figure S1) (INSTITUTO NACIONAL DE PESQUISAS ESPACIAIS (INPE), 2017). This reduction was a result of the strengthening of policies for prevention and control of deforestation in the region called Brazilian Legal Amazon, consolidated since the creation of the PPCDAm (*Plano de Ação para Prevenção e Controle do Desmatamento na Amazônia Legal*; Action Plan for Prevention and Control of Deforestation in the Legal Amazon) in 2004 (MINISTÉRIO DO MEIO AMBIENTE (MMA), 2013). During the first three phases of the PPCDAm (2004-2015), policies were created and actions implemented, including the creation and consolidation of near-real time systems for monitoring deforestation based on remote sensing, the intensification of law enforcement, the restriction of credit for illegal loggers, the creation and consolidation of conservation units and indigenous lands, as well as advances in land policy, such as the Rural Environmental Registry (*Cadastro*

*Ambiental Rural* – CAR) (MELLO; ARTAXO, 2017). However, from 2013 to 2019, an upward trend was observed in the official deforestation rates (INSTITUTO NACIONAL DE PESQUISAS ESPACIAIS (INPE), 2017), marked by an impressive rate of 10,129 $km^2$ in 2019, an increase of 34% compared to 2018 (7,536 $km^2$), the highest rate since 2008 (12,911 $km^2$). This upward trend was induced by environmental setbacks such as controversial changes in the Brazilian Forest Code in 2012 (BRANCALION et al., 2016), the recent weakening of deforestation enforcement, the dismantling of climate change policies (including the interruption of the PPCDAm from 2019), and the possibility regularization of public lands illegally grabbed (Bill nº 2,633/2020, former Provisional Measure nº 910/2019) (ASSOCIAÇÃO NACIONAL DOS SERVIDORES DE MEIO AMBIENTE (ASCEMA), 2020; BARLOW et al., 2020).

Although the PPCDAm was a key step for the reduction of the deforestation in the Brazilian Amazon, other external factors such as the soy and beef moratoria (NEPSTAD et al., 2014) also played a critical role. Companies, associated to the agribusiness, agREDD upon an embargo on soy and beef produced in illegal deforested areas. All these policies and actions inhibited illegal deforestation activities in the Brazilian Amazon, resulting in the significant decline of deforestation rates in Brazil after 2004. This pattern drove the overall trend of deforestation reduction across Amazonia.

Countries such as Ecuador, Guyana, Peru, and Suriname had, however, a significant increase in deforestation rates between 2001 and 2015. In Ecuador, the deforested areas were associated with increased commodity prices between 2005 and 2014, intensifying mineral and hydrocarbon extraction, agriculture production, logging, and palm cultivation (RAISG – AMAZONIAN NETWORK OF GEOREFERENCED SOCIO-ENVIRONMENTAL INFORMATION, 2015; LÓPEZ ACEVEDO, 2018). In Guyana (RAISG – AMAZONIAN NETWORK OF GEOREFERENCED SOCIO-ENVIRONMENTAL INFORMATION, 2015; DEZÉCACHE et al., 2017), Suriname (RAISG – AMAZONIAN NETWORK OF GEOREFERENCED SOCIO-ENVIRONMENTAL INFORMATION, 2015; DELVOYE; PARAHOE; LIBRETTO, 2018), and Peru (RAISG – AMAZONIAN

NETWORK OF GEOREFERENCED SOCIO-ENVIRONMENTAL INFORMATION, 2015; ASNER; TUPAYACHI, 2016), on the other hand, the increase in deforestation rates was mainly induced by activities related to illegal gold mining at different scales. Finally, countries such as Bolivia, Colombia, French Guiana, and Venezuela, had constant deforestation rates (no significant trends) between 2001 and 2015. These deforested areas were the result of agricultural, livestock, and mining activities (STEININGER et al., 2001; ARMENTERAS et al., 2006; RAISG – AMAZONIAN NETWORK OF GEOREFERENCED SOCIO-ENVIRONMENTAL INFORMATION, 2015; DEZÉCACHE et al., 2017), which potentiate the collateral impacts of edge effect on forest degradation and biodiversity loss (LAURANCE et al., 2018).

### 4.3.2 The collapse of above-ground carbon stocks in forest edges

Consistent with the decline in deforestation, we identified a significant decrease in the annual forest edge formation in Amazonia. The dynamics of forest edge formation result from the spatial and temporal patterns of deforestation, which defines the spatial arrangements and the geometries of the forest fragments (LAURANCE; LAURANCE; DELAMONICA, 1998; NUMATA et al., 2009). Landscapes arising from the deforestation process associated with the establishment of rural settlements (fish-bone pattern), have up to five times more forest edge areas per deforested land than landscapes dominated by large (regular shape) farms (LAURANCE; LAURANCE; DELAMONICA, 1998). The average rate of erosion of 11.47% within three years after forest edges creation and its subsequent increase to 42.80% after 12 years, found in our study, are lower than those found in previous studies at the local scale in the Amazon (NUMATA et al., 2009; HISSA et al., 2016). The lower rates found here are likely to be a result of two non-exclusive processes including a significant decrease in deforestation rates and the creation of more regular shape deforested polygons.

The drivers and historical trends of deforestation and forest edge creation are country-specific (NUMATA et al., 2009). Bolivia, Colombia, Venezuela, Peru and Suriname presented a large proportion of forest edges areas with one to six years old, which is explained by the intensification of deforestation in these countries in

recent years (KALAMANDEEN et al., 2018). The other Amazonian countries, as Brazil, have older forest edges areas, due to an older and more consolidate deforestation frontier, which stabilised by the end of the study period (KALAMANDEEN et al., 2018).

Our findings indicated that above-ground forest carbon progressively decreased in Amazonian Forest edges as a function of their ages. This pattern is corroborated by similar results found in Sabah, Malaysian Borneo (ORDWAY; ASNER, 2020). The losses observed in our study are greater in the first five years after the edge creation, which are consistent with field observations in controlled experiments in the Brazilian Central Amazon (LAURANCE et al., 1997; ALMEIDA et al., 2019) (Figure S4a). Following forest edge formation, mortality rates increase significantly (Figure S5c), amongst larger trees, which store most of the forest's carbon (LAURANCE et al., 2000; BRANDO et al., 2014). In addition, microclimatic changes, tend to increase wind turbulence and fire promoting an exacerbation of disturbance rates in the forest edges (LOVEJOY et al., 1986; KAPOS, 1989; CAMARGO; KAPOS, 1995; SIZER; TANNER, 1999; TRANCOSO, 2008). Together, these effects cause a steep initial reduction in carbon stocks following the edge formation. Subsequently, with the aging of the edges, turnover rates (LAURANCE et al., 1998), number of woody lianas (LAURANCE et al., 1997) and pioneer species increase, as a result of the successional process (NUMATA et al., 2017). Following this process, the plant community stablished in the forest edge tend to be better adapted to the new microclimatic conditions, sealing the edges (Figure S5d) and reducing the susceptibility to further microclimatic changes (CAMARGO; KAPOS, 1995; DIDHAM; LAWTON, 1999; D'ANGELO et al., 2004; LAURANCE et al., 2006). Although growth of new trees increases over time, turnover rates also increase (63), as a consequence of increasing mortality, so our age-carbon loss function (Figure S13) clearly capture the tendency of forest edges to reach an alternative post-fragmentation equilibrium state. This alternative state, which stabilizes between 6 and 15 years after the edge creation, is characterized by forests with lower above-ground biomass (AGB) than adjacent core areas. Field observations in controlled experiments in the Central Brazilian Amazon demonstrated a

significant reduction in canopy height as well as basal area and AGB up to 10 years after edge formation (ALMEIDA et al., 2019). The relationship between distance to edge and AGB was, however, no longer significant after 22 years of edge formation (ALMEIDA et al., 2019). It is important to note that, differently from Almeida et al. (ALMEIDA et al., 2019), in our analyses the AGB values are likely to remain below pre-fragmentation levels after 15 years, because most of the Amazonian edges are constantly exposed to the incidence of fire, which in the Brazilian Amazon can lead to a reduction in forest AGB of 24.8±6.9% after 31 years (SILVA et al., 2018b) (Figure S6). We expect the recovery of Amazonian Forest edges in few areas where secondary forests are growing adjacent to these edges, however these areas are likely to be minor as secondary forests in the Brazilian Amazon are limited to 34% (in 2018) of the total deforested area (1988-2018 period) (INSTITUTO NACIONAL DE PESQUISAS ESPACIAIS (INPE), 2017; SILVA JUNIOR et al., 2020c).

Figure 4.8 – Comparison between carbon losses calculated in this study and those calculated by Laurance et al. (1997) (LAURANCE et al., 1997). (a) Carbon loss average subset by classes of years after edge formation. (b) Magnitude of the difference between methods. Vertical bars are the standard deviations.

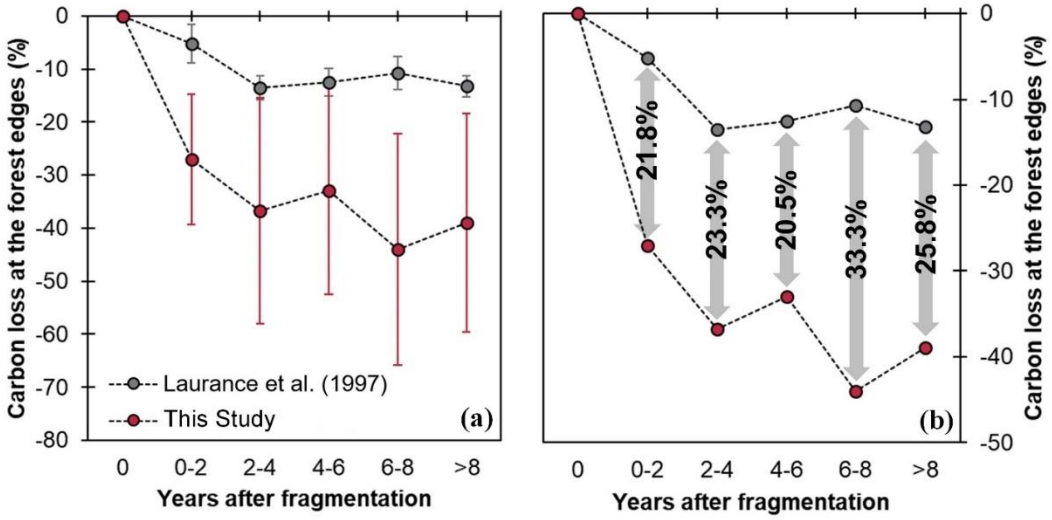

The estimated above-ground carbon (AGC) losses in our study are considerably higher (24.93±4.53% of difference) than that found by Laurance et al. (LAURANCE et al., 1997) in the local scale BDFFP long-term experiment (Figure S4b). These differences are expected as our Amazonia-wide analysis captures variations in factors influencing the stability of AGC in forest edges not contemplated by controlled local scales experiments such as: (i) multiple configurations of size, shape and types of land-use, and land-cover cover surrounding the forest edges (MESQUITA; DELAMÔNICA; LAURANCE, 1999) and mainly (ii) the impact of fires on forest edges (BRANDO et al., 2014; SILVA et al., 2018b). In Amazonia, fire typically occurs in forest edges (COCHRANE, 2001; COCHRANE; LAURANCE, 2002, 2008; ARMENTERAS; GONZÁLEZ; RETANA, 2013; ARMENTERAS et al., 2017; SILVA JUNIOR et al., 2018) by escaping from deforested areas, pastures and agricultural fields and leaking into surrounding forests (ARAGÃO et al., 2008; CANO-CRESPO et al., 2015). Moreover, fire in forest edges often damages the remaining trees, increasing their vulnerability to strong wind events, enhancing tree mortality rates (SILVÉRIO et al., 2019b). Finally, during the 21$^{st}$ century, Amazonia has been exposed to an increased frequency of extreme droughts (MARENGO; ESPINOZA, 2016; MARENGO et al., 2018), which may induce the reduction of forest carbon stocks, either by the direct effect of drought on tree mortality (BRIENEN et al., 2015) or by the collateral effect of increased fire incidence at the forest edges during these extreme events (ARAGÃO et al., 2007, 2018; SILVA JUNIOR et al., 2019a).

### 4.3.3 Implications for carbon emissions reduction policies

Here we showed at the Amazonian scale, that forest carbon loss induced by edge effect was one-third of the carbon loss caused by deforestation during the 2001-2015 period. Furthermore, our trend analysis showed that although deforestation-related carbon loss decreased significantly between 2001 and 2015, edge effect-related carbon loss remained unchanged. Knowing that part of the carbon losses in the forest edges is emitted to the atmosphere following the decomposition process, our findings clearly show that deforestation-induced edge effect can

indirectly increase emissions from deforestation alone by 37%, with implications for policies aiming to reduce in carbon emissions by avoiding deforestation.

To show the impact of neglecting carbon losses from edge effect on the calculation of gross deforestation emissions (Figure S7), we compared (Wilcoxon's test) carbon losses from each process before (between 2001 and 2004) and after (between 2005 and 2015) the implementation of the Action Plan for Prevention and Control of Deforestation in the Legal Amazon – PPCDAm (MINISTÉRIO DO MEIO AMBIENTE (MMA), 2013). The PPCDAm was the central policy responsible for the decline in deforestation rates in the Brazilian Amazon (MINISTÉRIO DO MEIO AMBIENTE (MMA), 2013; INSTITUTO NACIONAL DE PESQUISAS ESPACIAIS (INPE), 2017). We found that annual carbon loss associated to deforestation alone decreases significantly (41%, $W$=40 and $p$=0.02) from 187±21 Tg year$^{-1}$ in the pre-PPCDAm period to 111±39 Tg year$^{-1}$ in the post-PPCDAm period. The annual carbon loss associated to edge effect, conversely, in the pre-PPCDAm phase (43±6 Tg year$^{-1}$) was not statistically different ($W$=25 and $p$=0.75) from the value calculated for the post-PPCDAm period (40±7 Tg year$^{-1}$).

Figure 4.9 – Comparison between carbon losses from deforestation and edge effect before (between 2001 and 2004) and after (between 2005 and 2015) the creation of PPCDAm (MINISTÉRIO DO MEIO AMBIENTE (MMA), 2013) (Action Plan for Prevention and Control of Deforestation in Legal Amazon) in the Brazilian Amazon. (a) Losses from deforestation. (b) Losses from edge effect. The horizontal black line is the average, the red triangle is the median, the black vertical line is the standard deviation, and in blue the values of the statistic (*W*) and p-value (*p*) of the Wilcoxon statistical test.

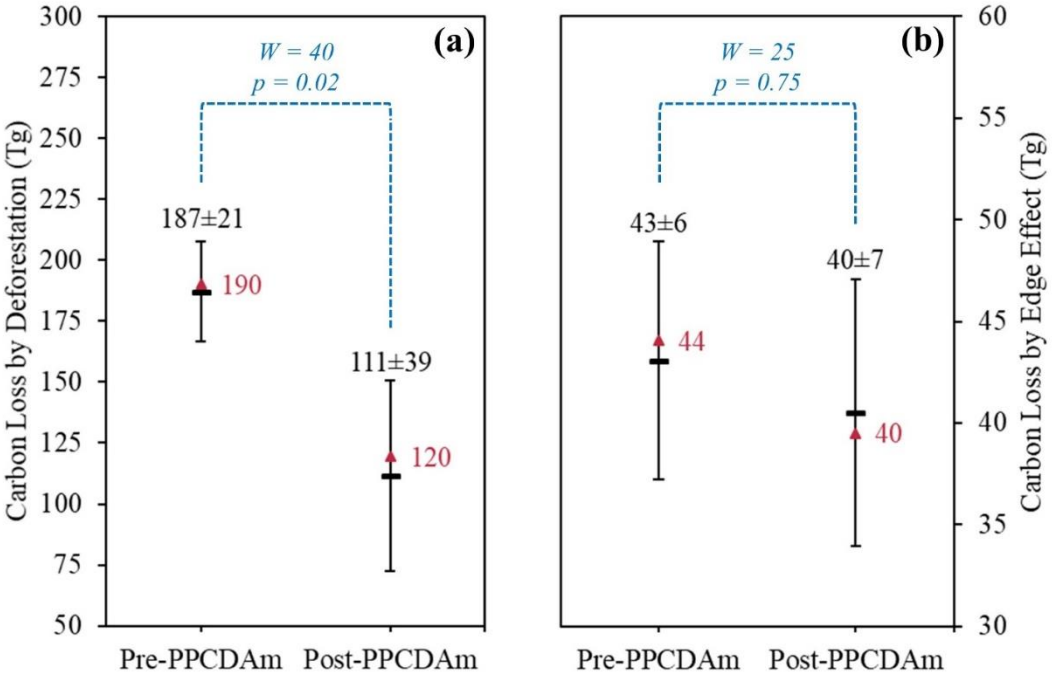


Our analysis points to two critical issues: First, because the carbon loss induced by edge effect is persistent over time, even with deforestation slowing down, extra emissions from the newly formed edges reduce de effectiveness of actions for reducing carbon emissions by avoiding deforestation, such as the REDD+ policy. The inclusion of the edge effect process into systems for Monitoring, Reporting, and Verifying emissions (MRV) is, hence crucial. Secondly, we show that reducing deforestation carbon loss does not change edge-induced carbon loss, indicating the need of new mechanisms to avoid or to compensate the potential carbon emissions associated to edge effect. These could be related to landscape planning, which is not only necessary to be implemented in Amazonian countries, but also in other tropical countries such as Africa and Asia. Besides, the recent deforestation upward trend in the Brazilian Amazon, has a negative implication, the increase of carbon losses from deforestation, directly, and edge effect induced by the creation of new forest edges.

Decreasing uncertainties in emissions estimates from land-use and land-cover change can support the establishment of more effective national actions, helping Amazonian countries to accomplish with emission reductions targets proposed at international climate agreements, such as the Paris Agreement. The Paris Agreement aims to establish volunteer emission reduction actions and targets by the signatory countries to be reached by 2025, to strengthen the global response to the threat of climate change (UNFCCC – FRAMEWORK CONVENTION ON CLIMATE CHANGE, 2015b). For combating the effects of climate change, it is critical to maintain the global average temperature rise below 2°C from pre-industrial levels and efforts to limit the temperature increase to 1.5°C (IPCC – INTERGOVERNMENTAL PANEL ON CLIMATE CHANGE, 2018). To achieve this goal, there is a pressing need for a 45% and 100% reduction in greenhouse gas emissions by 2030 and 2055, respectively (MASSON-DELMOTTE et al., 2018). Our results indicate that there is a significant missing source to be considered in the Amazonian carbon budget. Including carbon losses related to edge effect in regional and global carbon budgets is, hence, crucial for accurately estimate the land-use and land-cover change contribution to the atmospheric carbon burden. In conclusion, carbon losses associated to the edge effect in Amazonia are an additional unquantified carbon flux that can counteract carbon emissions avoided by reducing deforestation, compromising the Paris Agreement's bold targets.

## 4.4 Materials and methods

Our materials and methods are included in the following five steps: (i) forest cover mapping; (ii) identification of forest edges and quantification of age structure; (iii) carbon stock mapping from LiDAR data; (iv) carbon stock loss model by edge effect and deforestation; (v) statistical analysis; (vi) sources of uncertainty.

### 4.4.1 Forest cover mapping

We produced 16 annual forest cover maps from 2000 to 2015 with 30-m spatial resolution for Amazonia. The maps included old-growth forests, secondary forests (before 2000) and planted forests. We adopted the delimitation of the Amazonia *sensu latissimo* proposed by Eva et al. (EVA et al., 2005), excluding

the Andes and Planalto regions. This limit encompasses an area of 6,673,908 $km^2$, including areas from Brazil, Bolivia, Peru, Ecuador, Colombia, Venezuela, Guyana, Suriname, and French Guiana. All nine countries together host 95% of the remaining Amazonian old-growth forests (EVA et al., 2005).

To produce the forest cover maps, we used version 1.3 of the Global Forest Change dataset (https://earthenginepartners.appspot.com/science-2013-global-forest/download_v1.3.html) (HANSEN et al., 2013), which includes three products: (i) tree canopy cover (2000), (ii) forest cover loss (2001-2015) and (iii) forest cover gain (2000-2012) data. We also used the maximum water extent data (1984-2015) (https://global-surface-water.appspot.com) (PEKEL et al., 2016). All the data mentioned above are made available at 30-m spatial resolution. The temporal coverage of the datasets comprehends the pre-PPCDAm (between 2001 and 2004) and post-PPCDAm (between 2005 and 2015) period, implemented in the Brazilian Amazon for curbing illegal deforestation.

Initially, to produce the year 2000 forest map baseline, we applied the threshold of 80% tree canopy cover (Figure S8a) for defining the old-growth forest area, as suggested by Gasparini et al. (GASPARINI et al., 2019b) (Figure S8b). This threshold avoids the inclusion of non-forest formations (e.g., savannas) in Forest class (GASPARINI et al., 2019b). The forest class, hence, included all pixels with a percentage of tree canopy cover equal or greater than 80%, and as non-forest class all pixels with a tree canopy cover percentage of less than 80%. Subsequently, we removed all pixels with forest cover gain between 2000 and 2012 (Figure S8c). This procedure allowed the removal all secondary forest pixels start regrowing between 2000 and 2012. Wetland forests were also removed by intersecting the forest cover map with the map of flooded areas between 1984 and 2015 (Figure S8d).

Then, to obtain the forest maps (2001-2015), we removed year by year pixels with forest cover loss between 2001 and 2015 from the 2000 forest map, by using Boolean logic using the two sets of maps (Figure S8e). For instance, to obtain the 2001 forest map using this procedure, all pixels with forest cover loss in 2001

were removed from the 2000 forest map. This procedure was repeated across all years (2001-2015).

Finally, to avoid the effect of isolated single pixels, for both Forest and non- Forest classes, we applied a move window filter for all annual forest maps (16 maps in total). We adopted the Sieve algorithm (https://www.gdal.org/gdal_sieve.html) from the Geospatial Data Abstraction Library – GDAL (https://www.gdal.org). The GDAL Sieve algorithm removes pixels smaller than a provided threshold (give in pixels) and replaces them with the pixel of neighbour value. Here we used the five-pixel threshold, which includes patches greater than four pixels (0.0036 $km^2$ or 0.36 ha).

### 4.4.2 Identification of forest edges and quantification of age structure

Using the forest cover maps (Figure S9a), we produced 16 forest edges maps (2000 to 2015). For this study, we adopt a 100-m as the edge width, assuming the most significant AGC stocks loss typically occur within this distance in Amazonia (LAURANCE et al., 1997; NUMATA et al., 2017). However, due to the spatial resolution (30-m) of our data, we considered for our analyses a width of 120 m, equivalent to four pixels, to define the forest edges. Initially, we attributed a null value for each pixel corresponding to the Forest class for the 16 forest cover maps (Figure S9b). Subsequently, all pixels with the null value were filled with the Euclidean distance value (DANIELSSON, 1980) calculated from the non-forest class (Figure S9c). Finally, the calculated Euclidean distance was used to classify the pixels based on distance intervals, using three classes: non-forest class (equal to 0m), Forest class (greater than 120-m) and Forest-edge class (between 30 and 120m) (Figure S9d).

Using the forest edges maps, we produced 15 forest edges age maps (2001 to 2015). Firstly, we removed from the forest edges maps (2001 to 2015) all the edges in 2000, which had an area of 416,793 $km^2$ (6.25% of Amazonia territory), because of the impossibility of estimating the age of forest edges in the year 2000. This first step also removed all natural forest edges formed at the boundaries between forest-water and forest-savannas, which were not of interest

for our study. Then, we transform the forest edges maps into binary maps, where we assign the value of “1” to the forest edge class and “0” to the forest and non-Forest classes. Finally, we use the map algebra method to calculate the forest edges age, by summing the binary maps year by year cumulatively. From this procedure we obtained binary maps from 2001 to 2015, with the 2001 age map having only forest edges with one year old and the 2015 map having edges ranging from 1 to 15 years old (Figure S10).

### 4.4.3 Carbon stock mapping from LiDAR data

We produced 20 carbon maps with 50m spatial resolution, using a multitemporal LiDAR point clouds dataset, collected in 13 flight lines within the Brazilian Amazon (Figure S11 and Table S4). The LiDAR data were obtained from the Sustainable Landscapes Project (https://www.paisagenslidar.cnptia.embrapa.br), which were collected using a LiDAR Airborne System with flights carried out between 2012 and 2015, totalling an area of 153.17 $km^2$. All the LiDAR plots have a point density higher than four points per squared meters (LEITOLD et al., 2015) (Table S4).

Figure 4.10 – Spatial distribution of the LiDAR flight lines in Amazonia. Brazilian States: AC, Acre; AM, Amazonas; AP, Amapá; MA, Maranhão; MT, Mato Grosso; PA, Pará; RO, Rondônia; RR, Roraima; TO, Tocantins.

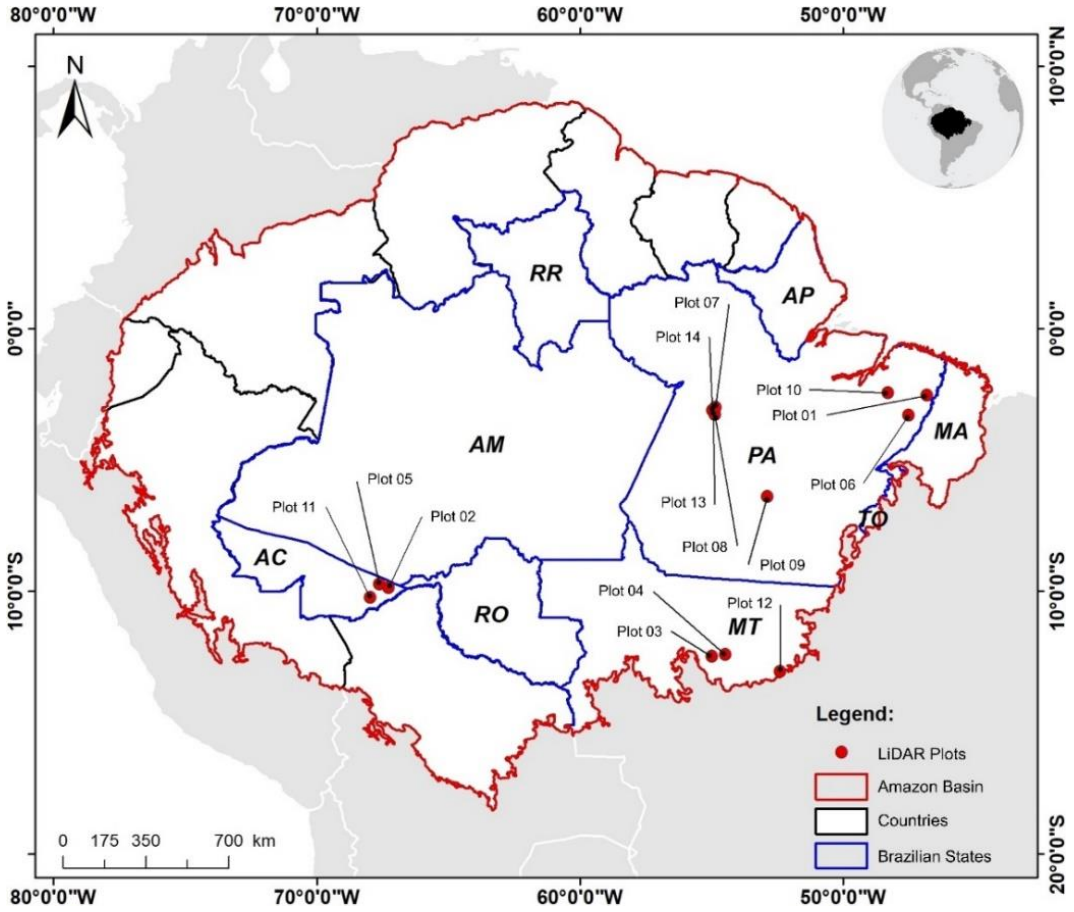

Table 4.5 – Technical specifications of the instrument, aircraft and data collection settings for the LiDAR flight lines.

| LiDAR Plots | Year of Acquisition | Average Return Density (points $m^{-2}$) | Average Density of First Return (points $m^{-2}$) | Average Flight Altitude (m) | Field of View (degree) |
|---|---|---|---|---|---|
| Plot 1 | 2013 | 16.80 | 9.30 | 853.40m | 11.00 |
| Plot 1 | 2014 | 38.20 | 17.20 | 853.40m | 11.00 |
| Plot 2 | 2013 | 33.39 | 15.57 | 900.00m | 11.10 |
| Plot 3 | 2013 | 38.34 | 25.84 | 853.00m | 9.80 |
| Plot 4 | 2015 | 38.59 | 29.82 | 850.00m | 12.00 |
| Plot 5 | 2013 | 66.61 | 30.48 | 900.00m | 11.10 |
| Plot 6 | 2013 | 11.78 | 6.58 | 853.40m | 11.00 |
| Plot 6 | 2014 | 40.00 | 17.75 | 853.40m | 11.00 |
| Plot 7 | 2015 | 49.53 | 26.40 | 850.00m | 12.00 |
| Plot 8 | 2015 | 58.67 | 29.16 | 850.00m | 12.00 |
| Plot 9 | 2012 | 30.10 | 20.40 | 850.00m | 11.00 |
| Plot 10 | 2013 | 24.25 | 15.14 | 853.40m | 9.80 |
| Plot 11 | 2014 | 40.70 | 18.40 | 900.00m | 11.10 |
| Plot 11 | 2013 | 10.80 | 5.20 | 900.00m | 11.10 |
| Plot 12 | 2012 | 13.70 | 7.05 | 850.00m | 11.00 |
| Plot 12 | 2014 | 41.05 | 16.70 | 853.00m | 10.00 |
| Plot 13 | 2012 | 36.90 | 23.11 | 850.00m | 11.10 |
| Plot 13 | 2013 | 29.95 | 17.12 | 853.40m | 11.00 |
| Plot 14 | 2012 | 38.90 | 23.90 | 850.00m | 11.10 |
| Plot 14 | 2013 | 29.95 | 17.12 | 853.40m | 11.00 |

We performed all LiDAR point clouds data processing in the FUSION 3.60 software (http://forsys.cfr.washington.edu/fusion/fusionlatest.html). Initially, we filtered the points classified as terrain for each LiDAR plot. Then, from the previously filtered points, we created Digital Terrain Models – DTM with 1-m spatial resolution (Figure S12a). Subsequently, we normalised (altitude-to-height conversion) all points classified as vegetation using the DTM, to create for each flight line a Canopy Height Model – CHM with -m spatial resolution (Figure S12b).

We used the methodology proposed by Longo et al. (LONGO et al., 2016) to calculate above-ground forest carbon (for living trees) using the LiDAR data. To apply this method, we first created a 50-m spatial resolution CHM, using the average of the canopy heights at 1-m spatial resolution (Figure S12c). Then, we

applied Equation 4.1 (LONGO et al., 2016) for each 50-m of spatial resolution pixel in the CHM map.

$$C_{Stock} = 0.025 \cdot CHM_{50m}^{1.99} \qquad (4.1)$$

where $C_{Stock}$ is the carbon stock of each pixel in kg $m^{-2}$ (subsequently converted to Mg $ha^{-1}$, multiplying the result by 10), and $CHM_{50m}$ is the pixel value at 50m of spatial resolution in the Canopy Height Model (CHM). This equation had an adjusted $R^2$ of 0.68 and a Mean Square Error of 4.33 kg C $m^{-2}$ (LONGO et al., 2016).

### 4.4.4 Carbon stock loss model by edge effect and deforestation

We use LiDAR carbon stock and forest edges age maps to model the carbon loss in forest edges as a function of edges age. Firstly, we overlaid the carbon stock map, of each LIDAR flight line, on the forest edge map to extract the carbon values for pixels in the forest edge and interior classes. For this approach, we considered the LiDAR collected at the same year as their respective forest edges age map. Then, we calculated the carbon average for the forest interior, which was consider as control areas, not impacted by edge effects (LAURANCE et al., 1997; NUMATA et al., 2017). We also calculated the carbon average for the forest edges stratified by their respective ages. Finally, we calculated the percentage difference between the forest interior and forest edges AGC stocks for each age, leading to 152 samples of the carbon loss percentage for different edge ages.

Based on the conceptual model proposed by Melito et al. (MELITO; METZGER; DE OLIVEIRA, 2018), we employed a non-linear rectangular hyperbolic regression (Michaelis-Menten kinetic equation, $R^2$=0.780) (Equation 2) using the average carbon loss stratified by forest edge ages (Figure S13a). From a bootstrap approach (KUSHARY; DAVISON; HINKLEY, 2000), we calculate the 95% confidence intervals for all equation parameters based on 1000 random repetitions with replacement using the “boot” package (Package ‘boot’) implemented in the R statistical software (R CORE TEAM, 2018) (version 3.4.4; https://www.r-project.org).

$$C_{Loss} = \frac{-42.815(\pm 2.966) \cdot E_{Age}}{0.836(\pm 0.411) + E_{Age}} + \varepsilon \qquad (4.2a)$$

$$\textit{Where } \varepsilon \sim N(0, 5.767^2) \qquad (4.2b)$$

where $C_{Loss}$ is the carbon stock loss in percentage as a function of forest edge age, $E_{Age}$ is the edge age for the specific year, -42.815 is the value of the α parameter, and 0.836 is the value of the β parameter, ε is the estimated error for the equation, and 5.767 is the residual standard error. The values in parentheses were obtained through the 1000 bootstrap interactions process and represent the variation of each parameter, considering a 95% confidence interval. From the Equation 2a decay curve, we calculated the individual carbon loss percentage for each forest edge age (Figure S13b and Tab. S5).

Figure 4.11 – Above-Ground Carbon Stock Loss Model by Edge Effect. (a) Fitting of the Michaelis-Menten kinetic curve on the measured values. (b) Carbon loss decay rate based on the model in Fig S13a.

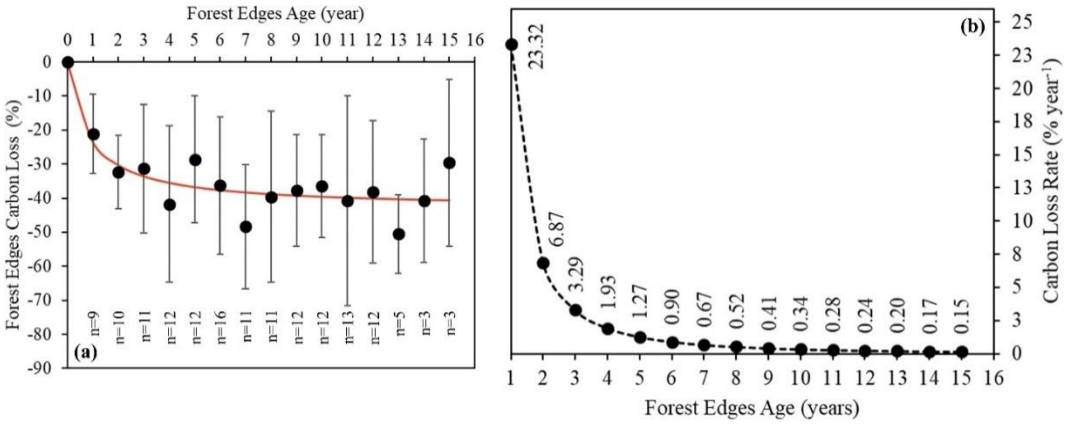

Table 4.6 - Carbon loss factor (f) for the calculation of carbon loss from edge effect.

| Forest Edges Ages (year) | Accumulated Carbon Loss (%) | Carbon Loss Rate (% year$^{-1}$) | Carbon Loss Factor (*f*) |
|---|---|---|---|
| 1 | 23.324 | 23.324 | 0.233 |
| 2 | 30.198 | 6.873 | 0.069 |
| 3 | 33.487 | 3.289 | 0.033 |
| 4 | 35.416 | 1.929 | 0.019 |
| 5 | 36.684 | 1.268 | 0.013 |
| 6 | 37.581 | 0.897 | 0.009 |
| 7 | 38.249 | 0.668 | 0.007 |
| 8 | 38.765 | 0.517 | 0.005 |
| 9 | 39.177 | 0.412 | 0.004 |
| 10 | 39.513 | 0.336 | 0.003 |
| 11 | 39.792 | 0.279 | 0.003 |
| 12 | 40.027 | 0.236 | 0.002 |
| 13 | 40.229 | 0.201 | 0.002 |
| 14 | 40.403 | 0.174 | 0.002 |
| 15 | 40.555 | 0.152 | 0.002 |

To extrap6late the percent changes in AGC stocks (carbon loss) from the forest edges, we first combined the annual age maps with a forest AGB density map a pixel-by-pixel approach (30-m spatial resolution), attributing to each edge pixel an initial (pre-edge formation) biomass value ($AGB_{Pixel}$). We carried out a similar procedure for the deforested pixels. We used the GFW (Global Forest Watch) forest biomass density map at 30-m spatial resolution, which was elaborated based on the method proposed by Baccini et al. (BACCINI et al., 2012) (https://data.globalforestwatch.org/datasets/aboveground-live-woody-biomass-density). This part of the method was implemented in Google Earth Engine - GEE platform (GORELICK et al., 2017).

For estimating Amazonia-wide edge effect on carbon loss between 2001 and 2015, we applied Equation 4.3 for each pixel.

$$CL_{Pixel} = L_{Factor} \cdot AGB_{Pixel} \cdot 0.5 \cdot 0.09 \qquad (4.3)$$

where $CL_{Pixel}$ is the pixel carbon loss at the forest edges given in Mg per pixel, $L_{Factor}$ is the loss factor for each forest edge age, calculated based on equation 2a (Table S5), $AGB_{Pixel}$ is the pre-edge or pre-deforestation AGB value of the pixel, obtained by the previous integration step, 0.5 is the AGB to AGC conversion

factor (CHAVE et al., 2005), and 0.09 is the conversion factor to transform carbon density in Mg ha$^{-1}$ to total carbon for the entire pixel area (0.09 ha).

For calculating the Amazonia-wide loss of C associated to the deforestation process, between 2001 and 2015, we applied Equation 4.4 for each pixel.

$$CL_{Pixel} = L_{Factor} . AGB_{Pixel} \cdot 0.5 \cdot 0.09 \qquad (4.4)$$

All terms in equation 4 are similar to those in equation 3, however, $L_{Factor}$ in this case is set to "1", indicating that all carbon stored in the pixel (100%) will be lost following the deforestation process.

Finally, to present in the maps the results of carbon losses across Amazonia associated to edge effect and deforestation, we aggregated all original pixels values at a 30-m spatial resolution into grid-cells with 10-km spatial resolution using the sum of the values.

### 4.4.5 Statistical analysis

Here we used nonparametric statistical approaches, for all analyses. For testing the temporal trends, we used the Mann-Kendall test and the Sen's Slope Estimator. To compare forest edges ages and carbon losses among Amazonian countries we used the Kruskal-Wallis test and the Wilcoxon test. All analyses were performed using the R statistical software (R CORE TEAM, 2018) (version 3.4.4; https://www.r-project.org). For the Kruskal-Wallis and the Wilcoxon test, we used the "agricolae" package (MENDIBURU, 2017), whereas for the Mann-Kendall test and the Sen's Slope Estimator the "wq" package (JASSBY; CLOERN, 2016) was used. For all statistical analysis, we adopted the significance level of 95% ($p \leq 0.05$).

To analyse the temporal trend in deforestation rates, forest edge increment, and forest carbon loss, we used the Mann-Kendall test (MANN, 1945; KENDALL, 1975). Then we calculated the magnitude of the changes by the application of Sen's Slope method (SEN, 1968). The Mann-Kendall test is used to assess whether there is a monotonic upward or downward trend over a time period, whereas the Sen's Slope Estimator, a robust nonparametric method with little

sensitivity to outliers, is used to estimate the magnitude of trends by the calculation of the median of the slopes of each pair of points in the data.

To verify the existence of significant differences in the forest edges ages among the Amazonian countries, we used the Kruskal-Wallis test (HETTMANSPERGER; MCKEAN, 2010). The Kruskal-Wallis test is equivalent to the Analysis of Variance (ANOVA), which compares three or more groups to test the hypothesis that they have the same distribution. To determine how the analysed variables, differ from each other, we performed a paired posthoc test. In the posthoc test, we used the Fisher's least significant difference criterion with Bonferroni adjustment methods correction (CONOVER, 1999b).

Finally, to verify the existence of significant differences in carbon losses associated to edge effect and deforestation between the period before (between 2001 and 2004) and after (between 2005 and 2015) the PPCDAm (Action Plan for Prevention and Control of Deforestation in the Legal Amazon) (MINISTÉRIO DO MEIO AMBIENTE (MMA), 2013) implementation, we used the Wilcoxon test for independent samples (HETTMANSPERGER; MCKEAN, 2010). The Wilcoxon test, which is equivalent to the student's t-test, compares two independents groups to test the hypothesis that they have the same median. We use the Fisher's least significant difference criterion with Bonferroni adjustment methods correction (CONOVER, 1999b).

### 4.4.6 Sources of uncertainty

Our estimations of carbon losses associated to edge effect and deforestation were performed from 2001 onwards due to the lack of forest-cover, forest-change, and biomass data for Amazonia before this period. Thus, our estimates do not account for historical carbon losses before 2001. In 2000 we estimate an area of edge-affected forests (including natural edges) of 416,793 $km^2$ (82% of the total edge area in 2015) within 120m of edge length, while accumulated deforestation in 2000 accounted for 591,414 $km^2$ (RAISG - AMAZONIAN NETWORK OF GEOREFERENCED SOCIO-ENVIRONMENTAL INFORMATION, 2015) across Amazonia.

Regarding the accuracy of remote sensing products, the 2000 forest map produced from the 80% tree cover percentage threshold has an overall accuracy of 82% (GASPARINI et al., 2019b), while forest cover change data has an overall accuracy of 99.5% (HANSEN et al., 2013). The biomass map (BACCINI et al., 2012) used has uncertainties from allometric equations, the LiDAR-based model, and the random forest model; however, we used the latest and improved map with a low level of uncertainty (https://data.globalforestwatch.org/datasets/aboveground-live-woody-biomass-density).

The effective edge distance of 120 m used was based on the well-documented landscape scale experiment in Central Brazilian Amazon (Manaus state) published by Laurence et al. (LAURANCE et al., 1997), although carbon loss may occur up to 300 m of edge (LAURANCE et al., 1997), making our carbon loss estimates conservative. Moreover, the variation of the penetrability of the carbon collapse from the edge to the interior of the forest throughout Amazonia is still unknown, making unfeasible at this stage the implementation of a function representing this variation in our analyses. The fix edge distance of 120 m, hence, is the most appropriated threshold, as it is conservative, comparable with other studies (NUMATA et al., 2010, 2011; HISSA et al., 2016) and with effects on forest biomass well documented in the literature. In our analysis, we assumed that the open and closed edges are equally impacted by edge effects, although these impacts may assume different magnitudes depending on the edge type, as suggested by Didham and Lawton (DIDHAM; LAWTON, 1999).

Although our forest carbon loss estimates associated to edge effect consider a global model for the entire Amazon, our approach represents an advance in relation to previous studies (NUMATA et al., 2010, 2011; PÜTZ et al., 2014; HISSA et al., 2016; BRINCK et al., 2017; MAXWELL et al., 2019), contributing to an improved understanding of the collateral impacts of deforestation on Amazonian carbon stocks. Finally, unlike previous studies (NUMATA et al., 2010, 2011; PÜTZ et al., 2014; HISSA et al., 2016; BRINCK et al., 2017; MAXWELL et al., 2019), our estimates of carbon loss were based for the first time on samples

derived from various regions of the Amazon, describing the gradual decay of carbon at forest edges over 15 years.

## 4.5 Graphical abstract

Figure 4.12 – Graphic summary of the main results found in chapter.

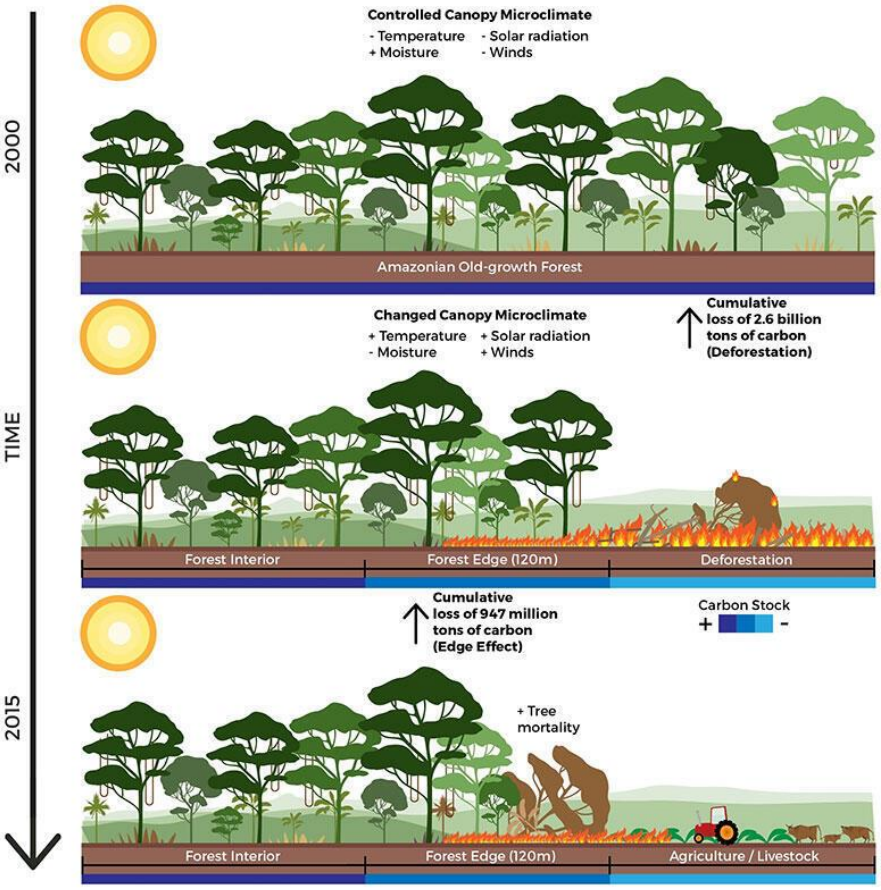

# 5 LARGE-SCALE CARBON COLLAPSE AT TROPICAL FOREST EDGES[5]

## 5.1 Introduction

The increase in the concentration of carbon dioxide ($CO_2$) in the atmosphere is a result of anthropogenic emissions, related to disturbances in carbon reservoirs due to the use of fossil fuels and land-use and land-cover changes (CIAIS et al., 2013). Thus, understanding the greenhouse gas emissions sources is an important tool for designing efficient policies to reduce emissions.

The Paris Climate Agreement (UNFCCC - FRAMEWORK CONVENTION ON CLIMATE CHANGE, 2015c; CLÉMENÇON, 2016), which deals with measures to reduce greenhouse gas emissions from 2020 on by the signatory countries, reinforces the need to strengthen the global response to the threat of climate change. Thus, it is necessary to keep the increase in the Earth's average global temperature below 2°C in relation to pre-industrial levels, and efforts must be made to limit the increase in temperature to up to 1.5°C compared to pre-industrial levels; for this would require a 45% reduction in greenhouse gas emissions by 2030 and 100% by 2055 (MASSON-DELMOTTE et al., 2018). However, at the 2021 United Nations Climate Change Conference (COP26) few advances in nations' ambitions to reduce their emissions were observed (ARORA; MISHRA, 2021; FERRANTE; FEARNSIDE, 2021).

In the tropical region, the process of deforestation has converted forests into agriculture, livestock, and urban areas (KISSINGER; HEROLD; SY, 2012; MALHI et al., 2014; CARTER et al., 2018). As a result, these forests declined from 1,965 million hectares in 1990 to 1,777 million hectares in 2015, totalling 10% of loss (KEENAN et al., 2015). This reduction compromises essential ecosystem services, such as biodiversity, climate regulation, carbon storage/cycling, and water supply (FOLEY, 2005; BACCINI et al., 2017). Tropical forests store

[5] This Chapter has not yet been published and will be submitted to the scientific journal Nature.

between 193 and 229 Pg of carbon in their biomass (SAATCHI et al., 2011; BACCINI et al., 2012).

Deforestation led to habitat loss, which alters the structure of the forest through the edge effect. Edge effect is a consequence of fragmentation, which can be measured or characterized by quantifying edge areas and number of patches, in addition to reducing the connectivity of forest remnants (FAHRIG, 2003; VILLARD; METZGER, 2014; VEDOVATO et al., 2016; SILVA JUNIOR et al., 2018, 2020a; TAUBERT et al., 2018). Edge effect adversely affects forest functioning, reducing carbon stocks and loss of diversity (LAURANCE et al., 1997, 2018; SILVA JUNIOR et al., 2020a). According to Haddad et al. (2015), about 70% of global forest remnants are subject to edge effects.

In the current climate crisis, which poses an urgent and potentially irreversible threat to human societies and the Earth (UNFCCC - FRAMEWORK CONVENTION ON CLIMATE CHANGE, 2015a), the tropical forest edges, which are an important source of atmospheric carbon (NUMATA et al., 2011; PÜTZ et al., 2014; BRINCK et al., 2017; SILVA JUNIOR et al., 2020a), are not yet explicitly measured and included in policies to reduce greenhouse gas emissions (SILVA JUNIOR et al., 2021a).

In the past, the large-scale understanding of the edge effect contribution to $CO_2$ emissions was limited by the lack of multi-temporal maps of forest cover with appropriate spatial resolution. Currently, the bound is a representative method of the variability of the tropical region. However, recent advances in remote sensing, especially with the widespread use of optical multitemporal data and LIDAR (Light Detection And Ranging) data, can fill these gaps.

Recent computational advances allow geospatial analysis on a planetary scale (GORELICK et al., 2017), adding to the availability of a long series of Earth observation data from the Landsat Program (WULDER et al., 2016), resulting in the first mapping of forest cover and loss on a global scale with improved detail (HANSEN et al., 2013; VANCUTSEM et al., 2021). In addition, recent advances in estimating forest biomass at large scale (LONGO et al., 2016; XU et al., 2017;

FERRAZ et al., 2018; POTAPOV et al., 2021) from remote sensing approach, provide quantitative and detailed information on the forest structure (GARCIA et al., 2017), create an unprecedented opportunity for exploration of these data in the context of the effect of forest fragmentation on the carbon stocks of tropical forests.

Therefore, in this study we aim to provide the first spatially and temporally explicit quantification od $CO_2$ emissions from forest edges and estimate the additional contribution to deforestation-induced carbon losses. Specifically, we: (i) analysed 31-years (1990-2020) of readily available 30-m spatial resolution Landsat-based forest cover change dataset (VANCUTSEM et al., 2021) to quantify the dynamics and age distribution of forest edges Tropical-wide; (ii) created a 100-m spatial resolution map of tropical carbon stocks in 2019 to build empirical carbon loss models as a function of forest edge age; and finally (iii) modelled the edge-induced carbon loss by applying the age-loss models across all tropical region. Our model is grounded on the observation (ORDWAY; ASNER, 2020; SILVA JUNIOR et al., 2020a) and concept (MELITO; METZGER; DE OLIVEIRA, 2018) that tropical forest edges formed by deforestation continuously reduce their carbon stocks with age. Thus, we hypothesize that direct $CO_2$ emissions by tropical deforestation are followed by incremental indirect carbon losses induced by the aging of forest edge, and which can be increased by the effect of degradation (selective logging and fire disturbances).

## 5.2 Impact of edge effects in tropical forests above ground carbon (AGC)

In the tropical region, previous evidence has showed a significant decline in aboveground biomass (AGB) within 100-m forest edges in Amazonia (LAURANCE; LAURANCE; DELAMONICA, 1998), 300-m in Congo basin (SHAPIRO et al., 2016), 448-m in Asia (QIE et al., 2017), and 500-m across the tropics (CHAPLIN-KRAMER et al., 2015). However, our finds revealed that the impact of edge effects surpass or match with already distances reported and vary between regions. We found that the edge effect in the tropical region can reduce aboveground carbon (AGC) within 369±45-m forest edges in America, 351±33-m in Africa and 415±61-m in Asia (Figure 5.1).

Figure 5.1 – Models and breakpoint (dashed vertical lines) for carbon stocks as a function of distance from forest edges for the three tropical regions.

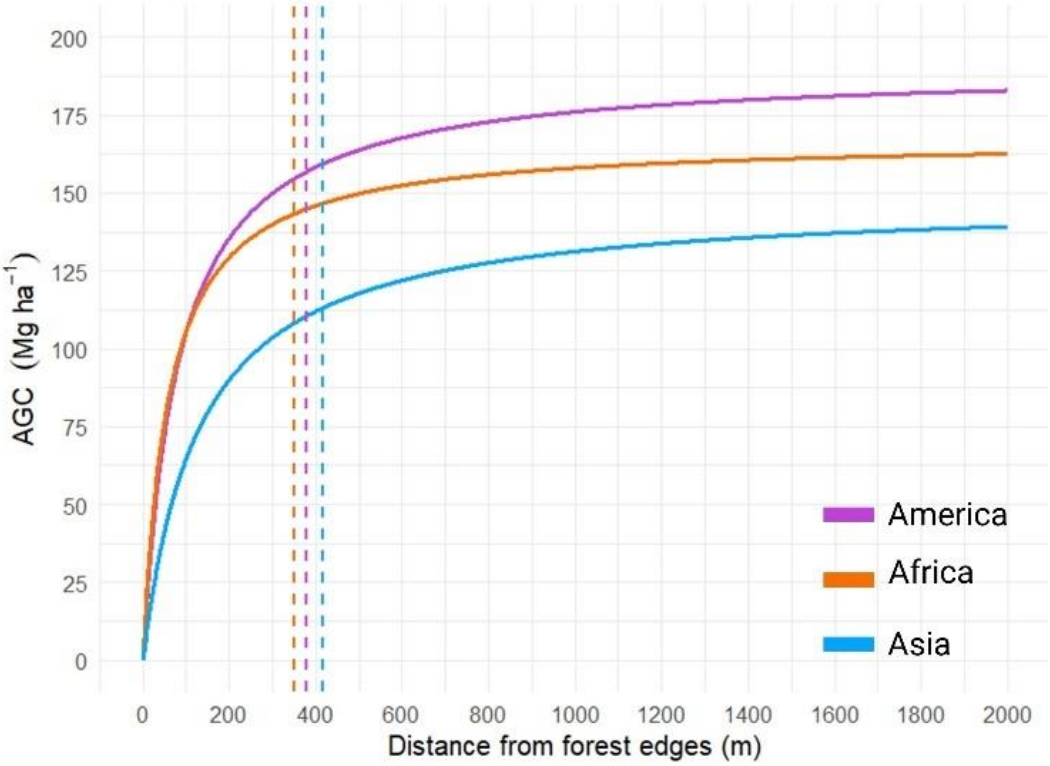


The complete decline of AGC within forest edges is not immediate after its creation. For example, Laurence et al. (1998) found a loss of up to 14% within the first four years after 100-m edges creation in Central Amazonia through field measurements. On the other hand, by a remote sensing approach, Silva-Junior et al. (2020a) found a loss of 37% within the first five years after 120-m edges creation considering a variety of Brazilian Amazon regions; attributed the greater AGC loss to fire disturbance (SILVA et al., 2018b; SILVA JUNIOR et al., 2018; PONTES-LOPES et al., 2021).

Based on these new finds, here we present an unprecedented 30-year analysis of the edge effect on tropical AGC. Additionally, we provide for the first time, the separate contribution of disturbances such as selective logging and fire to AGC losses at tropical forest edges.

Our age-loss models (Figure 5.2) showed that without the contribution of selective logging and fire disturbances, AGC losses in the first year after forest edge creation were 9%, 14%, and 32% for America, Africa, and Asia, respectively. For

America and Africa, the losses reached 16% and 21%, respectively, within four years after creating the edges, with a plateau after that period. On the other hand, losses reach 38% in Asia within the first three years after creating the edges before a plateau.

Figure 5.2 – Models of carbon stocks loss as a function of forest edge aging for the three tropical regions considering and removing the effect of forest edge degradation by other disturbances. For more details, please see the Method section.

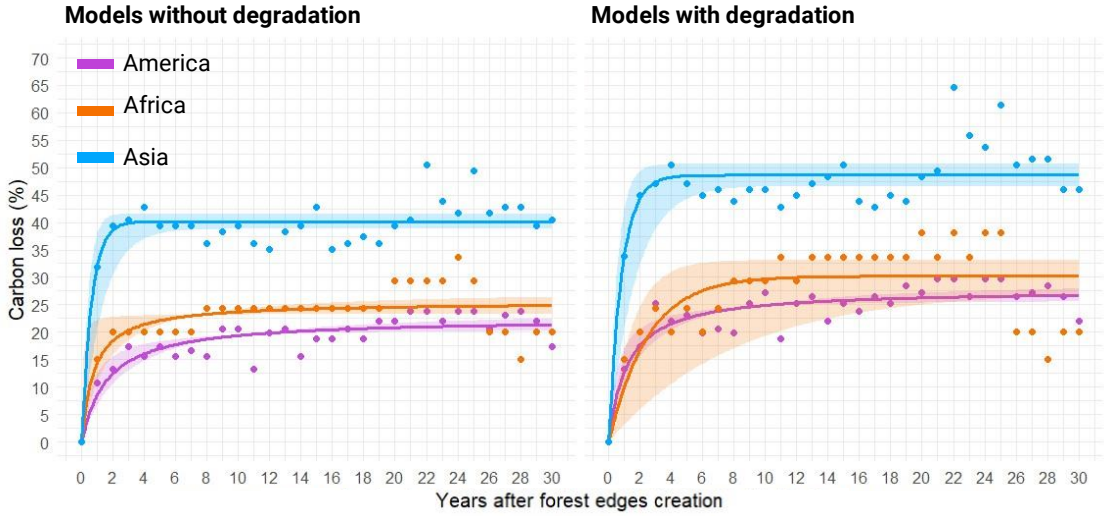


With selective logging and fire contribution, AGC losses in the first year after forest edge creation was 13%, 10%, and 34% for America, Africa, and Asia, respectively. Before a plateau in the models, America losses reached 23% within five years after creating the edges; Africa reached 28% of losses within six years; and Asia reached 47% of losses within six years. By the inclusion of selective logging and fire in our models, we found a carbon stock loss increase of 25% for America, 22% for Africa, and 21% for Asia within 30-years after creating forest edges. Thus, selective logging and fire disturbance cause a temporal prolongation and magnitude increase of carbon stocks collapse in tropical forest edges.

While our findings for tropical America are consistent with Laurance et al. (1997) for edges without selective logging and fire effects disturbance, and Silva-Junior et al. (2020a) with fire effect in Amazon region, losses for tropical Africa and Asia exceed the average loss founded across the tropics (CHAPLIN-KRAMER et al., 2015).

There are several AGC loss drivers at forest edges. The collapse of carbon stocks is explained by the increase in tree mortality after creating edges, especially the larger ones (LAURANCE et al., 2000; BRANDO et al., 2014), which store most of the forest's carbon; negative microclimatic changes within edges, as temperature and wind turbulence increase, plus moisture and evapotranspiration decreasing, led to an exacerbation tree mortality rate (LOVEJOY et al., 1986; KAPOS, 1989; CAMARGO; KAPOS, 1995; SIZER; TANNER, 1999; TRANCOSO, 2008; SILVÉRIO et al., 2019b; NUMATA et al., 2021). Besides, above average edge effect penetration found here can be attributed to an increased canopy dissection and insect or pathogen attack from edges to forest interior (BRIANT; GOND; LAURANCE, 2010). Fire escape (BAKER; BUNYAVEJCHEWIN; ROBINSON, 2008; ARMENTERAS; GONZÁLEZ; RETANA, 2013; CANO-CRESPO et al., 2015; SILVA et al., 2018b; SILVA JUNIOR et al., 2018; PONTES-LOPES et al., 2021) and selective logging (ASNER, 2005; HUANG; ASNER, 2010; MEDJIBE et al., 2011; MARTIN et al., 2015; LONGO et al., 2016; BUTARBUTAR et al., 2019; RANGEL PINAGÉ et al., 2019; D'OLIVEIRA et al., 2021) from human activities surrounding forest edges provide booster carbon stocks losses, which explain the additional loss found here by including these disturbances in our analysed models.

Following the initial tree mortality prosses, the plant community at forest edges tend to be better adapted to the new microclimatic conditions, sealing the edges, and reducing the susceptibility to further microclimatic changes (CAMARGO; KAPOS, 1995; DIDHAM; LAWTON, 1999; D'ANGELO et al., 2004; LAURANCE et al., 2006), as revelled by the plateau in our models for all tropical regions. However, although tree turnover rates increase due to increased mortality rates (LAURANCE et al., 2006), the original carbon stocks do not fully recover, evidenced by a significant reduction in trees' canopy height and the basal area within edges (ALMEIDA et al., 2019; MAEDA et al., 2022). This behaviour indicates that tropical forests edges reach an alternative post-fragmentation equilibrium state, with a lower carbon stock density (SILVA JUNIOR et al., 2020a).

## 5.3 Tropical forest edges AGB loss within environmental gradients

Although the mechanisms of AGC loss at tropical forest edges are well documented, for example in Brazilian Amazon (LAURANCE et al., 2018), poorly known how these losses vary across the tropical environmental gradients. Below we present the first tropical analysis of AGC loss within different environmental gradients, include: water deficit (MCWD), wind speed (WDSP), degradation (selective logging and fire; DGDT), maximum temperature (MXTP), edges age (EDAG), and distance from secondary forests (DFSF).

Our results showed that forest edges AGC losses was higher in regions with high MCWD levels (greater than 200 mm $year^{-1}$ for America, 160 mm $year^{-1}$ for America, and 40 mm $year^{-1}$ for Asia), while the losses reduced with the reduction of water stress (Figure 5.3a). On the other hand, our results regarding wind speed showed a greater AGC loss in regions with higher wind speed for America (greater than 1.4 m s-1) and Africa (greater than 1.3 m $s^{-1}$); however, this pattern is inverse in Asia (Figure 5.3b).

Figure 5.3 – Loess Regression of forest edges carbon loss as function of edges age for the gradient of MCWD (Maximum Cumulative Water Deficit) (a) and wind speed (b) for three tropical regions.

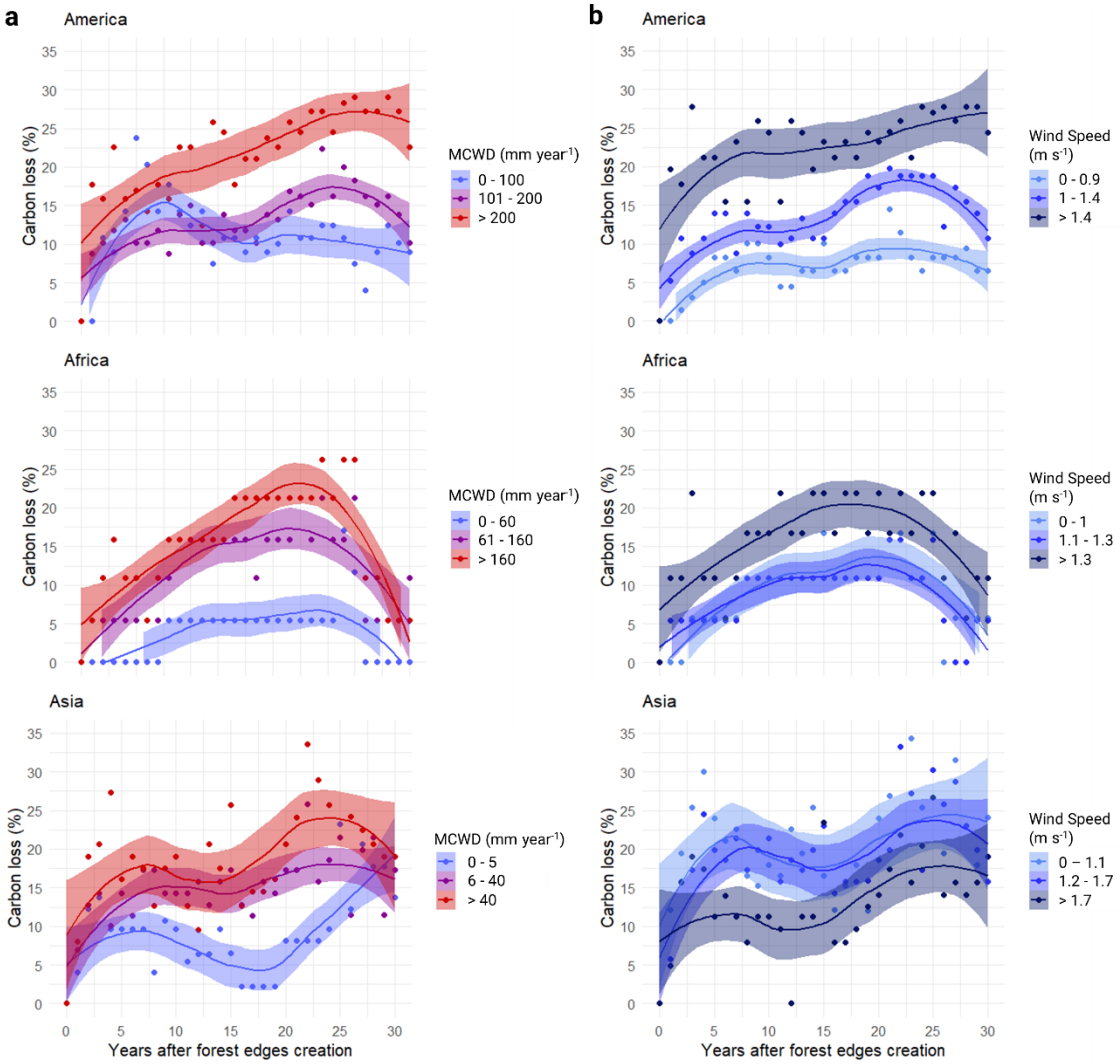


Our findings also showed that AGC losses at forest edges did not differ for America and Africa under different temperature gradients; however, losses in the Asian forest edges were markedly greater in areas with monthly maximum temperatures above 31.3 °C. The same pattern was observed for the distances of the ridges from secondary growth forests (Figure 5.4b). While the losses did not differ for different distances from secondary forests in America and Africa, in Asia, the minor AGC losses occurred at edges close to secondary forests (up to 500-m), while the largest occurred further away from them (greater than 1,000-m).

Figure 5.4 – Loess Regression of forest edges carbon loss as function of edges age for the gradient of maximum temperature (a) and distance from secondary forests (b) for three tropical region.

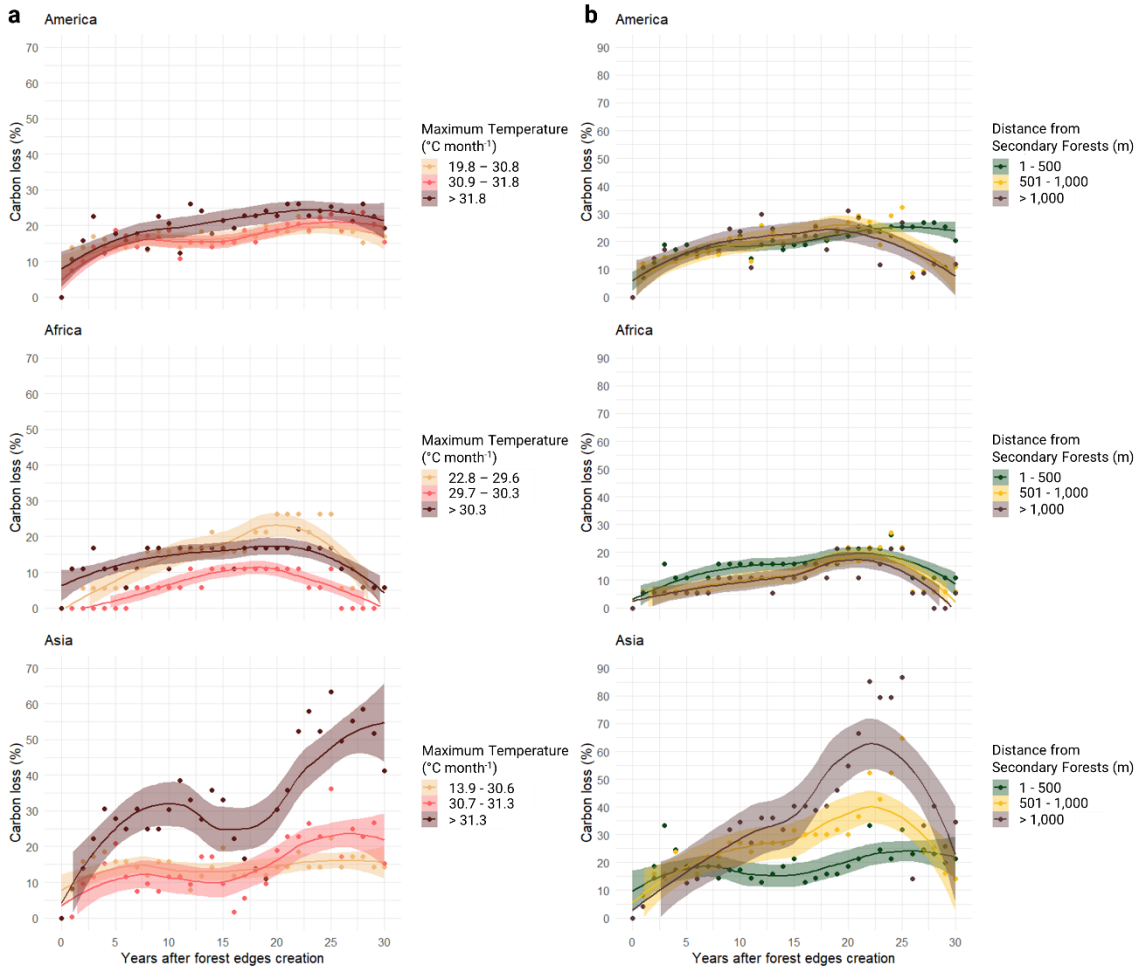


Figure 5.5 shows the importance of environmental factors for the loss of AGC within tropical forest edges using a random forest algorithm approach. Our analysis revealed lower importance of distance for secondary growth forests in the three analysed regions. In contrast, America and Africa presented the degradation with the most significant importance, while Asia presented the maximum temperature as the most important. However, we highlight the role of water deficit, maximum temperature, and wind speed for AGC loss in all tropical regions.

Figure 5.5 – Ranking the importance of environmental variables for carbon loss at forest edges using a random forest algorithm approach. Vertical bars are the 95% confidence interval.

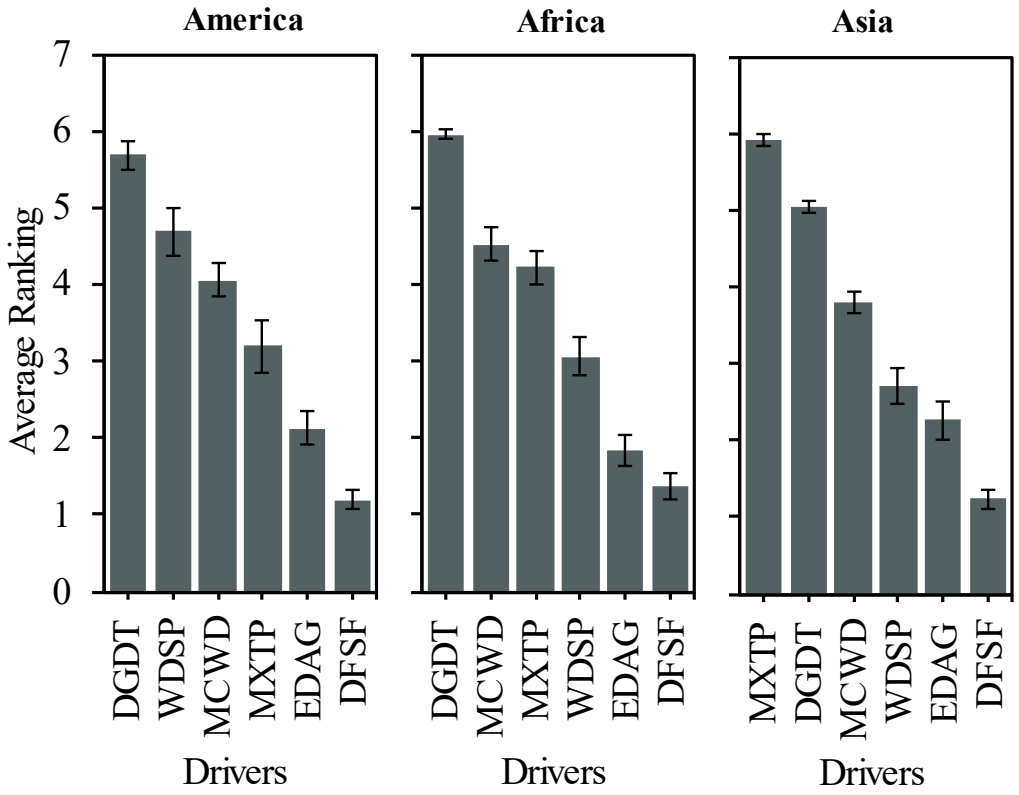


Our findings suggest that under current anthropogenic climate change crises (INTERGOVERNMENTAL PANEL ON CLIMATE CHANGE (IPCC), 2021), which causes more frequent and extreme drought (tropical region) and heat (Asia) events (WIGNERON et al., 2020), the edge effect will be potentiated; leading to a more AGC loss, and consequently, a more amount of carbon dioxide ($CO_2$) emitted into the atmosphere, contributing to Earth' warming. We also highlight the recovery trend of AGC in African forest edges after 30-years under different environmental gradients stratification, suggesting greater forest resilience than in America and Asia (BENNETT et al., 2021), corroborating previous on-the-ground findings (LEWIS et al., 2009; HUBAU et al., 2020; BENNETT et al., 2021).

## 5.4 Relationship between deforestation and forest edges formation in the tropics

Between 1990 and 2020, tropical forests lost 1,925,949 $km^2$ of cover, with a rate of 62,127±23,068 $km^2$ $year^{-1}$. America contributed 49% of all deforestation in the tropical region, followed by Asia (31%) and Africa (21%). After 30-years, the net area of forest edges in 2020 was equivalent to 56% (1,069,741 $km^2$) of all deforestation in the region.

On average, each squared kilometre of deforestation between 1990 and 2020 resulted in 0.59±0.23 $km^2$ $year^{-1}$ of forest edges in the tropical region; however, in Asia, this value was 0.40±0.41 $km^2$ $year^{-1}$, while America and Africa had 0.67±0.27 $km^2$ $year^{-1}$ and 2.11±3.50 $km^2$ $year^{-1}$ respectively. The variation in the arrangements and geometries of deforestation patches explains this disparity between deforestation-edges formation throughout tropical region (LAURANCE; LAURANCE; DELAMONICA, 1998; NUMATA et al., 2009). Studies in the Amazonia, for example, showed that rural settlements (fish-bone pattern, for example) with a pattern of multiple and smaller-scale deforestation produced five times more forest edges than landscapes with large farms with regular shape pattern (LAURANCE; LAURANCE; DELAMONICA, 1998). Our findings corroborate that the acceleration of deforestation rates leads to a critical increase of forest edges in the tropical region (FISCHER et al., 2021)

The peace and configuration of deforestation define the forest edges' creation and erosion (SILVA JUNIOR et al., 2020a), consequently determining its age composition (Figure 5.6). Considering all tropical forests, the age composition of edges showed that in 2020 about 48% of edges were over 15 years old, while another 31% of forest edges were aged up to 10 years. By region, America and Asia showed a similar pattern to the general one; however, 45% of all forest edges in Africa were over 20 years old. The composition of edge ages is crucial because it defines the amount of carbon stocks that have been lost and will be lost if these edges remain in the landscape (SILVA JUNIOR et al., 2020a).

Figure 5.6 – Age distribution of forest edges for three tropical regions in 2020.

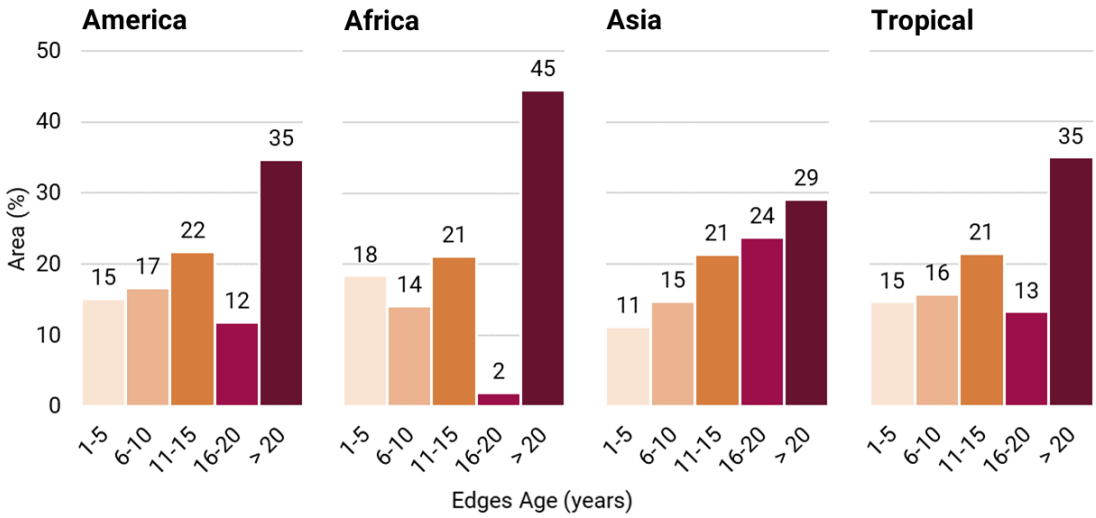


## 5.5 Tropical forest edges $CO_2$ emissions in the 1990-2020 period

By combining forest edge age maps and more conservative carbon stock loss models (without the effects of selective logging and fire), we estimate that between 1990 and 2020, tropical forests had a committed emission of 17,938 Tg $CO_2$ (an average of 579 ±190 Tg $CO_2$ $year^{-1}$) (Figure 5.7). This amount was equivalent to 19% of the committed emissions by deforestation (92,660 Tg CO2; an average of 2,989±1,098 Tg $CO_2$ $year^{-1}$) in the same period (Figure 5.7), being more conservative to the value (34%) found by Brinck.et al. (2017).

While the peak of emission from the edge effect occurred in 2019 (980 $CO_2$), the peak of emissions from deforestation occurred in 1986 (4,458 $CO_2$). The Mann-Kendall trend test showed that emissions from the edge effect between 1990 and 2020 increased significantly (MK=0.33 and p=0.01) at a rate of 12.27 Tg $CO_2$ $year^{-1}$, while emissions from deforestation showed no significant trend (MK=-0.07 and p=0.59).

Figure 5.7 – Annual and accumulated $CO_2$ emission by edge effect and deforestation for the tropical region between 1990 and 2020 (a). Contribution of each region to the total $CO_2$ emissions due to the edge effect and deforestation (b).

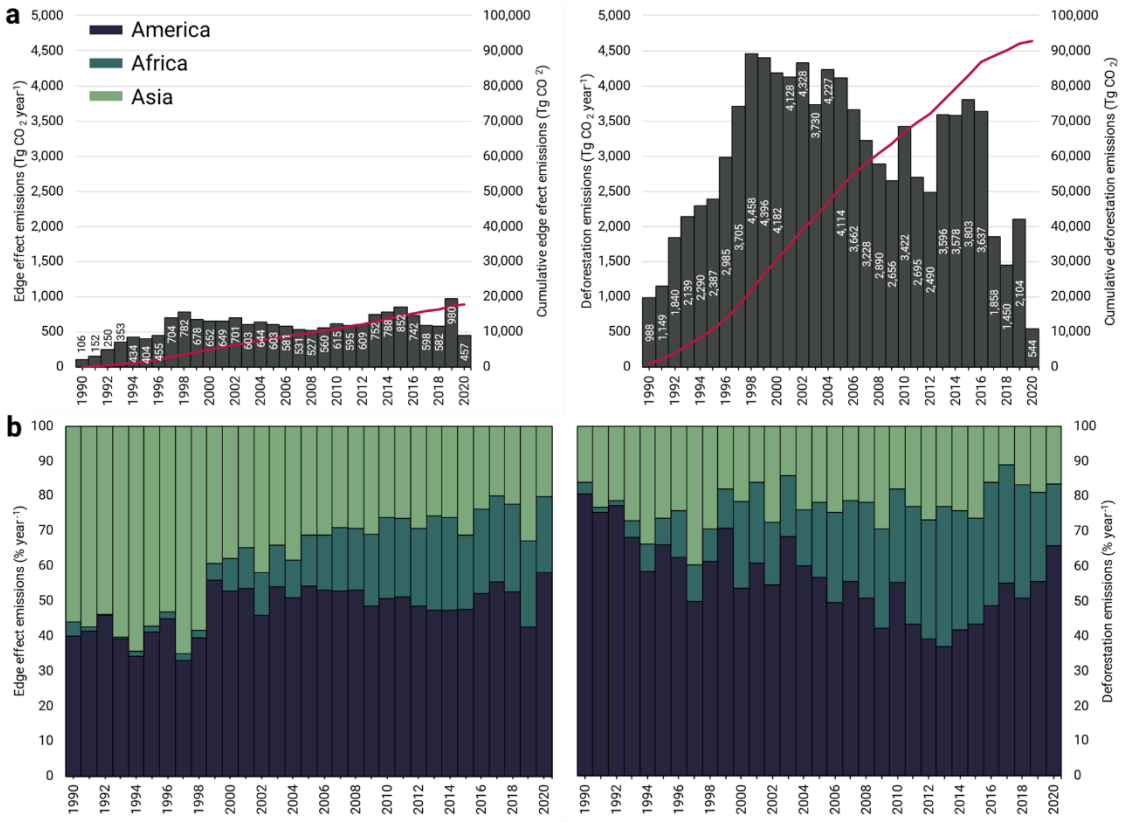


America contributed on average with more than half (57±11%) of emitted CO2 in the tropical region between 1990 and 2020; on the other hand, Africa and Asia accounted for more than half of the emissions due to the edge effect (52±24%). Annual edge emissions in America averaged 20±13% of emissions from deforestation, 15±19% in Africa, 35±18% in Asia, and 22±14% in the tropical region (Figure 5.7b).

The largest $CO_2$ emissions (greater than 5 Tg; Figure 5.8a) from forest edges were located mainly at the frontiers of deforestation in Amazonia, Congo Basin, and Asia (Figure 5.8b). However, $CO_2$ emission values of up to one teragram of $CO_2$ have been found in areas of intact forests (POTAPOV et al., 2017) in the more remote regions of the Amazonia, Congo Basin, and Kalimantan Island (Figure 5.8b). By estimating the equivalence of emissions by edge effect and deforestation (Figure 5.8c), we found that while at the frontiers of deforestation, the edge effect outweighs deforestation by up to 20%, in intact and more remote

areas of forest, emissions by edge effect can outweigh deforestation by more than 100%.

Figure 5.8 – Spatial distribution of the sum (within 1990-20 period at 10-km spatial resolution) of $CO_2$ emissions by edge effect (a) and deforestation (b). Spatialization of equivalence between emissions by edge effect and deforestation (c).

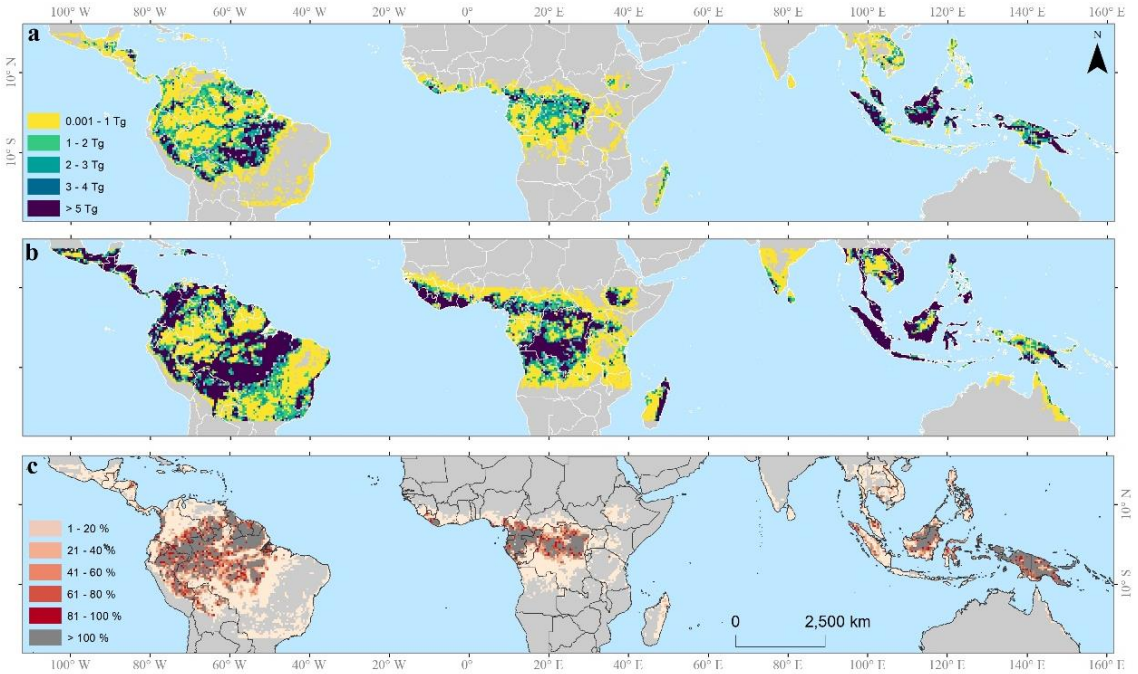


To understand the role of secondary forests to offset deforestation and edge effect emissions in the tropical region, we estimated its uptake potential in the 1990-2020 period (Table 5.2). Within the tropical region, we found that secondary forests reach a net uptake of 2,345 Tg $CO_2$ in 2020, offsetting 2.53% of deforestation emissions or 13.08% of edge effects emissions and 2.12% by the two emission sources combined. Regionally, African secondary forests offset only 1.54% of deforestation emissions, while Asian secondary forests 3.37%. Africa and Asia offset around 11% each of the edge effect emissions, while the American secondary forests 15.20%. The secondary forests offset between 1.35 and 2.58% in Africa and Asia by combining the two emission sources.

Table 5.1 - Secondary forest uptake within three tropical region between 1990 e 2020.

| Period (1990-2020) | America | Africa | Asia | Tropical |
|---|---|---|---|---|
| Secondary forest uptake (Tg $CO_2$) | 1,322 | 307 | 717 | 2,345 |
| Deforestation emissions offset (%) | 2.57 | 1.54 | 3.37 | 2.53 |
| Edges emissions offset (%) | 15.20 | 11.15 | 11.05 | 13.08 |
| Deforestation plus edge emissions offset (%) | 2.20 | 1.35 | 2.58 | 2.12 |

The offset values found here are much smaller than those previously (9.58±1.31%)[6] for Amazonia (NUNES et al., 2020; SILVA JUNIOR et al., 2020c; SMITH et al., 2020; HEINRICH et al., 2021a; SMITH et al., 2021), probably due to its shorter permanence time in the landscape, which avoids carbon accumulation over time. For example, in the Brazilian Amazon tropical forests, deforestation rates of secondary forests exceed rates for old-growth forests; thus, due to the gap in national legislation, this vegetation remains unprotects. Therefore, Brazil and other tropical nations must create mechanisms to protect secondary forests currently standing (HEINRICH et al., 2021a) and encourage the restoration of unused deforested areas (BRANCALION et al., 2019).

Additionally, we simulated a zero-deforestation scenario of tropical old- and secondary-growth forests from 2021 onwards. As a result, we found that secondary forests would have cumulatively uptake 4,471 Tg $CO_2$ from the atmosphere (90.62% higher than in 2020) at the end of 2030 and 11,779 Tg $CO_2$ (402.20% higher than in 2020) at the end of 2100. On the other hand, forest edges would have cumulatively emitted 18,878 Tg $CO_2$ (5.24% higher than in 2020) at the end of 2030 and 19,724 Tg $CO_2$ (9.96% higher than in 2020) at the end of 2100. Thus, secondary forests would have offset about 4.01% of accumulated deforestation emissions until 2020 combined with projected emissions by edge effect at the and 2030 and 10.48% at the and 2100.

[6] To estimate Heinrich et al. (2021) and Nunes et al. (2020) secondary forests offset we used deforestation emissions from Smith et al. (2020), about 3,522 Tg $CO_2$.

## 5.6 Edge effects with Implications for REDD

From our findings, here we use the Brazilian Amazon biome region to test the hypothesis that edge effects and forest fires can counteract Brazilian reducing emissions from deforestation (REDD) results (ARAGAO et al., 2010; SILVA JUNIOR et al., 2020a, 2021a).

Between 2006 and 2019 (Figure 5.8a), Brazil had a REDD result of 7,441 Tg $CO_2$ for the Amazon biome (UNFCCC, 2022). In the same period, forest edges emitted 2,640 Tg $CO_2$, forest fires 3,230 Tg $CO_2$, while secondary forests uptake 450 Tg $CO_2$, resulting in a net balance of 5,420 Tg $CO_2$. Even offset by the uptake of secondary forests, emissions from forest degradation (fire and edge effect) would have compromised 73% of Brazil's REDD results for the Amazon region.

Figure 5.9 – Carbon emissions end removal balance in the Brazilian Amazon between 2006 e 2019 (a). Brazilian REDD result for Amazon biome (b). *Secondary forest removal. **Forest Fires Emissions. *** Edge Effects Emissions.

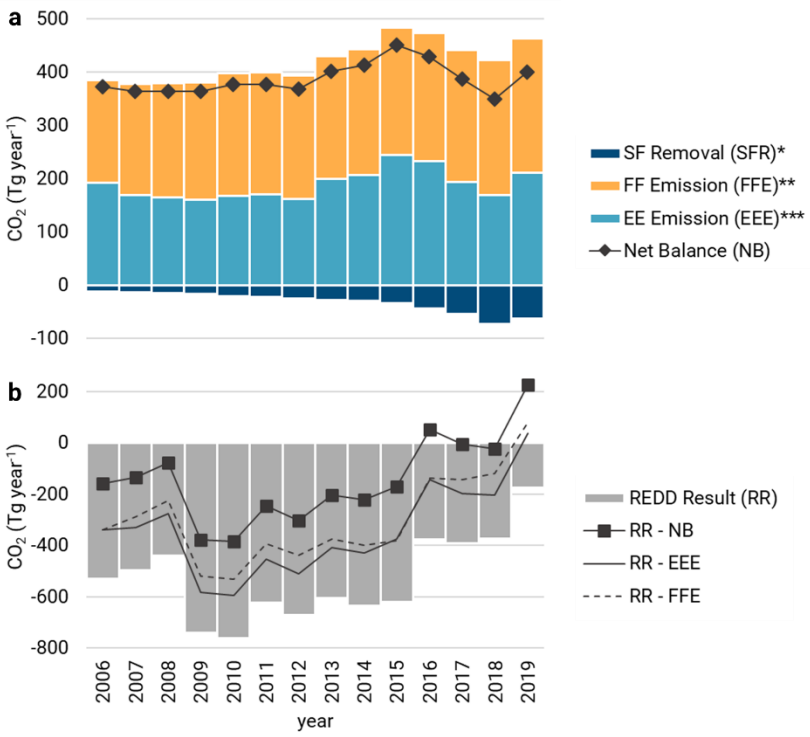


The analysis of the annual scale showed an even more worrying scenario. Brazil's REDD results have significantly (S=-0.41 and p=0.05) at a rate of 23.47 Tg $CO_2$ yr-1, induced mainly by increasing deforestation rates in the region from 2013

onwards (SILVA JUNIOR et al., 2021b). In all years, even with the removal of $CO_2$ by secondary forests, emissions from degradation reduced REDD results. However, in 2016 and 2019, net emissions from degradation compromised the entire REDD result, resulting in a positive emissions balance *Figure 5.8b).

These findings show that it is urgent to end the deforestation climb in the Brazilian Amazon, preventing emissions. In addition, we showed that edge effects and forest fires can compromise a national REDD strategy focused exclusively on reducing emissions from deforestation. When necessary, legal deforestation must be done based on territorial planning to create a minimum amount of forest edges. A fire management policy in the region is urgent to avoid uncontrolled fires (PIVELLO et al., 2021), especially during years of extreme drought (ARAGÃO et al., 2018; SILVA JUNIOR et al., 2019b). Finally, we argue that edge effect emissions should be quantified and reported explicitly with emissions from deforestation, allowing a better understanding the atmosphere $CO_2$ fluxes.

## 5.7 Methods[7]

Our methods are included in the following five steps:

1. Forest cover dynamics maps;
2. Mapping of forest edges and its age structure;
3. Carbon stock loss model by edge effect;
4. Carbon stock loss by edge effect under different environmental gradients;
5. Carbon dioxide ($CO_2$) emissions by edge effect and deforestation;
6. Tropical secondary forest $CO_2$ uptake potential between 1990 e 2020;
7. Analysis of Brazil's REDD result for Amazon biome;
8. Statistical analysis;
9. Sources of uncertainty.

[7] This method was adapted from Silva Junior et al. (2020a).

### 5.7.1 Forest cover dynamics maps

As primary dataset on forest cover dynamics, we used the unprecedented nearly 40-year mapping at 30-m spatial resolution of Tropical Moist Forests (TMF). From a time-series observations of the Landsat satellites, with images collected between 1982 and 2020, Vancutsem et al. (2021) mapped deforestation and forest degradation (by fire and selecting logging disturbances). In the TMF dataset, forest degradation events are changes at a forest pixel visible for less than 2.5-years. In contrast, deforestation (the total forest cover removal) are disturbances that last longer than 2.5-years. On the other hand, secondary forests were defined as pixels with forest regrowth after no forest cover for more than 2.5-years.

### 5.7.2 Mapping tropical carbon stocks for the year 2019

Considering that the last biomass map covering the tropical region is only available for the year 2018 (SANTORO; CARTUS, 2021), and our intention to analyse 30-years of edge effects impact, we prepared a biomass map for the year 2019 with 100-m spatial resolution. We used the global forest canopy height map (Figure 5.9) developed by Patapov et al. (2021) from GEDI (NASA's Global Ecosystem Dynamics Investigation pace-based LiDAR) and Landsat dataset. Patapov et al. (2021). highlighted that this dataset was able to detect and monitor deforestation, degradation, and recovery in tropical environments. The validations showed a Root Mean Squared Error (RMSE) of 6.60-m ($R^2$=0.62) using an independent set of GEDI samples and an RMSE of 9.07-m ($R^2$=0.61) using an airborne LiDAR dataset.

Figure 5.10 – Tree canopy hight map.

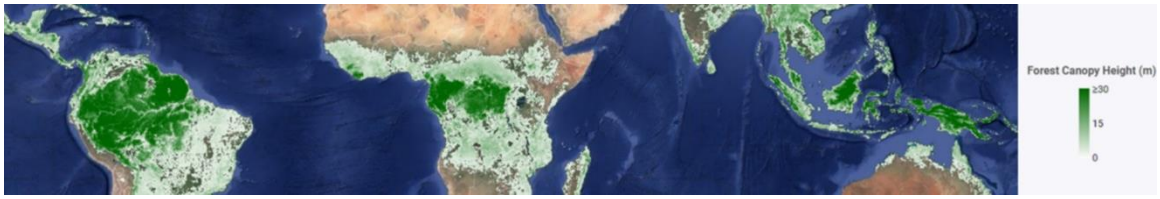


To estimate carbon stocks (Above Ground Carbon – AGC; in Tg $ha^{-1}$), we applied three equations from the literature that consider the tree canopy height (TCH; in

meters). For America we used Equation 5.1 ($R^2$ = 0.68 e RMSE = 43.30 Mg C $ha^{-1}$) by Longo et al. (2016), for Africa Equation 5.2 ($R^2$ = 0.76 e RMSE = 30.17 Mg C $ha^{-1}$) by Xu et al. (2017), and for Asia Equation 5.3 ($R^2$ = 0.81 e RMSE = 31,11 Mg C $ha^{-1}$) by Ferraz et al. (2018). All procedures were and following was performed (except were indicated otherwise) within the Google Earth Engine (GEE) platform (GORELICK et al., 2017).

$$AGC = 10 \cdot 0.025 \cdot TCH^{1.99} \quad (5.1)$$

$$AGC = 0.5 \cdot 1.88 \cdot TCH^{1.55} \quad (5.2)$$

$$AGC = 0.5 \cdot 0.03 \cdot TCH^{2.65} \quad (5.3)$$

Were, 0.5 is a factor to convert biomass into carbon stock (CHAVE et al., 2005), and 10 is a factor to convert carbon stocks from kg $m^{-2}$ into Tg $ha^{-1}$.

Firstly, original TCH map with 30-m spatial resolution was resampled (by the average of the original pixels) to 50-m and 100-m (for Africa) spatial resolution. Then the equations mentioned above were applied to the resampled TCH maps, thus obtaining the carbon stocks. Finally, for America and Asia, the stock map was resampled to 100-m spatial resolution for America and Asia, and 100-m spatial resolution for Africa (Figure 5.10).

Figure 5.11 – The 2019 above ground carbon (AGC) map.

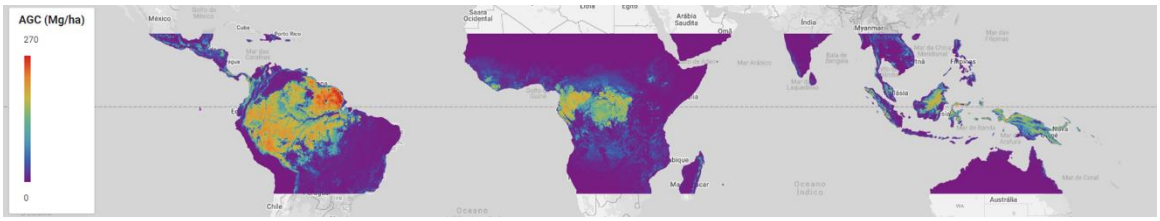


### 5.7.3 Mapping of forest edges and its age structure

Initially, we analysed the distance of carbon stocks as a function of their distance from the forest edge. This analysis served to identify the extent to which the reduction of stocks is significant from the edges to the forest's interior. We collected more than 977,000 random samples with a minimum distance of one kilometre between samples to avoid collecting within the same carbon stock pixel.

About 616,211, 107,438, and 254,939 samples were collected for America, Africa, and Asia. Only areas within forest in 2019 forest cover map were considered for sampling.

We performed analyses to identify the extent of carbon stock reduction from forest edges in the R software (R CORE TEAM, 2018). First, we only consider samples with a distance between 30 and 2,000-m from the forest edges because, after 2,000-m, stocks saturate as a function of distance. Then, we implemented a bootstrap approach (KUSHARY; DAVISON; HINKLEY, 2000) with 1,000 10% random resamples with replacement. To fit a model of stock growth as a function of edge distance (CHAPLIN-KRAMER et al., 2015), we adopted the Michaelis-Menten kinetic equation (Equation 5.4) through the "drc" R package (RITZ et al., 2015). To identify the distance threshold from forest edges where the reduction of carbon stocks is no longer significant, we performed a breaking-point analysis using the "segmented" R package (MUGGEO, 2016). Finally, the average and standard deviation of the parameters obtained from the 1,000 interactions were calculated.

$$AGC = \frac{\alpha \cdot E_{distance}}{\beta + E_{distance}} + \varepsilon \qquad (5.4)$$

Were AGC is the above ground carbon (Mg $ha^{-1}$)), α and β are parameters of the equation, $E_{distance}$ is the distance (meters) from the forest edges, and ε is the estimated error for the equation.

Thus, as shown earlier in the results, America had an average distance threshold of 379-m, Africa 351-m, and Arsia 415-m. Based on our forest cover data (30-m spatial resolution), we adopted the following widths in our forest edges mapping, 390-m, 360-m, and 420-m.

From 31-years of forest cover maps we calculated the Euclidean distance (DANIELSSON, 1980) from the edges to the forest's interior. Finally, from Euclidean distance we classified pixels based on distance intervals, using three classes: non-forest (equal to 0m), forest interior (greater than edge width) and forest edge class (between 30 and 360-420-m, depending on the region).

Using the 31-years forest edges maps, we produced 30 forest edges age maps (1990 to 2020). Firstly, we removed from the forest edges maps (1990 to 2020) all the edges in 1989 because we cannot estimate forest edges age in the 1989 year. This first step also removed all natural forest edges formed at the boundaries between forest-water and forest-savannas, which were not of interest for our study. Then, we transform the forest edges maps into binary maps, where we assign the value of "1" to the forest edges and "0" to the forest interior and non-forest cover. Finally, we use the map algebra method to calculate the forest edges age, by summing the binary maps year by year cumulatively. While the 1990 map had edges aged one year, the 2020 map was aged between one and thirty-one years.

### 5.7.4 Carbon stock loss model by edge effect

We use 2019 carbon stock map and 2019 forest edges age maps to fit models of carbon loss within forest edges as a function of its edges age. For all models, we used the median of carbon stocks in the forest interior (forest areas excluding the edges and limited to 2,000-m) as reference (control areas). Firstly, we overlaid the carbon stock map, on the forest edge map and 2019 cumulative forest degradation map (1982 to 2019) (VANCUTSEM et al., 2021) to extract carbon values for pixels in the edge and interior of degraded and non-degraded forests. Then, we calculated the median carbon values for forest edges stratified by their respective ages. Finally, with 30-years of data, we calculated the percentage difference between the forest interior and forest edges AGC for each age (carbon loss as percentage).

From carbon loss, edges age and based on the conceptual and remote-sensing-based model (Table 5.3) (MELITO; METZGER; DE OLIVEIRA, 2018; SILVA JUNIOR et al., 2020a), we employed in R software (R CORE TEAM, 2018) the non-linear rectangular hyperbolic regression of Michaelis-Menten kinetic model (Equation 5.5), and the Asymptotic regression model (Equation 5.6). Thus, we used the "drc" (RITZ et al., 2015) and “aomisc” (https://github.com/OnofriAndreaPG/aomisc) R packages.

$$C_{loss} = \frac{\alpha \cdot Y_{after}}{\beta + Y_{after}} (5.5)$$

$$C_{loss} = \alpha \cdot \left(1 - \exp\left(-\beta \cdot Y_{after}\right)\right) (5.6)$$

Were $C_{loss}$ being the amount of carbon stock loss measured as a proportion, and $Y_{after}$ is the number of years after the edges creation. The α and β are parameters of the equations.

Table 5.2 - Carbon loss factor (f) for the calculation of carbon loss from edge effect.

| Disturbance | Region | Equation | Coefficients | | RSE** |
|---|---|---|---|---|---|
| | | | a (*) | b (*) | |
| Non-degraded | America | 5 | 22.518(±1.875) | 1.615(±0.974) | 2.421 |
| | Africa | 5 | 25.500(±2.200) | 0.764(±0.715) | 3.742 |
| | Asia | 6 | 40.187(±1.387) | 1.625(±0.853) | 3.598 |
| Degraded | America | 5 | 27.785(±1.793) | 1.162(±0.642) | 2.695 |
| | Africa | 6 | 30.216(±2.893) | 0.405(±0.283) | 6.331 |
| | Asia | 6 | 48.615(±1.984) | 1.219(±0.621) | 5.074 |
| *95% confidence interval; **Residual Standard Error | | | | | |

### 5.7.5 Carbon stock loss by edge effect under different environmental gradients

Similar to the previous section, we calculated the carbon stocks loss for each forest edge age; however, we stratified each analysis for different environmental gradients including water deficit, monthly wind speed, maximum temperature, and distance from secondary forests. Thus, we fitted curves using Locally Weighted Scatterplot Smoothing - LOESS implemented in R software (R CORE TEAM, 2018), which is a local regression model (CLEVELAND; GROSSE; SHYU, 1992; CLEVELAND; LOADER, 1996). This method is a non-parametric strategy for fitting a smooth curve to data, where noisy data values, sparse data points or weak interrelationships interfere with your ability to see a line of best fit (TATE et al., 2005). He we used the span 0.75 (default setting) in LOESS analyses.

To analyse the water deficit in forest edges, we used the average (1981-2019 period) of Maximum Cumulative Water Deficit – MCWD (ARAGÃO et al., 2007; CAMPANHARO; SILVA JUNIOR, 2019) from the monthly Rainfall Estimates from Rain Gauge and Satellite Observation - CHIRPS (at 5-km spatial resolution) (FUNK et al., 2015). For monthly wind speed and maximum temperature average (1981-2019 period) we use the TerraClimate (Monthly Climate and Climatic Water Balance for Global Terrestrial Surfaces) dataset (4-km spatial resolution) (ABATZOGLOU et al., 2018). Finally, we calculated the distance from forest edges to the closest secondary forests (at 30-m spatial resolution) that grew between 1982 and 2019 and remained standing between in 2019 (VANCUTSEM et al., 2021).

We performed an independent approach to assess the importance of environmental variables (including degradation and age of forest edges). First, we created a reference map (at 100-m spatial resolution) with the median carbon stocks of the forest interior (forest region with up to 2,000-m from non-forest areas, excluding edge, degraded and secondary forest areas) across the tropical ecoregion (DINERSTEIN et al., 2017) using the original 2019 carbon stock map. Then, we overlay the two previous maps and calculate the percentage of loss of carbon stocks for each pixel of forest edges. Finally, we overlay the map with regionalized carbon loss values on the maps of environmental variables (including forest edges age and degradation) across more than 53,000 random samples (17,877 in America, 18,329 in Africa, and 18,260 in Asia; with one-kilometre distance among themselves) across all remaining forest edges in 2019.

From the samples of each tropical region in the we performed a machine learning approach. We used a “random-forest” model to assess which of the environmental variable were the most important in influencing the carbon loss within forest edges. The analysis was performed by the conditional random-forest model “cforest” available in the R package “caret” (KUHN, 2008). We implemented a bootstrap approach with 30 interactions in the R software, where 1,000 samples were randomly selected from the original samples dataset, which were then submitted to the random-forest model algorithm considering 500

decision trees (BEHNAMIAN et al., 2017). As our dataset include both continuous and categorical variables, the “cforest” random-forest model provides more accurate importance estimates compared to more traditional random-forest models (STROBL et al., 2007). For more information see Heinrich et al. (2021b).

### 5.7.6 Carbon dioxide ($CO_2$) emissions by edge effect and deforestation

We constructed a map of potential carbon stocks with a 30-m spatial resolution (Figure 5.11) for this step. For that, from the 2019 carbon stock map (100-m spatial resolution), we excluded all non-forest areas, forests within 500-m from the edges, degraded forests, and secondary growth forests. We then calculate the median carbon stocks for each ecoregion (DINERSTEIN et al., 2017) within the tropical region at 30-m spatial resolution. The ecoregions represent distinct biodiversity assemblages, including all taxa, not just vegetation, whose boundaries include the space required to sustain ecological processes (DINERSTEIN et al., 2017).

Figure 5.12 – Potential AGC map.

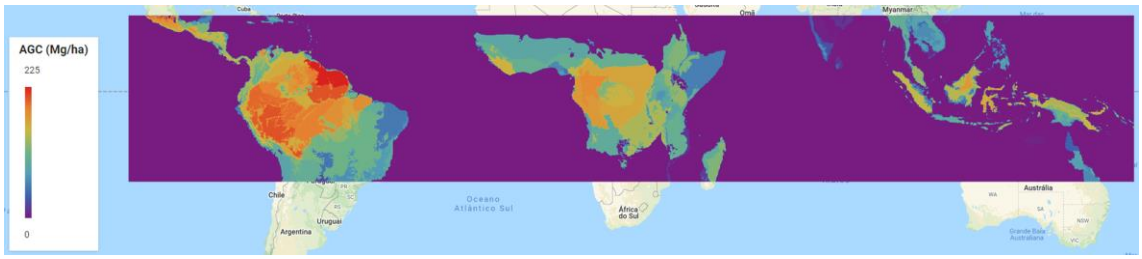


To extrapolate the carbon loss at forest edges in GEE platform, we first combined all the annual age maps with our potential AGB density map (30-m spatial resolution) in a pixel-by-pixel approach, attributing to each edge age pixel an initial (pre-edge formation) carbon value. We carried out a similar procedure for the deforested pixels. For estimating tropical-wide edge effect $CO_2$ emissions between 1990 and 2020, we applied Equation 7 for each pixel.

$$Emission_{Pixel} = Emission_{Factor} \cdot AGC_{Pixel} \cdot 0.09 \cdot 3.667 \quad (7)$$

where $Emission_{Pixel}$ is the pixel $CO_2$ emission at the forest edges given in Mg per pixel, $Emission_{Factor}$ is the emission factor for each forest edge age, calculated

based on non-degradation equation (Table 5.4), $AGC_{Pixel}$ is the pre-edge or pre-deforestation AGB value of the pixel, and 3.667 is the carbon to dioxide carbon factor conversion. To avoid double-counting, if a given pixel has lost carbon stocks due to the edge effect, that amount is discounted if there is a subsequent loss from deforestation in the same pixel. For calculating the tropical-wide $CO_2$ emissions from deforestation, between 1990 and 2020, we applied Equation 8 for each pixel.

$$Emission_{Pixel} = Emission_{Factor} . AGC_{Pixel} \cdot 0.09 \cdot 3.667 \quad (8)$$

All terms in Equation 8 are similar to those in Equation 7, however, $Emission_{Factor}$ in this case is set to “1”, indicating that all carbon stored in the pixel will be lost following the deforestation process.

Table 5.3 – Emission factor (f) for $CO_2$ amount calculation from edge effect.

| Forest edges age (year) | Emission Factor (*f*) | | |
|---|---|---|---|
| | America | Africa | Asia |
| 1 | 0.086 | 0.145 | 0.323 |
| 2 | 0.038 | 0.040 | 0.064 |
| 3 | 0.022 | 0.019 | 0.013 |
| 4 | 0.014 | 0.011 | 0.002 |
| 5 | 0.010 | 0.007 | 0.000 |
| 6 | 0.007 | 0.005 | 0.000 |
| 7 | 0.006 | 0.004 | 0.000 |
| 8 | 0.004 | 0.003 | 0.000 |
| 9 | 0.004 | 0.002 | 0.000 |
| 10 | 0.003 | 0.002 | 0.000 |
| 11 | 0.002 | 0.002 | 0.000 |
| 12 | 0.002 | 0.001 | 0.000 |
| 13 | 0.002 | 0.001 | 0.000 |
| 14 | 0.002 | 0.001 | 0.000 |
| 15 | 0.001 | 0.001 | 0.000 |
| 16 | 0.001 | 0.001 | 0.000 |
| 17 | 0.001 | 0.001 | 0.000 |
| 18 | 0.001 | 0.001 | 0.000 |
| 19 | 0.001 | 0.001 | 0.000 |
| 20 | 0.001 | 0.000 | 0.000 |
| 21 | 0.001 | 0.000 | 0.000 |
| 22 | 0.001 | 0.000 | 0.000 |
| 23 | 0.001 | 0.000 | 0.000 |
| 24 | 0.001 | 0.000 | 0.000 |
| 25 | 0.001 | 0.000 | 0.000 |
| 26 | 0.000 | 0.000 | 0.000 |
| 27 | 0.000 | 0.000 | 0.000 |
| 28 | 0.000 | 0.000 | 0.000 |
| 29 | 0.000 | 0.000 | 0.000 |
| 30 | 0.000 | 0.000 | 0.000 |
| 31 | 0.000 | 0.000 | 0.000 |

### 5.7.7 Tropical secondary forest $CO_2$ uptake potential between 1990 e 2020

We adopted the relative recovery curve (%) of above-ground biomass in tropical secondary forests (Table 5.4) proposed by Poorter et al. (2021) to estimate the uptake potential in the tropical region between 1990 e 2020.

Table 5.4 – Tropical secondary forest uptake factors.

| Secondary forest Age | Relative recovery (%) | Uptake factor (f) |
|---|---|---|
| 1 | 2.932 | 0.029 |
| 2 | 4.815 | 0.048 |
| 3 | 6.696 | 0.067 |
| 4 | 8.638 | 0.086 |
| 5 | 10.434 | 0.104 |
| 6 | 12.184 | 0.122 |
| 7 | 13.974 | 0.140 |
| 8 | 15.613 | 0.156 |
| 9 | 17.221 | 0.172 |
| 10 | 18.876 | 0.189 |
| 11 | 20.507 | 0.205 |
| 12 | 21.980 | 0.220 |
| 13 | 23.434 | 0.234 |
| 14 | 24.933 | 0.249 |
| 15 | 26.403 | 0.264 |
| 16 | 27.843 | 0.278 |
| 17 | 29.256 | 0.293 |
| 18 | 30.641 | 0.306 |
| 19 | 31.999 | 0.320 |
| 20 | 33.089 | 0.331 |
| 21 | 34.361 | 0.344 |
| 22 | 35.624 | 0.356 |
| 23 | 36.862 | 0.369 |
| 24 | 38.077 | 0.381 |
| 25 | 39.269 | 0.393 |
| 26 | 40.451 | 0.405 |
| 27 | 41.380 | 0.414 |
| 28 | 42.746 | 0.427 |
| 29 | 43.860 | 0.439 |
| 30 | 44.953 | 0.450 |
| 31 | 46.024 | 0.460 |

Through the secondary growth forests cover from Vancutsem et al. (2021) dataset, we calculate year by year the age of these forests when remaining in the year under analysis. Then, through the potential AGC map, we apply Equation 9 in a pixel approach.

$$Uptake_{Pixel} = AGC_{Pixel} \cdot f \cdot 3.667 \quad (9)$$

Were, $Uptake_{Pixel}$ is the amount of uptake $CO_2$ (in Tg) for a given year, $AGC_{Pixel}$ is a pixel in the potential AGC map, *f* is an uptake factor (Table 5.5) for a given secondary forest age, and 3.667 is a factor to convert carbon in $CO_2$.

### 5.7.8 Analysis of Brazil's REDD result for Amazon biome

To analyse Brazil's REDD results (UNFCCC - CONVENÇÃO-QUADRO DAS NAÇÕES UNIDAS SOBRE A MUDANÇA DO CLIMA, 2022) in a scenario of emissions from forest degradation, we used the same approach described above but with a specific spatial cut for the Brazilian Amazon biome. For the 2006-2019 period, we calculated the emissions by edge effect uptake from secondary forests.

Additionally, we calculated $CO_2$ emissions from forest fires for areas that burned only once between 2001 and 2019. We first combined three remote sensing products to produce annual maps of burned areas (CHUVIECO et al., 2018; GIGLIO et al., 2018; ALENCAR, 2022); then, we mapped the forests that burned only once outside the forest edges. Finally, we extract the total AGC from the potential map for each burned forest pixel and consider a carbon loss of 29.16% within one year after burn (ANDERSON et al., 2015), later converted into $CO_2$ (multiplied by the factor 3.667).

### 5.7.9 Statistical analysis

To test the significance of temporal trends, we used the non-parametric Mann-Kendall test (MANN, 1945; KENDALL, 1975) and the Sen's Slope estimator (SEN, 1968) to calc the magnitude of changes at time. All analyses were performed in R software (R CORE TEAM, 2018). For the we used the Mann-Kendall test and the Sen's Slope Estimator the "wq" package (JASSBY; CLOERN, 2016) was used. For all statistical analysis, we adopted the significance level of 95% ($p \leq 0.05$). The Mann-Kendall test is used to assess whether there is a monotonic upward or downward trend over a time period, whereas the Sen's Slope Estimator, a robust nonparametric method with little

sensitivity to outliers, is used to estimate the magnitude of trends by the calculation of the median of the slopes of each pair of points in the data.

### 5.7.10 Sources of uncertainty

Although the forest cover dataset is available for years prior 1990 (1982-1989 period), our edge effect and deforestation analyses were performed from 1990 onwards due to a lower density of Landsat data prior to 1990 (WULDER et al., 2019), which would lead to an underestimation of the forest cover changes mapping. Thus, our estimates do not account for historical forest changes before 1990.

While the equations and the base remote sensing product used to estimate carbon stocks in 2019 have been validated and uncertainties quantified, which gives security in the AGC values used, validations are still needed. As future steps, we defined a validation of our AGC estimates using airborne Lidar data already available for the tropical region.

In our analysis, we assumed that the open- and closed-edges are equally impacted by edge effects, although these impacts may assume different magnitudes depending on the edge type, as suggested by Didham and Lawton (1999) and Shapiro et al. (2016).

All uncertainties in our models and analyses were quantified and expressed as confidence intervals throughout the chapter. Besides, our approach and finds represents an advance in relation to previous studies (NUMATA et al., 2010, 2011; PÜTZ et al., 2014; HISSA et al., 2016; BRINCK et al., 2017; MAXWELL et al., 2019; SILVA JUNIOR et al., 2020a; QIN et al., 2021), contributing to an improved understanding of the carbon balance of tropical region. Finally, unlike previous studies (NUMATA et al., 2010, 2011; PÜTZ et al., 2014; HISSA et al., 2016; BRINCK et al., 2017; MAXWELL et al., 2019; SILVA JUNIOR et al., 2020a; QIN et al., 2021), our estimates of carbon loss were based for the first time on samples derived from all tropical region, describing the gradual decay of carbon at forest edges over unprecedent 30-years.

# 6 CONCLUDING REMARKS

We concluded that we were able to perform a comprehensive analysis of fragmented tropical forests and assess their impacts at different scales through remote sensing. The Chapter 2 presented the state of art of remote sensing of tropical fragmented forests.

From Chapter 3, we concluded that forest fires incidence and intensity vary with levels of habitat loss and forest fragmentation in the Central Brazilian Amazon. About 95% of active fires and the most intense ones occurred in the first kilometre from the forest edges. Furthermore, recent changes in the Brazilian forest code may lead to Amazonian landscapes with more fragmented forests.

From Chapter 4 we concluded that carbon losses associated with the edge effect in Amazonia (947 Tg C) corresponded to about one-third of losses from deforestation (2,592 Tg C). Despite a notable reduction of carbon losses from deforestation, the losses from the edge effect remained unchanged over time. Thus, carbon losses from edge effect are an additional unquantified flux that can counteract carbon emissions avoided by reducing deforestation.

From Chapter 5, we concluded that selective logging and fire degradation can increase carbon losses at forest edges for the tropical scale. Over time, carbon losses at forest edges vary along different environmental gradients, with degradation being the most important for losses in America and Africa and maximum temperature in Asia. Carbon losses resulted in $CO_2$ emission of 18 thousand teragrams, or the equivalent of 19% of emissions from deforestation (93 thousand teragrams). The uptake of $CO_2$ from the atmosphere by secondary tropical forests was not sufficient to offset these emissions.

Furthermore, we argue that the collateral $CO_2$ emissions from edge effect should be quantified and reported with emissions from deforestation for an inventory of greenhouse gases more consistent. Urgent actions are needed to restrain deforestation in Amazonia (SILVA JUNIOR et al., 2021b) and the tropical region. The protection of secondary tropical forests (SILVA JUNIOR et al., 2020b; HEINRICH et al., 2021b) and the incentive and investment in restoration

(BRANCALION et al., 2019) are indispensable tools to offset emissions from deforestation and the edge effect to guarantee the limitation of Earth warming.

## REFERENCES


ABATZOGLOU, J. T.; DOBROWSKI, S. Z.; PARKS, S. A.; HEGEWISCH, K. C. TerraClimate, a high-resolution global dataset of monthly climate and climatic water balance from 1958–2015. **Scientific Data**, v. 5, n. 1, e 170191, 2018.

AFRIYANTI, D.; KROEZE, C.; SAAD, A. Indonesia palm oil production without deforestation and peat conversion by 2050. **Science of the Total Environment**, v. 557/558, p. 562–570, jul. 2016.

ALENCAR, A. A. C.; SOLÓRZANO, L. A.; NEPSTAD, D. C. Modeling forest understory fires in an Eastern Amazonian Landscape. **Ecological Applications**, v. 14, n. sp4, p. 139–149, 2004.

ALMEIDA, D. R. A.; STARK, S. C.; SCHIETTI, J.; CAMARGO, J. L. C.; AMAZONAS, N. T.; GORGENS, E. B.; ROSA, D. M.; SMITH, M. N.; VALBUENA, R.; SALESKA, S.; ANDRADE, A.; MESQUITA, R.; LAURANCE, S. G.; LAURANCE, W. F.; LOVEJOY, T. E.; BROADBENT, E. N.; SHIMABUKURO, Y. E.; PARKER, G. G.; LEFSKY, M.; SILVA, C. A.; BRANCALION, P. H. S. Persistent effects of fragmentation on tropical rainforest canopy structure after 20 yr of isolation. **Ecological Applications**, v. 29, n. 6, 2019.

ALMEIDA, C. A.; COUTINHO, A. C.; ESQUERDO, J. C. D. M.; ADAMI, M.; VENTURI, A.; DINIZ, C. G.; DESSAY, N.; DURIEUX, L.; GOMES, A. R. High spatial resolution land use and land cover mapping of the Brazilian Legal Amazon in 2008 using Landsat-5/TM and MODIS data. **Acta Amazonica**, v. 46, n. 3, p. 291–302, 2016.

AMAZONIAN NETWORK OF GEOREFERENCED SOCIO-ENVIRONMENTAL INFORMATION (RAISG). **Deforestation in the Amazonia (1970-2013)**. Available from: https://www.amazoniasocioambiental.org/en/download/deforestation-in-the-amazonia-1970-2013-atlas/. Access on: 1 Jan. 2019.

ANDELA, N.; MORTON, D. C.; GIGLIO, L.; CHEN, Y.; VAN DER WERF, G. R.; KASIBHATLA, P. S.; DEFRIES, R. S.; COLLATZ, G. J.; HANTSON, S.; KLOSTER, S.; BACHELET, D.; FORREST, M.; LASSLOP, G.; LI, F.; MANGEON, S.; MELTON, J. R.; YUE, C.; RANDERSON, J. T. A human-driven decline in global burned area. **Science**, v. 356, n. 6345, p. 1356–1362, 2017.

ANDELA, N.; VAN DER WERF, G. R. Recent trends in African fires driven by cropland expansion and El Niño to La Niña transition. **Nature Climate Change**, v. 4, n. 9, p. 791–795, 2014.

ANDERSON, L. O.; ARAGÃO, L. E. O. C.; GLOOR, M.; ARAI, E.; ADAMI, M.; SAATCHI, S. S.; MALHI, Y.; SHIMABUKURO, Y. E.; BARLOW, J.; BERENGUER, E.; DUARTE, V. Disentangling the contribution of multiple land covers to fire-mediated carbon emissions in Amazonia during the 2010 drought. **Global Biogeochemical Cycles**, v. 29, n. 10, p. 1739–1753, 2015.

ALENCAR, A. A. **Algorithm Theoretical Basis Document (ATBD): MapBiomas Fire**. Available from: https://mapbiomas-br-site.s3.amazonaws.com/ATBD_MapBiomas_Fogo_Cole%C3%A7%C3%A3o_1.pdf.

ARAGÃO, L. E. O. C.; ANDERSON, L. O.; FONSECA, M. G.; ROSAN, T. M.; VEDOVATO, L. B.; WAGNER, F. H.; SILVA, C. V. J.; SILVA JUNIOR, C. H. L.; ARAI, E.; AGUIAR, A. P.; BARLOW, J.; BERENGUER, E.; DEETER, M. N.; DOMINGUES, L. G.; GATTI, L.; GLOOR, M.; MALHI, Y.; MARENGO, J. A.; MILLER, J. B.; PHILLIPS, O. L.; SAATCHI, S. 21st Century drought-related fires counteract the decline of Amazon deforestation carbon emissions. **Nature Communications**, v. 9, n. 1, p. 536, 2018.

ARAGÃO, L. E. O. C.; MALHI, Y.; BARBIER, N.; LIMA, A. A.; SHIMABUKURO, Y.; ANDERSON, L.; SAATCHI, S. Interactions between rainfall, deforestation and fires during recent years in the Brazilian Amazonia. **Philosophical transactions of the Royal Society of London. Series B, Biological sciences**, v. 363, n. 1498, p. 1779–85, 2008.

ARAGÃO, L. E. O. C.; MALHI, Y.; ROMAN-CUESTA, R. M.; SAATCHI, S.; ANDERSON, L. O.; SHIMABUKURO, Y. E. Spatial patterns and fire response of recent Amazonian droughts. **Geophysical Research Letters**, v. 34, n. 7, e L07701, 2007.

ARAGÃO, L. E. O. C.; SHIMABUKURO, Y. E. The incidence of fire in Amazonian forests with implications for REDD. **Science (New York, N.Y.)**, v. 328, p. 1275–1278, 2010.

ARAGAO, L. E. O. C.; SHIMABUKURO, Y. E.; ARAGÃO, L. E. O. C.; SHIMABUKURO, Y. E. The Incidence of Fire in Amazonian Forests with Implications for REDD. **Science**, v. 328, n. 5983, p. 1275–1278, 2010.

ARCHIBALD, S. Managing the human component of fire regimes: lessons from Africa. **Philosophical Transactions of the Royal Society B: Biological Sciences**, v. 371, n. 1696, e 20150346, 2016.

ARCHIBALD, S.; STAVER, A. C.; LEVIN, S. A. Evolution of human-driven fire regimes in Africa. **Proceedings of the National Academy of Sciences**, v. 109, n. 3, p. 847–852, 2012.

ARIMA, E. Y.; WALKER, R. T.; PERZ, S.; SOUZA, C. Explaining the fragmentation in the Brazilian Amazonian forest. **Journal of Land Use Science**, p. 1–21, 2015.

ARMENTERAS, D.; BARRETO, J. S.; TABOR, K.; MOLOWNY-HORAS, R.; RETANA, J. Changing patterns of fire occurrence in proximity to forest edges, roads and rivers between NW Amazonian countries. **Biogeosciences**, v. 14, n. 11, p. 2755–2765, 2017.

ARMENTERAS, D.; GONZÁLEZ, T. M.; RETANA, J. Forest fragmentation and edge influence on fire occurrence and intensity under different management types in Amazon forests. **Biological Conservation**, v. 159, p. 73–79, 2013.

ARMENTERAS, D.; RUDAS, G.; RODRIGUEZ, N.; SUA, S.; ROMERO, M. Patterns and causes of deforestation in the Colombian Amazon. **Ecological Indicators**, v. 6, n. 2, p. 353–368, 2006.

ARORA, N. K.; MISHRA, I. COP26: more challenges than achievements. **Environmental Sustainability**, v. 4, n. 4, p. 585–588, 2021.

ASNER, G. P. Selective logging in the brazilian Amazon. **Science**, v. 310, n. 5747, p. 480–482, 2005.

ASNER, G. P.; BROADBENT, E. N.; OLIVEIRA, P. J. C.; KELLER, M.; KNAPP, D. E.; SILVA, J. N. M. Condition and fate of logged forests in the Brazilian Amazon. **Proceedings of the National Academy of Sciences**, v. 103, n. 34, p. 12947–12950, 2006.

ASNER, G. P.; MASCARO, J. Mapping tropical forest carbon: Calibrating plot estimates to a simple LiDAR metric. **Remote Sensing of Environment**, v. 140, p. 614–624, 2014.

ASNER, G. P.; MASCARO, J.; MULLER-LANDAU, H. C.; VIEILLEDENT, G.; VAUDRY, R.; RASAMOELINA, M.; HALL, J. S.; VAN BREUGEL, M. A universal airborne LiDAR approach for tropical forest carbon mapping. **Oecologia**, v. 168, n. 4, p. 1147–1160, 2012.

ASNER, G. P.; POWELL, G. V. N.; MASCARO, J.; KNAPP, D. E.; CLARK, J. K.; JACOBSON, J.; KENNEDY-BOWDOIN, T.; BALAJI, A.; PAEZ-ACOSTA, G.; VICTORIA, E.; SECADA, L.; VALQUI, M.; HUGHES, R. F. High-resolution forest carbon stocks and emissions in the Amazon. **Proceedings of the National Academy of Sciences**, v. 107, n. 38, p. 16738–16742, 2010.

ASNER, G. P.; TUPAYACHI, R. Accelerated losses of protected forests from gold mining in the Peruvian Amazon. **Environmental Research Letters**, v. 12, n. 9, e 094004, 2016.

ASSOCIAÇÃO NACIONAL DOS SERVIDORES DE MEIO AMBIENTE (ASCEMA). **Cronologia de um desastre anunciado: Ações do governo Bolsonaro para desmontar as políticas de meio ambiente no Brasil**.Available from: http://www.ascemanacional.org.br/wp-content/uploads/2020/09/Dossie_Meio-Ambiente_Governo-Bolsonaro_revisado_02-set-2020-1.pdf. Access on: 2 Sept. 2020.

AUSTIN, K. G.; MOSNIER, A.; PIRKER, J.; MCCALLUM, I.; FRITZ, S.; KASIBHATLA, P. S. Shifting patterns of oil palm driven deforestation in Indonesia and implications for zero-deforestation commitments. **Land Use Policy**, v. 69, p. 41–48, 2017.

AVITABILE, V.; HEROLD, M.; HEUVELINK, G. B. M.; LEWIS, S. L.; PHILLIPS, O. L.; ASNER, G. P.; ARMSTON, J.; ASHTON, P. S.; BANIN, L.; BAYOL, N.; BERRY, N. J.; BOECKX, P.; DE JONG, B. H. J.; DEVRIES, B.; GIRARDIN, C. A. J.; KEARSLEY, E.; LINDSELL, J. A.; LOPEZ-GONZALEZ, G.; LUCAS, R.; MALHI, Y.; MOREL, A.; MITCHARD, E. T. A.; NAGY, L.; QIE, L.; QUINONES, M. J.; RYAN, C. M.; FERRY, S. J. W.; SUNDERLAND, T.; LAURIN, G. V.; GATTI, R. C.; VALENTINI, R.; VERBEECK, H.; WIJAYA, A.; WILLCOCK, S. An integrated pan-tropical biomass map using multiple reference datasets. **Global Change Biology**, v. 22, n. 4, p. 1406–1420, 2016.

BACCINI, A.; GOETZ, S. J.; WALKER, W. S.; LAPORTE, N. T.; SUN, M.; SULLA-MENASHE, D.; HACKLER, J.; BECK, P. S. A.; DUBAYAH, R.; FRIEDL, M. A.; SAMANTA, S.; HOUGHTON, R. A. Estimated carbon dioxide emissions from tropical deforestation improved by carbon-density maps. **Nature Climate Change**, v. 2, n. 3, p. 182–185, 2012.

BACCINI, A.; WALKER, W.; CARVALHO, L.; FARINA, M.; SULLA-MENASHE, D.; HOUGHTON, R. A. Tropical forests are a net carbon source based on aboveground measurements of gain and loss. **Science**, v. 358, n. 6360, p. 230–234, 2017.

BAKER, P. J.; BUNYAVEJCHEWIN, S.; ROBINSON, A. P. The impacts of large-scale, low-intensity fires on the forests of continental South-east Asia. **International Journal of Wildland Fire**, v. 17, n. 6, p. 782, 2008.

BARLOW, J.; BERENGUER, E.; CARMENTA, R.; FRANÇA, F. Clarifying Amazonia's burning crisis. **Global Change Biology**, v. 26, n. 2, p. 319–321, 2020.

BECKNELL, J. M.; KELLER, M.; PIOTTO, D.; LONGO, M.; NARA DOS-SANTOS, M.; SCARANELLO, M. A.; BRUNO DE OLIVEIRA CAVALCANTE, R.; PORDER, S. Landscape-scale lidar analysis of aboveground biomass distribution in secondary Brazilian Atlantic Forest. **Biotropica**, v. 50, n. 3, p. 520–530, 2018.

BEHNAMIAN, A.; MILLARD, K.; BANKS, S. N.; WHITE, L.; RICHARDSON, M.; PASHER, J. A Systematic Approach for Variable Selection With Random Forests: achieving stable variable importance values. **IEEE Geoscience and Remote Sensing Letters**, v. 14, n. 11, p. 1988–1992, 2017.

BENNETT, A. C et al. Resistance of African tropical forests to an extreme climate anomaly. **Proceedings of the National Academy of Sciences of the United States of America**, v. 118, n. 21, 2021.

BERENGUER, E.; FERREIRA, J.; GARDNER, T. A.; ARAGÃO, L. E. O. C.; DE CAMARGO, P. B.; CERRI, C. E.; DURIGAN, M.; OLIVEIRA, R. C. DE; VIEIRA, I. C. G.; BARLOW, J. A large-scale field assessment of carbon stocks in human-modified tropical forests. **Global Change Biology**, v. 20, n. 12, p. 3713–3726, 2014.

BONAN, G. B. Forests and climate change: forcings, feedbacks, and the climate benefits of forests. **Science**, v. 320, n. 5882, p. 1444–1449, 2008.

BONNINI, S.; CORAIN, L.; MAROZZI, M.; SALMASO, L. **Nonparametric hypothesis testing**. Chichester, UK: John Wiley & Sons, 2014. ISBN (9781118763490).

BOUCHER, D.; ELIAS, P.; LININGER, K.; MAY-TOBIN, C.; ROQUEMORE, S.; SAXON, E. **The root of the problem**: what's driving tropical deforestation today? Cambridge, Massachusetts: Union of Concerned Scientists, 2012.

BOWMAN, D. M. J. S.; BALCH, J.; ARTAXO, P.; BOND, W. J.; COCHRANE, M. A.; D'ANTONIO, C. M.; DEFRIES, R.; JOHNSTON, F. H.; KEELEY, J. E.; KRAWCHUK, M. A.; KULL, C. A.; MACK, M.; MORITZ, M. A.; PYNE, S.; ROOS, C. I.; SCOTT, A. C.; SODHI, N. S.; SWETNAM, T. W. The human dimension of fire regimes on Earth. **Journal of Biogeography**, v. 38, n. 12, p. 2223–2236, 2011.

BOWMAN, D. M. J. S.; BALCH, J. K.; ARTAXO, P.; BOND, W. J.; CARLSON, J. M.; COCHRANE, M. A.; D'ANTONIO, C. M.; DEFRIES, R. S.; DOYLE, J. C.; HARRISON, S. P.; JOHNSTON, F. H.; KEELEY, J. E.; KRAWCHUK, M. A.; KULL, C. A.; MARSTON, J. B.; MORITZ, M. A.; PRENTICE, I. C.; ROOS, C. I.; SCOTT, A. C.; SWETNAM, T. W.; VAN DER WERF, G. R.; PYNE, S. J. Fire in the Earth system. **Science (New York, N.Y.)**, v. 324, n. 5926, p. 481–4, 2009.

BRANCALION, P. H. S.; GARCIA, L. C.; LOYOLA, R.; RODRIGUES, R. R.; PILLAR, V. D.; LEWINSOHN, T. M. A critical analysis of the native vegetation protection law of Brazil (2012): updates and ongoing initiatives. **Natureza & Conservação**, v. 14, p. 1–15, 2016.

BRANCALION, P. H. S.; NIAMIR, A.; BROADBENT, E.; CROUZEILLES, R.; BARROS, F. S. M.; ALMEYDA ZAMBRANO, A. M.; BACCINI, A.; ARONSON, J.; GOETZ, S.; REID, J. L.; STRASSBURG, B. B. N.; WILSON, S.; CHAZDON, R. L. Global restoration opportunities in tropical rainforest landscapes. **Science Advances**, v. 5, n. 7, e eaav3223, 2019.

BRANDO, P. M.; BALCH, J. K.; NEPSTAD, D. C.; MORTON, D. C.; PUTZ, F. E.; COE, M. T.; SILVERIO, D.; MACEDO, M. N.; DAVIDSON, E. A; NOBREGA, C. C.; ALENCAR, A.; SOARES-FILHO, B. S. Abrupt increases in Amazonian tree mortality due to drought-fire interactions. **Proceedings of the National Academy of Sciences**, v. 111, n. 17, p. 6347–6352, 2014.

BRANDO, P. M.; NEPSTAD, D. C.; DAVIDSON, E. A.; TRUMBORE, S. E.; RAY, D.; CAMARGO, P. Drought effects on litterfall, wood production and belowground carbon cycling in an Amazon forest: results of a throughfall reduction experiment. **Philosophical Transactions of the Royal Society B: Biological Sciences**, v. 363, n. 1498, p. 1839–1848, 2008.

BRASIL. Lei Federal nº 12.727, de 17 de Outubro de 2012. **Diário Oficial da União**, 2012.

BRASIL. MINISTÉRIO DO MEIO AMBIENTE (MMA). **Plano de Ação para Prevenção e Controle do Desmatamento na Amazônia Legal (PPCDAm): 3ª fase (2012-2015) pelo uso sustentável e conservação da Floresta**. Brasíla: MMA, 2013. 174 p.

BRIANT, G.; GOND, V.; LAURANCE, S. G. W. Habitat fragmentation and the desiccation of forest canopies: A case study from eastern Amazonia. **Biological Conservation**, v. 143, n. 11, p. 2763–2769, 2010.

BRIENEN, R. J. W. et al. Long-term decline of the Amazon carbon sink. **Nature**, v. 519, n. 7543, p. 344–348, 2015.

BRINCK, K.; FISCHER, R.; GROENEVELD, J.; LEHMANN, S.; DANTAS DE PAULA, M.; PÜTZ, S.; SEXTON, J. O.; SONG, D.; HUTH, A. High resolution analysis of tropical forest fragmentation and its impact on the global carbon cycle. **Nature Communications**, v. 8, e 14855, 2017.

BROADBENT, E. N.; ASNER, G. P.; OLIVEIRA, P. J. C.; KNAPP, D. E.; KELLER, M.; SILVA, J. N. Forest fragmentation and edge effects from

deforestation and selective logging in the Brazilian Amazon. **Biological Conservation**, v. 141, n. 7, p. 1745–1757, 2008.

BURT, A.; DISNEY, M.; CALDERS, K. Extracting individual trees from lidar point clouds using treeseg. **Methods in Ecology and Evolution**, p. 2041–210X.13121, 2018.

BURTON, C.; RIFAI, S.; MALHI, Y. Inter-comparison and assessment of gridded climate products over tropical forests during the 2015/2016 El Niño. **Philosophical Transactions of the Royal Society B: Biological Sciences**, v. 373, n. 1760, e 20170406, 2018.

BUSH, M. B.; SILMAN, M. R.; MCMICHAEL, C.; SAATCHI, S. Fire, climate change and biodiversity in Amazonia: a Late-Holocene perspective. **Philosophical transactions of the Royal Society of London. Series B, Biological sciences**, v. 363, n. 1498, p. 1702–1795, 2008.

BUTARBUTAR, T.; SOEDIRMAN, S.; NEUPANE, P. R.; KÖHL, M. Carbon recovery following selective logging in tropical rainforests in Kalimantan, Indonesia. **Forest Ecosystems**, v. 6, n. 1, p. 36, 2019.

CABALLERO ESPEJO, J.; MESSINGER, M.; ROMÁN-DAÑOBEYTIA, F.; ASCORRA, C.; FERNANDEZ, L.; SILMAN, M. Deforestation and forest degradation due to gold mining in the peruvian Amazon: a 34-year perspective. **Remote Sensing**, v. 10, n. 12, p. 1903, 2018.

CAMARGO, J. L. C.; KAPOS, V. Complex edge effects on soil moisture and microclimate in central Amazonian forest. **Journal of Tropical Ecology**, v. 11, n. 2, p. 205–221, 1995.

CAMPANHARO, W. A.; SILVA JUNIOR, C. H. L. **Maximum Cumulative Water Deficit - MCWD:** a R language script. Available from: https://doi.org/10.5281/zenodo.2652629.

CANO-CRESPO, A.; OLIVEIRA, P. J. C.; BOIT, A.; CARDOSO, M.; THONICKE, K. Forest edge burning in the Brazilian Amazon promoted by escaping fires from managed pastures. **Journal of Geophysical Research: Biogeosciences**, v. 120, n. 10, p. 2095–2107, 2015.

CAPOBIANCO, J. P. R. **Biodiversidade na Amazônia brasileira**: avaliação e ações prioritárias para a conservação, uso sustentável e repartição de benefícios. São Paulo: Instituto Socioambiental, 2001. 540 p.

CARTER, S.; HEROLD, M.; AVITABILE, V.; DE BRUIN, S.; DE SY, V.; KOOISTRA, L.; RUFINO, M. C. Agriculture-driven deforestation in the tropics

from 1990–2015: emissions, trends and uncertainties. **Environmental Research Letters**, v. 13, n. 1, e 014002, 2018.

CASTIBLANCO, C.; ETTER, A.; AIDE, T. M. Oil palm plantations in Colombia: a model of future expansion. **Environmental Science & Policy**, v. 27, p. 172–183, 2013.

CHAPLIN-KRAMER, R.; RAMLER, I.; SHARP, R.; HADDAD, N. M.; GERBER, J. S.; WEST, P. C.; MANDLE, L.; ENGSTROM, P.; BACCINI, A.; SIM, S.; MUELLER, C.; KING, H. Degradation in carbon stocks near tropical forest edges. **Nature Communications**, v. 6, e 10158, 2015.

CHAVE, J.; ANDALO, C.; BROWN, S.; CAIRNS, M. A.; CHAMBERS, J. Q.; EAMUS, D.; FÖLSTER, H.; FROMARD, F.; HIGUCHI, N.; KIRA, T.; LESCURE, J.-P.; NELSON, B. W.; OGAWA, H.; PUIG, H.; RIÉRA, B.; YAMAKURA, T. Tree allometry and improved estimation of carbon stocks and balance in tropical forests. **Oecologia**, v. 145, n. 1, p. 87–99, 2005.

CHEN, Q. LiDAR remote sensing of vegetation biomass. In: WANG, G.; WENG, Q. (Ed.). **Remote sensing of natural resources**. [S.l.]: CRC Press, 2014. p. 399–420.

CHUVIECO, E.; LIZUNDIA-LOIOLA, J.; PETTINARI, M. L.; RAMO, R.; PADILLA, M.; TANSEY, K.; MOUILLOT, F.; LAURENT, P.; STORM, T.; HEIL, A.; PLUMMER, S. Generation and analysis of a new global burned area product based on MODIS 250 m reflectance bands and thermal anomalies. **Earth System Science Data**, v. 10, n. 4, p. 2015–2031, 2018.

CIAIS, P.; SABINE, C.; BALA, G.; BOPP, L.; BROVKIN, V.; CANADELL, J.; CHHABRA, A.; DEFRIES, R.; GALLOWAY, J.; HEIMANN, M.; JONES, C.; LE QUÉRÉ, C.; MYNENI, R.; PIAO, S.; THORNTON, P.; HEINZE, C.; TANS, P.; VESALA, T. Carbon and other biogeochemical cycles. In: INTERGOVERNMENTAL PANEL ON CLIMATE CHANGE (Ed.). **Climate change 2013** - the physical science basis. Cambridge: Cambridge University Press, 2013. v. 9781107057, p. 465–570.

CLÉMENÇON, R. The two sides of the Paris climate agreement. **The Journal of Environment & Development**, v. 25, n. 1, p. 3–24, 2016.

CLEVELAND, W. S.; GROSSE, E.; SHYU, W. M. Local regression models. In: CHAMBERS, J. M.; HASTIE, T. J. (Ed.). **Statistical models in S**. New York: Chapman and Hall, 1992. p. 309–376.

CLEVELAND, W. S.; LOADER, C. Smoothing by local regression: principles and methods. In: HÄRDLE, W.; SCHIMEK, M. G. **Statistical theory and computational aspect of smoking**. [S.l]: Springer, 1994.

COCHRANE, M. A. Synergistic interactions between habitat fragmentation and fire in evergreen tropical forests. **Conservation Biology**, v. 15, n. 6, p. 1515–1521, 2001.

COCHRANE, M. A. Fire science for rainforests. **Nature**, v. 421, n. 6926, p. 913–9, 2003.

COCHRANE, M. A.; LAURANCE, W. F. Fire as a large-scale edge effect in Amazonian forests. **Journal of Tropical Ecology**, v. 18, n. 3, p. 311–325, 26 maio 2002.

COCHRANE, M. A; LAURANCE, W. F. Synergisms among Fire, Land Use, and Climate Change in the Amazon. **AMBIO: A Journal of the Human Environment**, v. 37, n. 7, p. 522–527, 2008.

COE, M. T.; MARTHEWS, T. R.; COSTA, M. H.; GALBRAITH, D. R.; GREENGLASS, N. L.; IMBUZEIRO, H. M. A; LEVINE, N. M.; MALHI, Y.; MOORCROFT, P. R.; MUZA, M. N.; POWELL, T. L.; SALESKA, S. R.; SOLORZANO, L. A.; WANG, J. Deforestation and climate feedbacks threaten the ecological integrity of south-southeastern Amazonia. **Philosophical transactions of the Royal Society of London. Series B, Biological sciences**, v. 368, n. 1619, e. 20120155, 2013.

CONOVER, W. J. **Practical nonparametric statistics**. 3. ed. [S.l.]: John Wiley & Sons, 1999a. 592 p. ISBN (978-0471160687).

CONOVER, W. J. **Practical nonparametric statistics**. 3. ed. [S.l.]: John Wiley & Sons, 1999b. 592 p. ISBN (978-0471160687).

COOMES, D. A.; DALPONTE, M.; JUCKER, T.; ASNER, G. P.; BANIN, L. F.; BURSLEM, D. F. R. P.; LEWIS, S. L.; NILUS, R.; PHILLIPS, O. L.; PHUA, M.-H.; QIE, L. Area-based vs tree-centric approaches to mapping forest carbon in Southeast Asian forests from airborne laser scanning data. **Remote Sensing of Environment**, v. 194, p. 77–88, 2017.

CURTIS, P. G.; SLAY, C. M.; HARRIS, N. L.; TYUKAVINA, A.; HANSEN, M. C. Classifying drivers of global forest loss. **Science**, v. 361, n. 6407, p. 1108–1111, 2018.

D'ANGELO, S. A.; ANDRADE, A. C. S.; LAURANCE, S. G.; LAURANCE, W. F.; MESQUITA, R. C. G. Inferred causes of tree mortality in fragmented and intact

Amazonian forests. **Journal of Tropical Ecology**, v. 20, n. 2, p. 243–246, 2004.

DANIAU, A.-L.; SANCHEZ GONI, M. F.; MARTINEZ, P.; URREGO, D. H.; BOUT-ROUMAZEILLES, V.; DESPRAT, S.; MARLON, J. R. Orbital-scale climate forcing of grassland burning in southern Africa. **Proceedings of the National Academy of Sciences**, v. 110, n. 13, p. 5069–5073, 2013.

DANIELSSON, P.-E. Euclidean distance mapping. **Computer Graphics and Image Processing**, v. 14, n. 3, p. 227–248, 1980.

DE PAULA, M. D.; COSTA, C. P. A.; TABARELLI, M. Carbon storage in a fragmented landscape of Atlantic forest: the role played by edge-affected habitats and emergent trees. **Tropical Conservation Science**, v. 4, n. 3, p. 349–358, 2011.

DEFRIES, R. S.; RUDEL, T.; URIARTE, M.; HANSEN, M. Deforestation driven by urban population growth and agricultural trade in the twenty-first century. **Nature Geoscience**, v. 3, n. 3, p. 178–181, 2010.

DELVOYE, K.; PARAHOE, M.; LIBRETTO, H. Suriname: an exposed interior. In: UNGAR, M. (Ed.). **The 21st century fight for the Amazon**. Cham: Springer International Publishing, 2018. p. 149–170.

DEZÉCACHE, C.; FAURE, E.; GOND, V.; SALLES, J.-M.; VIEILLEDENT, G.; HÉRAULT, B. Gold-rush in a forested El Dorado: deforestation leakages and the need for regional cooperation. **Environmental Research Letters**, v. 12, n. 3, e 034013, . 2017.

DIDHAM, R. K.; LAWTON, J. H. Edge structure determines the magnitude of changes in microclimate and vegetation structure in topical forest fragments. **Biotropica**, v. 31, n. 1, p. 17–30, 1999.

DINERSTEIN, E.; OLSON, D.; JOSHI, A.; VYNNE, C.; BURGESS, N. D.; WIKRAMANAYAKE, E.; HAHN, N.; PALMINTERI, S.; HEDAO, P.; NOSS, R.; HANSEN, M.; LOCKE, H.; ELLIS, E. C.; JONES, B.; BARBER, C. V.; HAYES, R.; KORMOS, C.; MARTIN, V.; CRIST, E.; SECHREST, W.; PRICE, L.; BAILLIE, J. E. M.; WEEDEN, D.; SUCKLING, K.; DAVIS, C.; SIZER, N.; MOORE, R.; THAU, D.; BIRCH, T.; POTAPOV, P.; TURUBANOVA, S.; TYUKAVINA, A.; DE SOUZA, N.; PINTEA, L.; BRITO, J. C.; LLEWELLYN, O. A.; MILLER, A. G.; PATZELT, A.; GHAZANFAR, S. A.; TIMBERLAKE, J.; KLÖSER, H.; SHENNAN-FARPÓN, Y.; KINDT, R.; LILLESØ, J.-P. B.; VAN BREUGEL, P.; GRAUDAL, L.; VOGE, M.; AL-SHAMMARI, K. F.; SALEEM, M. An ecoregion-based approach to protecting half the terrestrial realm. **BioScience**, v. 67, n. 6, p. 534–545, 2017.

D’OLIVEIRA, M. V. N.; FIGUEIREDO, E. O.; DE ALMEIDA, D. R. A.; OLIVEIRA, L. C.; SILVA, C. A.; NELSON, B. W.; DA CUNHA, R. M.; DE ALMEIDA PAPA, D.; STARK, S. C.; VALBUENA, R. Impacts of selective logging on Amazon forest canopy structure and biomass with a LiDAR and photogrammetric survey sequence. **Forest Ecology and Management**, v. 500, e 119648, 2021.

DUNCANSON, L. I.; NIEMANN, K. O.; WULDER, M. A. Integration of GLAS and Landsat TM data for aboveground biomass estimation. **Canadian Journal of Remote Sensing**, v. 36, n. 2, p. 129–141, 2010.

EUROPEAN SPACE AGENCY (ESA). **Land cover CCI product user guide version 2.0**. Available from: <http://maps.elie.ucl.ac.be/CCI/viewer/download/ESACCI-LC-Ph2-PUGv2_2.0.pdf>. Access on: 10 Apr. 2017.

EVA, H.; HUBER, O.; ACHARD, F.; BALSLEV, H.; BECK, S.; BEHLING, H.; BELWARD, A.; BEUCHLE, R.; CLEEF, A.; COLCHESTER, M.; DUIVENVOORDEN; HOOGMOED, M.; JUNK, W.; KABAT, P.; B. KRUIJIT; MALHI, Y.; MÜLLER, J. M.; PEREIRA, J. M.; PERES, C.; PRANCE, G. T.; ROBERTS, J.; SALO, J. **A proposal for defining the geographical boundaries of Amazonia**. Luxembourg: Publications Office, 2005. 38 p. ISBN (92-79-00012-8).

FAHRIG, L. Effects of habitat fragmentation on biodiversity. **Annual Review of Ecology, Evolution, and Systematics**, v. 34, n. 1, p. 487–515, 2003.

FEARNSIDE, P. M. Desmatamento na Amazônia brasileira: história, índices e conseqüências. **Megadiversidade**, v. 1, n. 1, p. 113–123, 2005.

FERRANTE, L.; FEARNSIDE, P. M. Brazil’s deception threatens climate goals. **Science**, v. 374, n. 6575, p. 1569–1569, 2021.

FERRAZ, A.; SAATCHI, S.; XU, L.; HAGEN, S.; CHAVE, J.; YU, Y.; MEYER, V.; GARCIA, M.; SILVA, C.; ROSWINTIART, O.; SAMBOKO, A.; SIST, P.; WALKER, S.; PEARSON, T. R. H.; WIJAYA, A.; SULLIVAN, F. B.; RUTISHAUSER, E.; HOEKMAN, D.; GANGULY, S. Carbon storage potential in degraded forests of Kalimantan, Indonesia. **Environmental Research Letters**, v. 13, n. 9, e 095001, 2018.

FERREIRA, L. V.; LAURANCE, W. F. Effects of forest fragmentation on mortality and damage of selected trees in central Amazonia. **Conservation Biology**, v. 11, n. 3, p. 797–801, 1997.

FISCHER, R.; TAUBERT, F.; MÜLLER, M. S.; GROENEVELD, J.; LEHMANN, S.; WIEGAND, T.; HUTH, A. Accelerated forest fragmentation leads to critical increase in tropical forest edge area. **Science Advances**, v. 7, n. 37, 2021.

FITZHERBERT, E.; STRUEBIG, M.; MOREL, A.; DANIELSEN, F.; BRUHL, C.; DONALD, P.; PHALAN, B. How will oil palm expansion affect biodiversity? **Trends in Ecology & Evolution**, v. 23, n. 10, p. 538–545, 2008.

FOLEY, J. A. Global consequences of land use. **Science**, v. 309, n. 5734, p. 570–574, 2005.

FRIEDL, M.; SULLA-MENASHE, D. **MCD12Q1 MODIS/Terra+Aqua land cover type yearly L3 global 500m SIN grid V006**. Available from: <https://doi.org/10.5067/MODIS/MCD12Q1.006>. Access on: 1 Jan. 2019.

FUNK, C.; PETERSON, P.; LANDSFELD, M.; PEDREROS, D.; VERDIN, J.; SHUKLA, S.; HUSAK, G.; ROWLAND, J.; HARRISON, L.; HOELL, A.; MICHAELSEN, J. The climate hazards infrared precipitation with stations—a new environmental record for monitoring extremes. **Scientific Data**, v. 2, n. 1, e 150066, 2015.

GARCIA, M.; SAATCHI, S.; FERRAZ, A.; SILVA, C. A.; USTIN, S.; KOLTUNOV, A.; BALZTER, H. Impact of data model and point density on aboveground forest biomass estimation from airborne LiDAR. **Carbon Balance and Management**, v. 12, n. 1, p. 4, 2017.

GASPARINI, K. A. C.; SILVA JUNIOR, C. H. L.; SHIMABUKURO, Y. E.; ARAI, E.; ARAGÃO, L. E. O. C. E; SILVA, C. A.; MARSHALL, P. L. Determining the frest threshold for the Amazon basin from the treecover2000 GFC data. **Sensors**, 2019a. Submited.

GASPARINI, K. A. C.; SILVA JUNIOR, C. H. L.; SHIMABUKURO, Y. E.; ARAI, E.; ARAGÃO, L. E. O. C. E; SILVA, C. A.; MARSHALL, P. L. Determining a threshold to delimit the amazonian forests from the tree canopy cover 2000 GFC data. **Sensors**, v. 19, n. 22, e 5020, 2019b.

GERWING, J. J. Degradation of forests through logging and fire in the eastern Brazilian Amazon. **Forest Ecology and Management**, v. 157, n. 1–3, p. 131–141, 2002.

GIBBONS, J. D.; CHAKRABORTI, S. Nonparametric statistical inference. In: LOVRIC, M. (Ed.). **International encyclopedia of statistical science**. Berlin, Heidelberg: Springer, 2011. p. 977–979.

GIBBS, H. K.; RAUSCH, L.; MUNGER, J.; SCHELLY, I.; MORTON, D. C.; NOOJIPADY, P.; SOARES-FILHO, B.; BARRETO, P.; MICOL, L.; WALKER, N. F. Brazil's Soy Moratorium. **Science**, v. 347, n. 6220, p. 377–378, 2015.

GIBBS, H. K.; RUESCH, A. S.; ACHARD, F.; CLAYTON, M. K.; HOLMGREN, P.; RAMANKUTTY, N.; FOLEY, J. A. Tropical forests were the primary sources of new agricultural land in the 1980s and 1990s. **Proceedings of the National Academy of Sciences**, v. 107, n. 38, p. 16732–16737, 2010.

GIGLIO, L.; BOSCHETTI, L.; ROY, D. P.; HUMBER, M. L.; JUSTICE, C. O. The collection 6 MODIS burned area mapping algorithm and product. **Remote Sensing of Environment**, v. 217, p. 72–85, 2018.

GIGLIO, L.; DESCLOITRES, J.; JUSTICE, C. O.; KAUFMAN, Y. J. An enhanced contextual fire detection algorithm for MODIS. **Remote Sensing of Environment**, v. 87, n. 2–3, p. 273–282, 2003.

GIGLIO, L.; SCHROEDER, W.; JUSTICE, C. O. The collection 6 MODIS active fire detection algorithm and fire products. **Remote Sensing of Environment**, v. 178, p. 31–41, 2016.

GIONGO, M.; KOEHLER, H. S.; MACHADO, S. DO A.; KIRCHNER, F. F.; MARCHETTI, M. LiDAR: princípios e aplicações florestais. **Pesquisa Florestal Brasileira**, v. 30, n. 63, p. 231–244, 2010.

GLOBAL FOREST WATCH (GFW). **globalforestwatch**. Available from: http://data.globalforestwatch.org/datasets/aboveground-live-woody-biomass-density. Access on: 1 Jan. 2019.

GONZALEZ DE TANAGO, J.; LAU, A.; BARTHOLOMEUS, H.; HEROLD, M.; AVITABILE, V.; RAUMONEN, P.; MARTIUS, C.; GOODMAN, R. C.; DISNEY, M.; MANURI, S.; BURT, A.; CALDERS, K. Estimation of above-ground biomass of large tropical trees with terrestrial LiDAR. **Methods in Ecology and Evolution**, v. 9, n. 2, p. 223–234, 2018.

GORELICK, N.; HANCHER, M.; DIXON, M.; ILYUSHCHENKO, S.; THAU, D.; MOORE, R. Google Earth Engine: planetary-scale geospatial analysis for everyone. **Remote Sensing of Environment**, v. 202, p. 18–27, 2017.

GRACE, J. Understanding and managing the global carbon cycle. **Journal of Ecology**, v. 92, n. 2, p. 189–202, 2004.

GRACE, J.; MITCHARD, E.; GLOOR, E. Perturbations in the carbon budget of the tropics. **Global Change Biology**, p. 3238–3255, 2014.

HADDAD, N. M.; BRUDVIG, L. A.; CLOBERT, J.; DAVIES, K. F.; GONZALEZ, A.; HOLT, R. D.; LOVEJOY, T. E.; SEXTON, J. O.; AUSTIN, M. P.; COLLINS, C. D.; COOK, W. M.; DAMSCHEN, E. I.; EWERS, R. M.; FOSTER, B. L.; JENKINS, C. N.; KING, A. J.; LAURANCE, W. F.; LEVEY, D. J.; MARGULES, C. R.; MELBOURNE, B. A.; NICHOLLS, A. O.; ORROCK, J. L.; SONG, D.-X.; TOWNSHEND, J. R. Habitat fragmentation and its lasting impact on Earth's ecosystems. **Science Advances**, v. 1, n. 2, e1500052, 2015.

HANCOCK, S.; ARMSTON, J.; HOFTON, M.; SUN, X.; TANG, H.; DUNCANSON, L. I.; KELLNER, J. R.; DUBAYAH, R. The GEDI simulator: a large-footprint waveform lidar simulator for calibration and validation of spaceborne missions. **Earth and Space Science**, e 2018EA000506, 2019.

HANSEN, M. C.; POTAPOV, P. V; MOORE, R.; HANCHER, M.; TURUBANOVA, S. A; TYUKAVINA, A.; THAU, D.; STEHMAN, S. V; GOETZ, S. J.; LOVELAND, T. R.; KOMMAREDDY, A.; EGOROV, A.; CHINI, L.; JUSTICE, C. O.; TOWNSHEND, J. R. G. High-resolution global maps of 21st-century forest cover change. **Science**, v. 342, n. 6160, p. 850–853, 2013.

HANSEN, M. C.; WANG, L.; SONG, X.-P.; TYUKAVINA, A.; TURUBANOVA, S.; POTAPOV, P. V.; STEHMAN, S. V. The fate of tropical forest fragments. **Science Advances**, v. 6, n. 11, eaax8574, 2020.

HANSEN, M.; POTAPOV, P.; MARGONO, B.; STEHMAN, S.; TURUBANOVA, S.; TYUKAVINA, A. Response to comment on "High-resolution global maps of 21st-century forest cover change." **Science**, v. 344, n. 6187, p. 981–981, 2014.

HASSEBO, Y. Active remote sensing: Lidar SNR improvements. In: ESCALANTE-RAMIREZ, B. (Ed.). **Remote sensing - advanced techniques and platforms**. Rijeka: InTech, 2012. p. 474.

HAYES, J. J.; ROBESON, S. M. Relationships between fire severity and post-fire landscape pattern following a large mixed-severity fire in the Valle Vidal, New Mexico, USA. **Forest Ecology and Management**, v. 261, n. 8, p. 1392–1400, 2011.

HEINRICH, V. H. A.; DALAGNOL, R.; CASSOL, H. L. G.; ROSAN, T. M.; DE ALMEIDA, C. T.; SILVA JUNIOR, C. H. L.; CAMPANHARO, W. A.; HOUSE, J. I.; SITCH, S.; HALES, T. C.; ADAMI, M.; ANDERSON, L. O.; ARAGÃO, L. E. O. C. Large carbon sink potential of secondary forests in the Brazilian Amazon to mitigate climate change. **Nature Communications**, v. 12, n. 1, e 1785, 2021a.

HEINRICH, V. H. A.; DALAGNOL, R.; CASSOL, H. L. G.; ROSAN, T. M.; DE ALMEIDA, C. T.; SILVA JUNIOR, C. H. L.; CAMPANHARO, W. A.; HOUSE, J. I.; SITCH, S.; HALES, T. C.; ADAMI, M.; ANDERSON, L. O.; ARAGÃO, L. E. O.

C. Large carbon sink potential of secondary forests in the Brazilian Amazon to mitigate climate change. **Nature Communications**, v. 12, n. 1, e 1785, 2021b.

HEROLD, M.; VAN GROENESTIJN, A.; KOOISTRA, L.; KALOGIROU, V.; ARINO, O. **Land cover CCI user requirements document**. Louvain-la-Neuve, Belgium: ESA, 2011.

HETTMANSPERGER, T. P.; MCKEAN, J. W. **Robust nonparametric statistical methods**. 2.ed. [S.l.]: CRC Press, 2010. 554 p. ISBN (9781439809082).

HIBBARD, K.; JANETOS, A.; VAN VUUREN, D. P.; PONGRATZ, J.; ROSE, S. K.; BETTS, R.; HEROLD, M.; FEDDEMA, J. J. Research priorities in land use and land-cover change for the Earth system and integrated assessment modelling. **International Journal of Climatology**, v. 30, n. 13, p. 2118–2128, 2010.

HISSA, L. D. B. V.; MÜLLER, H.; AGUIAR, A. P. D.; HOSTERT, P.; LAKES, T. Historical carbon fluxes in the expanding deforestation frontier of Southern Brazilian Amazonia (1985–2012). **Regional Environmental Change**, p. 1–13, 2016.

HOLDSWORTH, A. R.; UHL, C. Fire in Amazonian selectively logged rain forest and the potential for fire reduction. **Ecological Applications**, v. 7, n. 2, p. 713–725, 1997.

HOSHEN, J.; KOPELMAN, R. Percolation and cluster distribution. I. Cluster multiple labeling technique and critical concentration algorithm. **Physical Review B**, v. 14, n. 8, p. 3438–3445, 1976.

HOUGHTON, R. A.; HALL, F.; GOETZ, S. J. Importance of biomass in the global carbon cycle. **Journal of Geophysical Research: Biogeosciences**, v. 114, n. 3, 2009.

HOUGHTON, R. A.; HOUSE, J. I.; PONGRATZ, J.; VAN DER WERF, G. R.; DEFRIES, R. S.; HANSEN, M. C.; LE QUÉRÉ, C.; RAMANKUTTY, N. Carbon emissions from land use and land-cover change. **Biogeosciences**, v. 9, n. 12, p. 5125–5142, 2012.

HU, T.; SU, Y.; XUE, B.; LIU, J.; ZHAO, X.; FANG, J.; GUO, Q. Mapping global forest aboveground biomass with spaceborne LiDAR, optical imagery, and forest inventory data. **Remote Sensing**, v. 8, n. 7, e 565, 2016.

HUANG, M.; ASNER, G. P. Long-term carbon loss and recovery following selective logging in Amazon forests. **Global Biogeochemical Cycles**, v. 24, n. 3, 2010.

HUBAU, W. et al. Asynchronous carbon sink saturation in African and Amazonian tropical forests. **Nature**, v. 579, n. 7797, 2020.

INSTITUTO NACIONAL DE PESQUISAS ESPACIAIS (INPE). **PRODES - monitoramento da floresta amazônica brasileira por satélite**. Available from: <http://www.obt.inpe.br/prodes/>. Access on: 1 jan. 2018.

INSTITUTO NACIONAL DE PESQUISAS ESPACIAIS (INPE). **Monitoramento de queimadas**. Available from: http://www.inpe.br/queimadas/portal. Access on: 1 jan. 2018.

INTERGOVERNMENTAL PANEL ON CLIMATE CHANGE (IPCC). **Climate change 2021**: the physical science basis. Available from: https://www.ipcc.ch/report/sixth-assessment-report-working-group-i/. Access on: 12 Mar. 2021.

INTERGOVERNMENTAL PANEL ON CLIMATE CHANGE (IPCC). **Special report on global warming of 1.5 °C:** summary for policymakers. Available from: https://www.ipcc.ch/sr15/chapter/spm/. Access on: 1 Jan. 2019.

JASSBY, A. D.; CLOERN, J. E. **Package 'wq.'** Available from: https://cran.r-project.org/web/packages/wq/wq.pdf. Access on: 19 May 2016.

JIMENEZ, J. C.; BARICHIVICH, J.; MATTAR, C.; TAKAHASHI, K.; SANTAMARÍA-ARTIGAS, A.; SOBRINO, J. A.; MALHI, Y. Spatio-temporal patterns of thermal anomalies and drought over tropical forests driven by recent extreme climatic anomalies. **Philosophical Transactions of the Royal Society B: Biological Sciences**, v. 373, n. 1760, e 20170300, 2018.

JIMÉNEZ-MUÑOZ, J. C.; MATTAR, C.; BARICHIVICH, J.; SANTAMARÍA-ARTIGAS, A.; TAKAHASHI, K.; MALHI, Y.; SOBRINO, J. A.; SCHRIER, G. VAN DER. Record-breaking warming and extreme drought in the Amazon rainforest during the course of El Niño 2015–2016. **Scientific Reports**, v. 6, p. 33130, 2016.

JUÁREZ-OROZCO, S. M.; SIEBE, C.; FERNÁNDEZ Y FERNÁNDEZ, D. Causes and effects of forest fires in tropical rainforests: a bibliometric approach. **Tropical Conservation Science**, v. 10, e 194008291773720, 2017.

JUCKER, T.; ASNER, G. P.; DALPONTE, M.; BRODRICK, P. G.; PHILIPSON, C. D.; VAUGHN, N. R.; TEH, Y. A.; BRELSFORD, C.; BURSLEM, D. F. R. P.; DEERE, N. J.; EWERS, R. M.; KVASNICA, J.; LEWIS, S. L.; MALHI, Y.; MILNE, S.; NILUS, R.; PFEIFER, M.; PHILLIPS, O. L.; QIE, L.; RENNEBOOG, N.; REYNOLDS, G.; RIUTTA, T.; STRUEBIG, M. J.; SVÁTEK, M.; TURNER, E. C.; COOMES, D. A. Estimating aboveground carbon density and its uncertainty

in Borneo's structurally complex tropical forests using airborne laser scanning. **Biogeosciences**, v. 15, n. 12, p. 3811–3830, 2018.

JUNG, M. LecoS — A python plugin for automated landscape ecology analysis. **Ecological Informatics**, v. 31, p. 18–21, 2016.

KALAMANDEEN, M.; GLOOR, E.; MITCHARD, E.; QUINCEY, D.; ZIV, G.; SPRACKLEN, D.; SPRACKLEN, B.; ADAMI, M.; ARAGÃO, L. E. O. C.; GALBRAITH, D. Pervasive rise of small-scale deforestation in Amazonia. **Scientific Reports**, v. 8, n. 1, e 1600, 2018.

KAPOS, V. Effects of isolation on the water status of forest patches in the brazilian Amazon. **Journal of Tropical Ecology**, v. 5, n. 2, p. 173–185, 1989.

KEENAN, R. J.; REAMS, G. A.; ACHARD, F.; DE FREITAS, J. V.; GRAINGER, A.; LINDQUIST, E. Dynamics of global forest area: Results from the FAO global forest resources assessment 2015. **Forest Ecology and Management**, v. 352, p. 9–20, 2015.

KENDALL, M. G. **Rank correlation methods**. London: Charles Griffin, 1975.

KISSINGER, G.; HEROLD, M.; SY, V. DE. **Drivers of deforestation and forest degradation**: a synthesis report for REDD+ policy makers. Vancouver Canada: Lexeme Consulting, 2012.

KOH, L. P.; WILCOVE, D. S. Is oil palm agriculture really destroying tropical biodiversity? **Conservation Letters**, v. 1, n. 2, p. 60–64, 2008.

KOH, L. P.; WILCOVE, D. S. Oil palm: disinformation enables deforestation. **Trends in Ecology & Evolution**, v. 24, n. 2, p. 67–68, 2009.

KUHN, M. Building predictive models in R using the caret Package. **Journal of Statistical Software**, v. 28, n. 5, 2008.

KUSHARY, D.; DAVISON, A. C.; HINKLEY, D. V. Bootstrap methods and their application. **Technometrics**, v. 42, n. 2, p. 216, 2000.

LARGE, A. R. G.; HERITAGE, G. L. Laser scanning– evolution of the discipline. In: HERITAGE, G. L.; LARGE, A. R. G. (Ed.). **Laser scanning for the environmental sciences**. Oxford, UK: Wiley-Blackwell, 2009. p. 1–20.

LAURANCE, W. F.; CAMARGO, J. L. C.; FEARNSIDE, P. M.; LOVEJOY, T. E.; WILLIAMSON, G. B.; MESQUITA, R. C. G.; MEYER, C. F. J.; BOBROWIEC, P. E. D.; LAURANCE, S. G. W. An Amazonian rainforest and its fragments as a laboratory of global change. **Biological Reviews**, 2017.

LAURANCE, W. F.; CAMARGO, J. L. C.; FEARNSIDE, P. M.; LOVEJOY, T. E.; WILLIAMSON, G. B.; MESQUITA, R. C. G.; MEYER, C. F. J.; BOBROWIEC, P. E. D.; LAURANCE, S. G. W. An Amazonian rainforest and its fragments as a laboratory of global change. **Biological Reviews**, v. 93, n. 1, p. 223–247, 2018.

LAURANCE, W. F.; DELAMÔNICA, P.; LAURANCE, S. G.; VASCONCELOS, H. L.; LOVEJOY, T. E. Rainforest fragmentation kills big trees. **Nature**, v. 404, n. 6780, p. 836–836,. 2000.

LAURANCE, W. F.; FERREIRA, L. V.; MERONA, J. M. R.; LAURANCE, S. G. Rain forest fragmentation and the dynamics of amazonian tree communities. **Ecology**, v. 79, n. 6, e 2032, 1998.

LAURANCE, W. F.; LAURANCE, S. G.; DELAMONICA, P. Tropical forest fragmentation and greenhouse gas emissions. **Forest Ecology and Management**, v. 110, n. 1–3, p. 173–180, 1998.

LAURANCE, W. F.; LAURANCE, S. G.; FERREIRA, L. V.; RANKIN-DE-MERONA, J. M.; GASCON, C.; LOVEJOY, T. E. Biomass collapse in Amazonian forest fagments. **Science**, v. 278, n. 5340, p. 1117–1118, 1997.

LAURANCE, W. F.; NASCIMENTO, H. E. M.; LAURANCE, S. G.; ANDRADE, A. C.; FEARNSIDE, P. M.; RIBEIRO, J. E. L.; CAPRETZ, R. L. RAIN FOREST FRAGMENTATION AND THE PROLIFERATION OF SUCCESSIONAL TREES. **Ecology**, v. 87, n. 2, p. 469–482, 2006.

LAURANCE, W. F.; VASCONCELOS, H. L. Consequências ecológicas da fragmentação florestal na Amazônia. **Oecologia Brasiliensis**, v. 13, n. 3, p. 434–451, 2009.

LAURANCE, W. F.; WILLIAMSON, G. B. Positive feedbacks among forest fragmentation, drought, and climate change in the Amazon. **Conservation Biology**, v. 15, n. 6, p. 1529–1535, 2001.

LE MAIRE, G.; MARSDEN, C.; NOUVELLON, Y.; GRINAND, C.; HAKAMADA, R.; STAPE, J.-L.; LACLAU, J.-P. MODIS NDVI time-series allow the monitoring of Eucalyptus plantation biomass. **Remote Sensing of Environment**, v. 115, n. 10, p. 2613–2625, 2011.

LE PAGE, Y.; MORTON, D.; HARTIN, C.; BOND-LAMBERTY, B.; PEREIRA, J. M. C.; HURTT, G.; ASRAR, G. Synergy between land use and climate change increases future fire risk in Amazon forests. **Earth System Dynamics**, v. 8, n. 4, p. 1237–1246, 2017.

LEFSKY, M. A.; COHEN, W. B.; PARKER, G. G.; HARDING, D. J. Lidar remote sensing for ecosystem studies. **BioScience**, v. 52, n. 1, p. 19–30, 2002.

LEITOLD, V.; KELLER, M.; MORTON, D. C.; COOK, B. D.; SHIMABUKURO, Y. E. Airborne lidar-based estimates of tropical forest structure in complex terrain: opportunities and trade-offs for REDD+. **Carbon Balance and Management**, v. 10, n. 1, p. 3, e 2015.

LEWIS, S. L.; EDWARDS, D. P.; GALBRAITH, D. Increasing human dominance of tropical forests. **Science**, v.349, n.6250, p.827-832, 2015.

LEWIS, S. L.; LOPEZ-GONZALEZ, G.; SONKÉ, B.; AFFUM-BAFFOE, K.; BAKER, T. R.; OJO, L. O.; PHILLIPS, O. L.; REITSMA, J. M.; WHITE, L.; COMISKEY, J. A.; DJUIKOUO K, M. N.; EWANGO, C. E. N.; FELDPAUSCH, T. R.; HAMILTON, A. C.; GLOOR, M.; HART, T.; HLADIK, A.; LLOYD, J.; LOVETT, J. C.; MAKANA, J. R.; MALHI, Y.; MBAGO, F. M.; NDANGALASI, H. J.; PEACOCK, J.; PEH, K. S. H.; SHEIL, D.; SUNDERLAND, T.; SWAINE, M. D.; TAPLIN, J.; TAYLOR, D.; THOMAS, S. C.; VOTERE, R.; WÖLL, H. Increasing carbon storage in intact African tropical forests. **Nature**, v. 457, n. 7232, 2009.

LIU, Y. Y.; VAN DIJK, A. I. J. M.; DE JEU, R. A. M.; CANADELL, J. G.; MCCABE, M. F.; EVANS, J. P.; WANG, G. Recent reversal in loss of global terrestrial biomass. **Nature Climate Change**, p. 1–5, 2015.

LIU, Z.; HE, C.; WU, J. The relationship between habitat loss and fragmentation during urbanization: an empirical evaluation from 16 world cities. **PLOS ONE**, v. 11, n. 4, e0154613, 2016.

LOHBERGER, S.; STÄNGEL, M.; ATWOOD, E. C.; SIEGERT, F. Spatial evaluation of Indonesia's 2015 fire-affected area and estimated carbon emissions using Sentinel-1. **Global Change Biology**, v. 24, n. 2, p. 644–654, 2018.

LONGO, M.; KELLER, M.; DOS-SANTOS, M. N.; LEITOLD, V.; PINAGÉ, E. R.; BACCINI, A.; SAATCHI, S.; NOGUEIRA, E. M.; BATISTELLA, M.; MORTON, D. C. Aboveground biomass variability across intact and degraded forests in the Brazilian Amazon. **Global Biogeochemical Cycles**, v. 30, n. 11, p. 1639–1660, 2016.

LÓPEZ ACEVEDO, V. Ecuador: rainforest under Siege. In: UNGAR, M. (Ed.). **The 21st century fight for the Amazon**. Cham: Springer International, 2018. p. 93–113.

LOVEJOY, T. E.; BIERREGAARD, R. O.; RYLANDS, A. B.; MALCOM, J. R.; QUINTELA, C. E.; HARPER, L. H.; BROWN JR, K. S.; POWELL, A. H.; POWELL, G. V. N.; SCHUBART, H. O. R.; HAYS, M. B. Edge and other effects of isolation on Amazon forest fragments. In: SOULÉ, M. E. (Ed.). **Conservation biology**: the science of scarcity and diversity. Massachusetts: Sinauer Press, 1986. p. 257–285.

MAEDA, E. E.; NUNES, M. H.; CALDERS, K.; MOURA, Y. M. DE; RAUMONEN, P.; TUOMISTO, H.; VERLEY, P.; VINCENT, G.; ZUQUIM, G.; CAMARGO, J. L. Shifts in structural diversity of Amazonian forest edges detected using terrestrial laser scanning. **Remote Sensing of Environment**, v. 271, e 112895, 2022.

MALHI, Y. The carbon balance of tropical forest regions, 1990–2005. **Current Opinion in Environmental Sustainability**, v. 2, n. 4, p. 237–244, 2010.

MALHI, Y.; GARDNER, T. A.; GOLDSMITH, G. R.; SILMAN, M. R.; ZELAZOWSKI, P. Tropical forests in the anthropocene. **Annual Review of Environment and Resources**, v. 39, n. 1, p. 125–159, 2014.

MALHI, Y.; ROBERTS, J. T.; BETTS, R. A.; KILLEEN, T. J.; LI, W.; NOBRE, C. A. Climate change, deforestation, and the fate of the Amazon. **Science**, v. 319, n. 5860, p. 169–172, 2008.

MANN, H. B. Nonparametric tests against trend. **Econometrica**, v. 13, n. 3, p. 245, 1945.

MARENGO, J. A.; ESPINOZA, J. C. Extreme seasonal droughts and floods in Amazonia: causes, trends and impacts. **International Journal of Climatology**, v. 36, n. 3, p. 1033–1050, 2016.

MARENGO, J. A.; SOUZA, C. M.; THONICKE, K.; BURTON, C.; HALLADAY, K.; BETTS, R. A.; ALVES, L. M.; SOARES, W. R. Changes in climate and land use over the Amazon region: current and future variability and trends. **Frontiers in Earth Science**, v. 6, 2018.

MARTIN, P. A.; NEWTON, A. C.; PFEIFER, M.; KHOO, M.; BULLOCK, J. M. Impacts of tropical selective logging on carbon storage and tree species richness: a meta-analysis. **Forest Ecology and Management**, v. 356, p. 224–233, 2015.

MARTONE, M.; RIZZOLI, P.; WECKLICH, C.; GONZÁLEZ, C.; BUESO-BELLO, J.-L.; VALDO, P.; SCHULZE, D.; ZINK, M.; KRIEGER, G.; MOREIRA, A. The global forest/non-forest map from TanDEM-X interferometric SAR data. **Remote Sensing of Environment**, v. 205, p. 352–373, 2018.

MASCARO, J.; DETTO, M.; ASNER, G. P.; MULLER-LANDAU, H. C. Evaluating uncertainty in mapping forest carbon with airborne LiDAR. **Remote Sensing of Environment**, v. 115, n. 12, p. 3770–3774, 2011.

MASSON-DELMOTTE, V.; ZHAI, P.; PÖRTNER, H.-O.; ROBERTS, D.; SKEA, J.; SHUKLA, P. R.; PIRANI, A.; MOUFOUMA-OKIA, W.; PÉAN, C.; PIDCOCK, R.; CONNORS, S.; MATTHEWS, J. B. R.; CHEN, Y.; ZHOU, X.; GOMIS, M. I.; LONNOY, E.; MAYCOCK, T.; TIGNOR, M.; WATERFIELD, T. **Global warming of 1.5°C**: summary for policymakers. [S.l.]: IPCC, 2018.

MATAVELI, G. A. V.; SILVA, M. E. S.; PEREIRA, G.; DA SILVA CARDOZO, F.; KAWAKUBO, F. S.; BERTANI, G.; COSTA, J. C.; DE CÁSSIA RAMOS, R.; DA SILVA, V. V. Satellite observations for describing fire patterns and climate-related fire drivers in the Brazilian savannas. **Natural Hazards and Earth System Sciences**, v. 18, n. 1, p. 125–144, 2018.

MAUYA, E. W.; HANSEN, E. H.; GOBAKKEN, T.; BOLLANDSÅS, O. M.; MALIMBWI, R. E.; NÆSSET, E. Effects of field plot size on prediction accuracy of aboveground biomass in airborne laser scanning-assisted inventories in tropical rain forests of Tanzania. **Carbon Balance and Management**, v. 10, n. 1, p. 10, 2015.

MAXWELL, S. L.; EVANS, T.; WATSON, J. E. M.; MOREL, A.; GRANTHAM, H.; DUNCAN, A.; HARRIS, N.; POTAPOV, P.; RUNTING, R. K.; VENTER, O.; WANG, S.; MALHI, Y. Degradation and forgone removals increase the carbon impact of intact forest loss by 626%. **Science Advances**, v. 5, n. 10, e eaax2546, 2019.

MCGARIGAL, K. **Fragstats help**. Available from: http://www.umass.edu/landeco/research/fragstats/documents/fragstats.help.4.2.pdf. Access on: 21 Apr. 2015.

MEDJIBE, V. P.; PUTZ, F. E.; STARKEY, M. P.; NDOUNA, A. A.; MEMIAGHE, H. R. Impacts of selective logging on above-ground forest biomass in the Monts de Cristal in Gabon. **Forest Ecology and Management**, v. 262, n. 9, p. 1799–1806, 2011.

MELITO, M.; METZGER, J. P.; DE OLIVEIRA, A. A. Landscape-level effects on aboveground biomass of tropical forests: a conceptual framework. **Global Change Biology**, v. 24, n. 2, p. 597–607, 2018.

MELLO, N. G. R.; ARTAXO, P. Evolução do plano de ação para prevenção e controle do desmatamento na Amazônia Legal. **Revista do Instituto de Estudos Brasileiros**, n. 66, p. 108, 2017.

MENDIBURU, F. DE. **Statistical procedures for agricultural research**. Available from: https://cran.r-project.org/web/packages/agricolae/agricolae.pdf. Access on: 1 Jan. 2017.

MESQUITA, R. C. G.; DELAMÔNICA, P.; LAURANCE, W. F. Effect of surrounding vegetation on edge-related tree mortality in Amazonian forest fragments. **Biological Conservation**, v. 91, n. 2–3, p. 129–134, 1999.

MITCHARD, E. T. A.; SAATCHI, S. S.; WHITE, L. J. T.; ABERNETHY, K. A.; JEFFERY, K. J.; LEWIS, S. L.; COLLINS, M.; LEFSKY, M. A.; LEAL, M. E.; WOODHOUSE, I. H.; MEIR, P. Mapping tropical forest biomass with radar and spaceborne LiDAR in Lopé National Park, Gabon: overcoming problems of high biomass and persistent cloud. **Biogeosciences**, v. 9, n. 1, p. 179–191, 2012.

MUGGEO, V. M. R. Testing with a nuisance parameter present only under the alternative: a score-based approach with application to segmented modelling. **Journal of Statistical Computation and Simulation**, v. 86, n. 15, p. 3059–3067, 2016.

NASCIMENTO, H. E. M.; LAURANCE, W. F. Biomass dynamics in Amazonian forest fragments. **Ecological Applications**, v. 14, n. sp4, p. 127–138, 2004.

NEPSTAD, D. C.; TOHVER, I. M.; RAY, D.; MOUTINHO, P.; CARDINOT, G. Mortality of large trees and lianas following experimental drought in an Amazon forest. **Ecology**, v. 88, n. 9, p. 2259–2269, 2007.

NEPSTAD, D.; LEFEBVRE, P.; LOPES DA SILVA, U.; TOMASELLA, J.; SCHLESINGER, P.; SOLORZANO, L.; MOUTINHO, P.; RAY, D.; GUERREIRA BENITO, J. Amazon drought and its implications for forest flammability and tree growth: a basin-wide analysis. **Global Change Biology**, v. 10, n. 5, p. 704–717, 2004.

NEPSTAD, D.; MCGRATH, D.; STICKLER, C.; ALENCAR, A.; AZEVEDO, A.; SWETTE, B.; BEZERRA, T.; DIGIANO, M.; SHIMADA, J.; SEROA DA MOTTA, R.; ARMIJO, E.; CASTELLO, L.; BRANDO, P.; HANSEN, M. C.; MCGRATH-HORN, M.; CARVALHO, O.; HESS, L. Slowing Amazon deforestation through public policy and interventions in beef and soy supply chains. **Science**, v. 344, n. 6188, p. 1118–1123, 2014.

NUMATA, I.; COCHRANE, M. A. Forest fragmentation and its potential implications in the brazilian Amazon between 2001 and 2010. **Open Journal of Forestry**, v. 2, n. 4, p. 265–271, 2012.

NUMATA, I.; COCHRANE, M. A.; ROBERTS, D. A.; SOARES, J. V. Determining dynamics of spatial and temporal structures of forest edges in

South Western Amazonia. **Forest Ecology and Management**, v. 258, n. 11, p. 2547–2555, 2009.

NUMATA, I.; COCHRANE, M. A.; ROBERTS, D. A.; SOARES, J. V.; SOUZA, C. M.; SALES, M. H. Biomass collapse and carbon emissions from forest fragmentation in the Brazilian Amazon. **Journal of Geophysical Research**, v. 115, n. G3, e G03027, 2010.

NUMATA, I.; COCHRANE, M. A.; SOUZA JUNIOR, C. M.; SALES, M. H. Carbon emissions from deforestation and forest fragmentation in the Brazilian Amazon. **Environmental Research Letters**, v. 6, n. 4, e 044003, 2011.

NUMATA, I.; KHAND, K.; KJAERSGAARD, J.; COCHRANE, M. A.; SILVA, S. S. Forest evapotranspiration dynamics over a fragmented forest landscape under drought in southwestern Amazonia. **Agricultural and Forest Meteorology**, v. 306, e 108446, 2021.

NUMATA, I.; SILVA, S. S.; COCHRANE, M. A.; D'OLIVEIRA, M. V. Fire and edge effects in a fragmented tropical forest landscape in the southwestern Amazon. **Forest Ecology and Management**, v. 401, p. 135–146, 2017.

NUNES, S.; OLIVEIRA, L.; SIQUEIRA, J.; MORTON, D. C.; SOUZA, C. M. Unmasking secondary vegetation dynamics in the Brazilian Amazon. **Environmental Research Letters**, v. 15, n. 3, e 034057, 2020.

OLIVEIRA FILHO, F. J. B.; METZGER, J. P. Thresholds in landscape structure for three common deforestation patterns in the Brazilian Amazon. **Landscape Ecology**, v. 21, n. 7, p. 1061–1073, 2006.

ORDWAY, E. M.; ASNER, G. P. Carbon declines along tropical forest edges correspond to heterogeneous effects on canopy structure and function. **Proceedings of the National Academy of Sciences**, v. 117, n. 14, p. 7863–7870, 2020.

PAN, Y.; BIRDSEY, R. A.; FANG, J.; HOUGHTON, R.; KAUPPI, P. E.; KURZ, W. A.; PHILLIPS, O. L.; SHVIDENKO, A.; LEWIS, S. L.; CANADELL, J. G.; CIAIS, P.; JACKSON, R. B.; PACALA, S. W.; MCGUIRE, A. D.; PIAO, S.; RAUTIAINEN, A.; SITCH, S.; HAYES, D. A large and persistent carbon sink in the World's forests. **Science**, v. 333, n. 6045, p. 988–993, 2011.

PEKEL, J.-F.; COTTAM, A.; GORELICK, N.; BELWARD, A. S. High-resolution mapping of global surface water and its long-term changes. **Nature**, v. 540, n. 7633, p. 418–422, 2016.

PEREIRA, I.; MENDONÇA DO NASCIMENTO, H.; BONI VICARI, M.; DISNEY, M.; DELUCIA, E.; DOMINGUES, T.; KRUIJT, B.; LAPOLA, D.; MEIR, P.;

NORBY, R.; OMETTO, J.; QUESADA, C.; RAMMIG, A.; HOFHANSL, F. Performance of laser-based electronic devices for structural analysis of Amazonian Terra-Firme forests. **Remote Sensing**, v. 11, n. 5, e 510, 2019.

PEREIRA, R.; ZWEEDE, J.; ASNER, G. P.; KELLER, M. Forest canopy damage and recovery in reduced-impact and conventional selective logging in eastern Para, Brazil. **Forest Ecology and Management**, v. 168, n. 1–3, p. 77–89, 2002.

PINHEIRO, T. F.; ESCADA, M. I. S.; VALERIANO, D. M.; HOSTERT, P.; GOLLNOW, F.; MÜLLER, H. Forest degradation associated with logging frontier expansion in the Amazon: the BR-163 region in southwestern Pará, Brazil. **Earth Interactions**, v. 20, n. 17, p. 1–26, 2016.

PIVELLO, V. R.; VIEIRA, I.; CHRISTIANINI, A. V.; RIBEIRO, D. B.; DA SILVA MENEZES, L.; BERLINCK, C. N.; MELO, F. P. L.; MARENGO, J. A.; TORNQUIST, C. G.; TOMAS, W. M.; OVERBECK, G. E. Understanding Brazil's catastrophic fires: causes, consequences and policy needed to prevent future tragedies. **Perspectives in Ecology and Conservation**, v. 19, n. 3, p. 233–255, 2021.

PONTES-LOPES, A.; SILVA, C. V. J.; BARLOW, J.; RINCÓN, L. M.; CAMPANHARO, W. A.; NUNES, C. A.; DE ALMEIDA, C. T.; SILVA JÚNIOR, C. H. L.; CASSOL, H. L. G.; DALAGNOL, R.; STARK, S. C.; GRAÇA, P. M. L. A.; ARAGÃO, L. E. O. C. Drought-driven wildfire impacts on structure and dynamics in a wet Central Amazonian forest. **Proceedings of the Royal Society B: Biological Sciences**, v. 288, n. 1951, e 20210094, 2021.

POORTER, L. et al. Multidimensional tropical forest recovery. **Science**, v. 374, n. 6573, p. 1370–1376, 2021.

POTAPOV, P.; HANSEN, M. C.; LAESTADIUS, L.; TURUBANOVA, S.; YAROSHENKO, A.; THIES, C.; SMITH, W.; ZHURAVLEVA, I.; KOMAROVA, A.; MINNEMEYER, S.; ESIPOVA, E. The last frontiers of wilderness : tracking loss of intact forest landscapes from 2000 to 2013. **Science Advances**, v. 3, n.1, 2017.

POTAPOV, P.; LI, X.; HERNANDEZ-SERNA, A.; TYUKAVINA, A.; HANSEN, M. C.; KOMMAREDDY, A.; PICKENS, A.; TURUBANOVA, S.; TANG, H.; SILVA, C. E.; ARMSTON, J.; DUBAYAH, R.; BLAIR, J. B.; HOFTON, M. Mapping global forest canopy height through integration of GEDI and Landsat data. **Remote Sensing of Environment**, v. 253, e 112165, 2021.

PÜTZ, S.; GROENEVELD, J.; HENLE, K.; KNOGGE, C.; MARTENSEN, A. C.; METZ, M.; METZGER, J. P.; RIBEIRO, M. C.; DE PAULA, M. D.; HUTH, A.

Long-term carbon loss in fragmented Neotropical forests. **Nature Communications**, v. 5, e 5037, 2014.

QGIS DEVELOPMENT TEAM. **QGIS Geographic Information System**. Available from: <http://qgis.osgeo.org>. Access on: 22 jun. 2016.

QIE, L. et al. Long-term carbon sink in Borneo's forests halted by drought and vulnerable to edge effects. **Nature Communications**, v. 8, n. 1, 2017.

QIN, Y.; XIAO, X.; WIGNERON, J.-P.; CIAIS, P.; BRANDT, M.; FAN, L.; LI, X.; CROWELL, S.; WU, X.; DOUGHTY, R.; ZHANG, Y.; LIU, F.; SITCH, S.; MOORE, B. Carbon loss from forest degradation exceeds that from deforestation in the Brazilian Amazon. **Nature Climate Change**, v. 11, n. 5, p. 442–448, 2021.

R CORE TEAM. **R:** a language and environment for statistical computing. R Foundation for Statistical Computing, Vienna, Austria. Available from: <https://www.r-project.org/>. Access on: 1 Jan. 2018.

RANGEL PINAGÉ, E.; KELLER, M.; DUFFY, P.; LONGO, M.; DOS-SANTOS, M.; MORTON, D. Long-term impacts of selective logging on Amazon forest dynamics from multi-temporal airborne LiDAR. **Remote Sensing**, v. 11, n. 6, p. 709, 2019.

REUTEBUCH, S. E.; ANDERSEN, H.-E.; MCGAUGHEY, R. J. Light Detection and Ranging (LIDAR): an emerging tool for multiple resource inventory. **Journal of Forestry**, v. 103, n. 6, p. 286- 292, 2005.

RIITTERS, K.; WICKHAM, J.; O'NEILL, R.; JONES, B.; SMITH, E. Global-scale patterns of forest fragmentation. **Ecology and Society**, 2000.

RIPLEY, B. D. **Local polynomial regression fitting**. Available from: <http://stat.ethz.ch/R-manual/R-devel/library/stats/html/loess.html>. Access on: 1 Jan. 2018.

RITZ, C.; BATY, F.; STREIBIG, J. C.; GERHARD, D. Dose-response analysis using R. **PLOS ONE**, v. 10, n. 12, e0146021, 2015.

ROSAN, T. M.; ANDERSON, L. O.; VEDOVATO, L. Assessing the oigin of hot pixels in extreme climate yYears in the brazilian Amazon. **Revista Brasileira de Cartografia**, v. 69, n. 4, p. 731–741, 2017.

RUESCH, A.; GIBBS, H. K. **New IPCC Tier-1 global biomass carbon map for the year 2000**. Oak Ridge, Tennessee: Oak Ridge National Laboratory, 2008.

SAATCHI, S. S.; HARRIS, N. L.; BROWN, S.; LEFSKY, M.; MITCHARD, E. T. A; SALAS, W.; ZUTTA, B. R.; BUERMANN, W.; LEWIS, S. L.; HAGEN, S.; PETROVA, S.; WHITE, L.; SILMAN, M.; MOREL, A. Benchmark map of forest carbon stocks in tropical regions across three continents. **Proceedings of the National Academy of Sciences**, v. 108, n. 24, p. 9899–9904, 2011.

SAITO, É. A.; FONSECA, L. M. G.; ESCADA, M. I. S.; KORTING, T. S. Efeitos da mudança de escala em padrões de desmatamento na Amazônia. **Revista Brasileira de Cartografia**, v. 63, n. 3, p. 401–414, 2011.

SANTORO, M.; CARTUS, O. **ESA Biomass Climate Change Initiative (Biomass_cci)**: global datasets of forest above-ground biomass for the years 2010, 2017 and 2018, v3. [S.l.]: NERC EDS, 2021.

SEN, P. K. Estimates of the regression coefficient based on Kendall's Tau. **Journal of the American Statistical Association**, v. 63, n. 324, p. 1379, 1968.

SEXTON, J. O.; SONG, X.-P.; FENG, M.; NOOJIPADY, P.; ANAND, A.; HUANG, C.; KIM, D.-H.; COLLINS, K. M.; CHANNAN, S.; DIMICELI, C.; TOWNSHEND, J. R. Global, 30-m resolution continuous fields of tree cover: Landsat-based rescaling of MODIS vegetation continuous fields with lidar-based estimates of error. **International Journal of Digital Earth**, v. 6, n. 5, p. 427–448, 2013.

SHAPIRO, A. C.; AGUILAR-AMUCHASTEGUI, N.; HOSTERT, P.; BASTIN, J.-F. Using fragmentation to assess degradation of forest edges in Democratic Republic of Congo. **Carbon Balance and Management**, v. 11, n. 1, p. 11, 2016.

SHIMADA, M.; ITOH, T.; MOTOOKA, T.; WATANABE, M.; SHIRAISHI, T.; THAPA, R.; LUCAS, R. New global forest/non-forest maps from ALOS PALSAR data (2007–2010). **Remote Sensing of Environment**, v. 155, p. 13–31, 2014.

SIEGERT, F.; RUECKER, G.; HINRICHS, A.; HOFFMANN, A. A. Increased damage from fires in logged forests during droughts caused by El Niño. **Nature**, v. 414, n. 6862, p. 437–440, 2001.

SILVA, C. A.; SAATCHI, S.; GARCIA, M.; LABRIERE, N.; KLAUBERG, C.; FERRAZ, A.; MEYER, V.; JEFFERY, K. J.; ABERNETHY, K.; WHITE, L.; ZHAO, K.; LEWIS, S. L.; HUDAK, A. T. Comparison of small- and large-footprint lidar characterization of tropical forest aboveground structure and biomass: a case study from central Gabon. **IEEE Journal of Selected Topics in Applied Earth Observations and Remote Sensing**, v. 11, n. 10, p. 3512–3526, 2018a.

SILVA, C. V. J.; ARAGÃO, L. E. O. C.; BARLOW, J.; ESPIRITO-SANTO, F.; YOUNG, P. J.; ANDERSON, L. O.; BERENGUER, E.; BRASIL, I.; FOSTER BROWN, I.; CASTRO, B.; FARIAS, R.; FERREIRA, J.; FRANÇA, F.; GRAÇA, P. M. L. A.; KIRSTEN, L.; LOPES, A. P.; SALIMON, C.; SCARANELLO, M. A.; SEIXAS, M.; SOUZA, F. C.; XAUD, H. A. M. Drought-induced Amazonian wildfires instigate a decadal-scale disruption of forest carbon dynamics. **Philosophical Transactions of the Royal Society B: Biological Sciences**, v. 373, n. 1760, e 20180043, 2018b.

SILVA JUNIOR, C.; ARAGÃO, L.; FONSECA, M.; ALMEIDA, C.; VEDOVATO, L.; ANDERSON, L. Deforestation-Induced Fragmentation Increases Forest Fire Occurrence in Central Brazilian Amazonia. **Forests**, v. 9, n. 6, p. 305, 2018.

SILVA JUNIOR, C. H. L. **Dinâmica da formação de bordas florestais e seu impacto nos estoques de carbono na Bacia Amazônica utilizando sensoriamento remoto**. 2018. 183 p. Dissertação (Mestrado em Sensoriamento Remoto) - Instituto Nacional de Pesquisas Espaciais - INPE, São José dos Campos, 2018. Available from: http://urlib.net/8JMKD3MGP3W34P/3QEKUAS.

SILVA JUNIOR, C. H. L.; ANDERSON, L. O.; SILVA, A. L.; ALMEIDA, C. T.; DALAGNOL, R.; PLETSCH, M. A. J. S.; PENHA, T. V.; PALOSCHI, R. A.; ARAGÃO, L. E. O. C. Fire responses to the 2010 and 2015/2016 Amazonian droughts. **Frontiers in Earth Science**, v. 7, n. 97, p. 1–16, 2019a.

SILVA JUNIOR, C. H. L.; ANDERSON, L. O.; SILVA, A. L.; ALMEIDA, C. T.; DALAGNOL, R.; PLETSCH, M. A. J. S.; PENHA, T. V.; PALOSCHI, R. A.; ARAGÃO, L. E. O. C. Fire responses to the 2010 and 2015/2016 Amazonian droughts. **Frontiers in Earth Science**, v. 7, n. 97, p. 1–16, 2019b.

SILVA JUNIOR, C. H. L.; ARAGÃO, L. E. O. C.; ANDERSON, L. O.; FONSECA, M. G.; SHIMABUKURO, Y. E.; VANCUTSEM, C.; ACHARD, F.; BEUCHLE, R.; NUMATA, I.; SILVA, C. A.; MAEDA, E. E.; LONGO, M.; SAATCHI, S. S. Persistent collapse of biomass in Amazonian forest edges following deforestation leads to unaccounted carbon losses. **Science Advances**, v. 6, n. 40, e eaaz8360, 2020a.

SILVA JUNIOR, C. H. L.; CARVALHO, N. S.; PESSÔA, A. C. M.; REIS, J. B. C.; PONTES-LOPES, A.; DOBLAS, J.; HEINRICH, V.; CAMPANHARO, W.; ALENCAR, A.; SILVA, C.; LAPOLA, D. M.; ARMENTERAS, D.; MATRICARDI, E. A. T.; BERENGUER, E.; CASSOL, H.; NUMATA, I.; HOUSE, J.; FERREIRA, J.; BARLOW, J.; GATTI, L.; BRANDO, P.; FEARNSIDE, P. M.; SAATCHI, S.; SILVA, S.; SITCH, S.; AGUIAR, A. P.; SILVA, C. A.; VANCUTSEM, C.; ACHARD, F.; BEUCHLE, R.; SHIMABUKURO, Y. E.; ANDERSON, L. O.;

ARAGÃO, L. E. O. C. Amazonian forest degradation must be incorporated into the COP26 agenda. **Nature Geoscience**, v. 14, n. 9, p. 634–635, 2021a.

SILVA JUNIOR, C. H. L.; CELENTANO, D.; ROUSSEAU, G. X.; DE MOURA, E. G.; VARGA, I. VAN D.; MARTINEZ, C.; MARTINS, M. B. Amazon forest on the edge of collapse in the Maranhão State, Brazil. **Land Use Policy**, v. 97, e 104806, 2020b.

SILVA JUNIOR, C. H. L.; HEINRICH, V. H. A.; FREIRE, A. T. G.; BROGGIO, I. S.; ROSAN, T. M.; DOBLAS, J.; ANDERSON, L. O.; ROUSSEAU, G. X.; SHIMABUKURO, Y. E.; SILVA, C. A.; HOUSE, J. I.; ARAGÃO, L. E. O. C. Benchmark maps of 33 years of secondary forest age for Brazil. **Scientific Data**, v. 7, n. 1, p. 269, 2020c.

SILVA JUNIOR, C. H. L.; PESSÔA, A. C. M.; CARVALHO, N. S.; REIS, J. B. C.; ANDERSON, L. O.; ARAGÃO, L. E. O. C. The Brazilian Amazon deforestation rate in 2020 is the greatest of the decade. **Nature Ecology & Evolution**, v. 5, n. 2, p. 144–145, 2021b.

SILVÉRIO, D. V.; BRANDO, P. M.; BUSTAMANTE, M. M. C.; PUTZ, F. E.; MARRA, D. M.; LEVICK, S. R.; TRUMBORE, S. E. Fire, fragmentation, and windstorms: a recipe for tropical forest degradation. **Journal of Ecology**, v. 107, n. 2, p. 656–667, 2019a.

SILVÉRIO, D. V.; BRANDO, P. M.; BUSTAMANTE, M. M. C.; PUTZ, F. E.; MARRA, D. M.; LEVICK, S. R.; TRUMBORE, S. E. Fire, fragmentation, and windstorms: a recipe for tropical forest degradation. **Journal of Ecology**, v. 107, n. 2, p. 656–667, 2019b.

SIZER, N.; TANNER, E. V. J. Responses of woody plant seedlings to edge formation in a lowland tropical rainforest, Amazonia. **Biological Conservation**, v. 91, n. 2–3, p. 135–142, 1999.

SMITH, C. C.; ESPÍRITO-SANTO, F. D. B.; HEALEY, J. R.; YOUNG, P. J.; LENNOX, G. D.; FERREIRA, J.; BARLOW, J. Secondary forests offset less than 10% of deforestation-mediated carbon emissions in the Brazilian Amazon. **Global Change Biology**, v. 26, n. 12, p. 7006–7020, 2020.

SMITH, C. C.; HEALEY, J.; BERENGUER, E.; YOUNG, P. J.; TAYLOR, B.; ELIAS, F.; ESPÍRITO-SANTO, F.; BARLOW, J. Old-growth forest loss and secondary forest recovery across Amazonian countries. **Environmental Research Letters**, 2021.

SOARES-FILHO, B.; RAJAO, R.; MACEDO, M.; CARNEIRO, A.; COSTA, W.; COE, M.; RODRIGUES, H.; ALENCAR, A. Cracking Brazil's forest code. **Science**, v. 344, n. 6182, p. 363–364, 2014.

STAVROS, E. N.; SCHIMEL, D.; PAVLICK, R.; SERBIN, S.; SWANN, A.; DUNCANSON, L.; FISHER, J. B.; FASSNACHT, F.; USTIN, S.; DUBAYAH, R.; SCHWEIGER, A.; WENNBERG, P. ISS observations offer insights into plant function. **Nature Ecology & Evolution**, v. 1, n. 7, e0194, 2017.

STEININGER, M. K.; TUCKER, C. J.; TOWNSHEND, J. R. G.; KILLEEN, T. J.; DESCH, A.; BELL, V.; ERSTS, P. Tropical deforestation in the Bolivian Amazon. **Environmental Conservation**, v. 28, n. 2, p. 127–134, 2001.

STICKLER, C. M.; NEPSTAD, D. C.; AZEVEDO, A. A.; MCGRATH, D. G. Defending public interests in private lands: compliance, costs and potential environmental consequences of the Brazilian Forest Code in Mato Grosso. **Philosophical Transactions of the Royal Society B: Biological Sciences**, v. 368, n. 1619, e 20120160, 2013.

STROBL, C.; BOULESTEIX, A.-L.; ZEILEIS, A.; HOTHORN, T. Bias in random forest variable importance measures: Illustrations, sources and a solution. **BMC Bioinformatics**, v. 8, n. 1, p. 25, 2007.

STYSLEY, P. R.; COYLE, D. B.; KAY, R. B.; FREDERICKSON, R.; POULIOS, D.; CORY, K.; CLARKE, G. Long term performance of the High Output Maximum Efficiency Resonator (HOMER) laser for NASA′s Global Ecosystem Dynamics Investigation (GEDI) lidar. **Optics & Laser Technology**, v. 68, p. 67–72, 2015.

SULLIVAN, M. J. P. et al. Diversity and carbon storage across the tropical forest biome. **Scientific Reports**, v. 7, e 39102, 2017.

TATE, N. J.; BRUNSDON, C.; CHARLTON, M.; FOTHERINGHAM, A. S.; JARVIS, C. H. Smoothing/filtering LiDAR digital surface models: experiments with loess regression and discrete wavelets. **Journal of Geographical Systems**, v. 7, n. 3–4, p. 273–290, 2005.

TAUBERT, F.; FISCHER, R.; GROENEVELD, J.; LEHMANN, S.; MÜLLER, M. S.; RÖDIG, E.; WIEGAND, T.; HUTH, A. Global patterns of tropical forest fragmentation. **Nature**, v. 554, n. 7693, p. 519–522, 2018.

TRANCOSO, R. **Hydrological impacts of deforestation in small catchments in Brazilian Amazonia**. 2008. Manaus: National Institute for Amazonian Research - INPA, 2008.

TROPEK, R.; SEDLA EK, O.; BECK, J.; KEIL, P.; MUSILOVA, Z.; IMOVA, I.; STORCH, D. Comment on “High-resolution global maps of 21st-century forest cover change.” **Science**, v. 344, n. 6187, p. 981–981, 2014.

TURUBANOVA, S.; POTAPOV, P. V; TYUKAVINA, A.; HANSEN, M. C. Ongoing primary forest loss in Brazil, Democratic Republic of the Congo, and Indonesia. **Environmental Research Letters**, v. 13, n. 7, e 074028, 2018.

UHL, C.; BARRETO, P.; VIDAL, E.; AMARAL, P.; BARROS, A. C.; SOUZA, C.; JOHNS, J.; GERWING, J. Natural resource management in the brazilian Amazon. **BioScience**, v. 47, n. 3, p. 160–168, 1997.

UHL, C.; VIEIRA, I. C. G. Ecological Impacts of selective logging in the brazilian Amazon: a case study from the Paragominas region of the State of Para. **Biotropica**, v. 21, n. 2, p. 98, 1989.

UNITED NATIONS FRAMEWORK CONVENTION ON CLIMATE CHANGE (UNFCCC). **Lima REDD+ Information Hub**. 2017. Available from: http://redd.mma.gov.br/en/information-hub-brazil/the-lima-redd-information-hub.

UNITED NATIONS FRAMEWORK CONVENTION ON CLIMATE CHANGE (UNFCCC). **Adoção do acordo de Paris**. Available from: https://antigo.mma.gov.br/clima/convencao-das-nacoes-unidas/acordo-de-paris.html.

UNITED NATIONS FRAMEWORK CONVENTION ON CLIMATE CHANGE (UNFCCC). **The Paris Agreement**. Available from: https://unfccc.int/process-and-meetings/the-paris-agreement/the-paris-agreement. Access on: 1 Jan. 2019b.

UNITED NATIONS FRAMEWORK CONVENTION ON CLIMATE CHANGE (UNFCCC). **Adoção do Acordo de Paris**. Available from: https://nacoesunidas.org/wp-content/uploads/2016/04/Acordo-de-Paris.pdf. Access on: 12 Dec. 2015c.

UNITED NATIONS FRAMEWORK CONVENTION ON CLIMATE CHANGE (UNFCCC). **Forest reference emission levels**. Available from: https://redd.unfccc.int/fact-sheets/forest-reference-emission-levels.html. Access on: 1 Jan. 2019.

VANCUTSEM, C.; ACHARD, F.; PEKEL, J.-F.; VIEILLEDENT, G.; CARBONI, S.; SIMONETTI, D.; GALLEGO, J.; ARAGÃO, L. E. O. C.; NASI, R. Long-term (1990–2019) monitoring of forest cover changes in the humid tropics. **Science Advances**, v. 7, n. 10, eabe1603, 2021.

VANCUTSEM, C.; FRÉDÉRIC, A. Mapping intact and degraded humid forests over the tropical belt from 32 years of Landsat time series. In: ESA LIVING PLANET SYMPOSIUM, 2016. **Proceedings...** 2016.

VEDOVATO, L. B.; FONSECA, M. G.; ARAI, E.; ANDERSON, L. O.; ARAGÃO, L. E. O. C. The extent of 2014 forest fragmentation in the Brazilian Amazon. **Regional Environmental Change**, v. 16, n. 8, p. 2485–2490, 2016.

VELASCO GOMEZ, M. D.; BEUCHLE, R.; SHIMABUKURO, Y.; GRECCHI, R.; SIMONETTI, D.; EVA, H. D.; ACHARD, F. A long-term perspective on deforestation rates in the Brazilian Amazon. **ISPRS - International Archives of the Photogrammetry, Remote Sensing and Spatial Information Sciences**, v. 40, n. 7W3, p. 539–544, 2015.

VERISSIMO, A.; BARRETO, P.; MATTOS, M.; TARIFA, R.; UHL, C. Logging impacts and prospects for sustainable forest management in an old Amazonian frontier: the case of Paragominas. **Forest Ecology and Management**, v. 55, n. 1–4, p. 169–199, dez. 1992.

VIEIRA, S.; DE CAMARGO, P. B.; SELHORST, D.; DA SILVA, R.; HUTYRA, L.; CHAMBERS, J. Q.; BROWN, I. F.; HIGUCHI, N.; DOS SANTOS, J.; WOFSY, S. C.; TRUMBORE, S. E.; MARTINELLI, L. A. Forest structure and carbon dynamics in Amazonian tropical rain forests. **Oecologia**, v. 140, n. 3, p. 468–479, 2004.

VIJAY, V.; PIMM, S. L.; JENKINS, C. N.; SMITH, S. J. The impacts of oil palm on recent deforestation and biodiversity loss. **PLOS ONE**, v. 11, n. 7, e0159668, 2016a.

VIJAY, V.; PIMM, S. L.; JENKINS, C. N.; SMITH, S. J. The impacts of oil palm on recent deforestation and biodiversity loss. **PLOS ONE**, v. 11, n. 7, e0159668, 2016b.

VILLARD, M.-A.; METZGER, J. P. Beyond the fragmentation debate: a conceptual model to predict when habitat configuration really matters. **Journal of Applied Ecology**, v. 51, n. 2, p. 309–318, 2014.

WEHR, A.; LOHR, U. Airborne laser scanning—an introduction and overview. **ISPRS Journal of Photogrammetry and Remote Sensing**, v. 54, n. 2–3, p. 68–82, 1999.

WEISSE, M. J.; NAUGHTON-TREVES, L. C. Conservation beyond park boundaries: the Impact of buffer zones on deforestation and mining concessions in the peruvian Amazon. **Environmental Management**, v. 58, n. 2, p. 297–311, 2016.

WICKE, B.; SIKKEMA, R.; DORNBURG, V.; FAAIJ, A. Exploring land use changes and the role of palm oil production in Indonesia and Malaysia. **Land Use Policy**, v. 28, n. 1, p. 193–206, 2011.

WIGNERON, J. P.; FAN, L.; CIAIS, P.; BASTOS, A.; BRANDT, M.; CHAVE, J.; SAATCHI, S.; BACCINI, A.; FENSHOLT, R. Tropical forests did not recover from the strong 2015–2016 El Niño event. **Science Advances**, v. 6, n. 6, 2020.

WOOSTER, M. J.; ROBERTS, G.; PERRY, G. L. W.; KAUFMAN, Y. J. Retrieval of biomass combustion rates and totals from fire radiative power observations: FRP derivation and calibration relationships between biomass consumption and fire radiative energy release. **Journal of Geophysical Research**, v. 110, n. D24, e D24311, 2005.

WULDER, M. A.; LOVELAND, T. R.; ROY, D. P.; CRAWFORD, C. J.; MASEK, J. G.; WOODCOCK, C. E.; ALLEN, R. G.; ANDERSON, M. C.; BELWARD, A. S.; COHEN, W. B.; DWYER, J.; ERB, A.; GAO, F.; GRIFFITHS, P.; HELDER, D.; HERMOSILLA, T.; HIPPLE, J. D.; HOSTERT, P.; HUGHES, M. J.; HUNTINGTON, J.; JOHNSON, D. M.; KENNEDY, R.; KILIC, A.; LI, Z.; LYMBURNER, L.; MCCORKEL, J.; PAHLEVAN, N.; SCAMBOS, T. A.; SCHAAF, C.; SCHOTT, J. R.; SHENG, Y.; STOREY, J.; VERMOTE, E.; VOGELMANN, J.; WHITE, J. C.; WYNNE, R. H.; ZHU, Z. Current status of Landsat program, science, and applications. **Remote Sensing of Environment**, v. 225, p. 127–147, 2019.

WULDER, M. A.; WHITE, J. C.; LOVELAND, T. R.; WOODCOCK, C. E.; BELWARD, A. S.; COHEN, W. B.; FOSNIGHT, E. A.; SHAW, J.; MASEK, J. G.; ROY, D. P. The global Landsat archive: status, consolidation, and direction. **Remote Sensing of Environment**, v. 185, p. 271–283, 2016.

XU, L.; SAATCHI, S. S.; SHAPIRO, A.; MEYER, V.; FERRAZ, A.; YANG, Y.; BASTIN, J.-F.; BANKS, N.; BOECKX, P.; VERBEECK, H.; LEWIS, S. L.; MUANZA, E. T.; BONGWELE, E.; KAYEMBE, F.; MBENZA, D.; KALAU, L.; MUKENDI, F.; ILUNGA, F.; EBUTA, D. Spatial distribution of carbon stored in forests of the Democratic Republic of Congo. **Scientific Reports**, v. 7, n. 1, p. 15030, 2017.

ZOLKOS, S. G.; GOETZ, S. J.; DUBAYAH, R. A meta-analysis of terrestrial aboveground biomass estimation using lidar remote sensing. **Remote Sensing of Environment**, v. 128, p. 289–298, 2013.